Université d'Ottawa • University of Ottawa

Université d'Ottawa • University of Ottawa

FACULTÉ DES ÉTUDES SUPÉRIEURES ET POSTDOCTORALES

FACULTY OF GRADUATE AND POSTDOCTORAL STUDIES

Shahbaz ASIF

AUTEUR DE LA THÈSE - AUTHOR OF THESIS

M. A. Sc. (Environmental Engineering)

GRADE - DEGREE

Department of Civil Engineering

FACULTÉ, ÉCOLE, DÉPARTEMENT - FACULTY, SCHOOL, DEPARTMENT

TITRE DE LA THÈSE - TITLE OF THE THESIS

Two-dimensional Depth-average Phytoplankton Growth Modeling in the Rideau River (Black Rapids - Hog's Back Reach)

R. Frenette

DIRECTEUR DE LA THÈSE - THESIS SUPERVISOR

F. Pick

CO-DIRECTEUR DE LA THÈSE - THESIS CO-SUPERVISOR

EXAMINATEURS DE LA THÈSE - THESIS EXAMINERS

P. Champagne

R. Droste

Y. Secretan

J.-M. De Koninck, Ph.D.

LE DOYEN DE LA FACULTÉ DES ÉTUDES SUPÉRIEURES ET POSTDOCTORALES

DEAN OF THE FACULTY OF GRADUATE AND POSTDOCTORAL STUDIES

TWO-DIMENSIONAL DEPTH-AVERAGED PHYTOPLANKTON GROWTH MODELLING IN THE RIDEAU RIVER (BLACK RAPIDS-HOG'S BACK REACH)

by
Shahbaz Asif

A thesis
presented to the University of Ottawa in partial fulfillment of the requirements for
Master of Applied Science in Environmental Engineering

Department of Environmental Engineering
University of Ottawa
Ottawa, Canada
K1N 6N5

May 2004

The M.A.Sc. in Environmental Engineering is a joint program
with Carleton University administered by the
Ottawa-Carleton Institute for Environmental Engineering (OCIENE)

Your file Votre référence
ISBN: 0-494-01402-4
Our file Notre référence
ISBN: 0-494-01402-4

ACKNOWLEDGEMENTS

I would like to thank my supervisors, Drs. Richard Frenette and Frances Pick for their invaluable guidance, encouragement and availability throughout this study.

I am grateful to Dr. Yves Secretan and INRS-EAU for providing us the hydrodynamic and transport model, source code of the transport model, short training and continuous support on the model.

Furthermore, I would like to express appreciation to Drs. Ronald Droste, Pascale Champagne and Yves Secretan for their useful comments and suggestions.

I am grateful to the staff of City of Ottawa, Canadian Museum of Nature, Parks Canada, Environment Canada, Rideau Valley Conservation Authority and Baird and Associates for their support in the data collection.

I would like to thank my wife and children for their continued support and patience throughout this study.

Funding for this research was partly provided through University of Ottawa Inter-Faculty Research fund managed by Drs. Frances Pick and Richard Frenette.

ABSTRACT

Eutrophication is the excessive growth of aquatic plants due to over-fertilization of aquatic systems. Increased nutrient loading increases the capacity of a water body to support a greater production of suspended algae or phytoplankton. Increased concentrations of phytoplankton can cause deleterious effects on water quality such as low dissolved oxygen levels during night-time, higher levels of total suspended solids, and aesthetic problems associated with water colour, taste and odour.

Within rivers, the spatial distribution of phytoplankton depends on various factors: these are hydrological (discharge, water-residence time), chemical (nutrient concentrations), physical (light conditions) and biotic (grazing, competition) in nature. Flow velocity has a significant impact on phytoplankton growth and dispersion.

The Rideau River is a moderately enriched lowland river in eastern Ontario that is sensitive to eutrophication. The urbanization and rural development within the Rideau River watershed has increased the loading of nutrients from point and non-point sources. Total phosphorus (TP) increases along the course of the Rideau River and exceeds the Provincial Water Quality Objectives for Ontario (PWQO) guidelines in the downstream sections of the River past Kars.

The present study was carried out to model the algal growth in Black Rapids-Hog's Back reach of the Rideau River. In this study a two-dimensional depth-averaged hydrodynamic model (HYDROSIM) and a transport model (DISPERSIM) both packaged in a GUI called MODELEUR were used. The model has been developed by Scientific Research Institute (INRS-EAU), Quebec. A model for growth and transport of algae was developed which was incorporated in the existing transport model, DISPERSIM.

The simulated results of velocity vectors from HYDROSIM showed an agreement with the Acoustic Flowmeter For Remote Areas (AFFRA) measurements although the simulated values were always on the lower side. The modelling results of MIKE3D and a study carried out in 1997 support the results of the flow modelling in the present study.

The Phytoplankton element was successfully added in the DISPERSIM model. The results of the phytoplankton growth and transport model matched well with the measurements of suspended chlorophyll-a in Mooney's Bay for July 03, 2000 simulation. The simulated values for June 05, 2000 and July 20, 2000 were also reasonably close to the measured values. The model under-estimated the measured values for August 08, 2000 simulation by 59%. The internal loading of phosphorus could be a source of error for August 08, 2000 simulation as the available data indicated development of anoxic conditions in deep zones in the Mooney's Bay during this period. The errors are also associated with lack of information on point sources. Modelling the variables such as k_e and T as nodal properties will also improve the results. Modelling phytoplankton as several different groups of species would be a better approach but data regarding taxonomy would be required to assess the type of species at a particular period and location.

TABLE OF CONTENTS

LIST OF TABLES

LIST OF FIGURES

SYMBOLS AND NOTATION

AFFRA	Acoustic Flowmeter For Remote Areas
C	Chezy's roughness
Cal	Calorie
Chl *a*	Chlorophyll-a
d	Day(s)
D/S	Downstream
Eh	Redox potential
E_7	Eh adjusted to pH 7
EPA	Environmental Protection Agency
GSC	Geodetic Survey of Canada
GUI	Graphical Users' Interface
ly	Langleys
MOE	Ministry of the Environment (Ontario)
N	Manning's Roughness Coefficient
NAD	North American Datum
NITER	Number of Iterations
NPREC	Number of Pre-conditioning
NRDEM	Number of restart
Pe_H	Hydrodynamic Peclet Number
Pe_T	Transport Peclet Number
RP	Reactive Phosphorus
SRP	Soluble Reactive Phosphorus
TMDL	Total Maximum Daily Loads
TNDF	Total number of degree of freedom
TP	Total phosphorus
1-D	One Dimensional
2-D	Two Dimensional
3-D	Three Dimensional

Greek Notation

μ_{global}	Global viscosity
μ_M	Molecular viscosity
μ_T	Eddy viscosity
μ_N	Numerical viscosity
g	Acceleration due to gravity
ρ	Density of water

CHAPTER 1

1 INTRODUCTION

1.1 Problem Definition

Eutrophication is the excessive growth of aquatic plants due to over-fertilization of aquatic systems. The over-fertilization occurs due to an abundance of nutrients in the waters [Thomann et al., 1987]. Increased nutrient loading increases the capacity of a water body to support a greater production of suspended algae or phytoplankton [Reynolds, 1984]. Increased concentrations of phytoplankton can cause deleterious effects on water quality such as low dissolved oxygen levels during night-time, higher levels of total suspended solids, aesthetic problems associated with water colour, taste and odour. Dying algae produce compounds, which act like surfactants and produce foam on the surface, especially downstream of weirs and falls. The relationship between nutrients and algal biomass has been well-established for lakes and reservoirs, but the relationship in flowing waters is more complex.

Within rivers, the spatial distribution of phytoplankton depends on various factors: these are hydrological (discharge, water-residence time), chemical (nutrient concentrations), physical (light conditions) and biotic (grazing, competition) in nature. Flow velocity has a significant impact on phytoplankton growth and dispersion. Rivers with milder slope and low velocities retain plankton sufficiently long in dead/storage zones to allow the establishment of plankton communities [Reynolds, 1995]. In a study carried out on the River Severn, U.K., it was observed that dead zone concentrations exceeded those in main channel by a factor of 1 to 2.5 and some were even greater [Reynolds, 2000].

The following study focuses on modelling the spatial and temporal distribution of algae within a moderately enriched lowland river in eastern Ontario, the Rideau River. The urbanization and rural development within the Rideau River watershed has increased the loading of nutrients from

point and non-point sources. Total phosphorus (TP) increases along the course of the Rideau River and exceeds the Provincial Water Quality Objectives for Ontario (PWQO) guidelines in the downstream sections of the River past Kars [The Rideau River Round Table, 2001]. The phytoplankton concentration decreases as the River flows out of the Lower Rideau Lake and gradually builds up along the upstream reach of the River and then again decreases in the downstream part near Kars (Fig. 1.1), [The Rideau River Round Table, 2001]. Several of the catchments between Black Rapids and Hog's Back discharge storm-water directly into the River without treatment, although implementation of facilities is being considered [Baird & Associates, 2000].

1.2 Study Area

The Rideau River is located in southeastern Ontario (Fig.1.1) and flows northeast for 110 km from its headwaters in Lower Rideau Lake before discharging into the Ottawa River at Ottawa (45°27'N, 75°42'W). The average annual discharge of the Rideau is 40 $m^3 s^{-1}$ and the watershed area at Ottawa is 3830 km^2 [The Rideau River Round Table, 2001]. There are few small tributaries contributing to the flow of the Rideau and the Lake feeds most of its discharge. Approximately 70% of the watershed area is agricultural land and the remainder is either forested or urban [Basu and Pick, 1997]. The primary uses of the river are for recreation and water supply, and there are no major industries located along the Rideau's course.

In the present study, a reach of the Rideau River between Black Rapids and Hog's Back was selected. On the eastern side of the Mooney's Bay [Fig. 1.1] is a beach used for swimming and other water sports by local residents. The area surrounding the Rideau River in this reach is mainly urban [Baird & Associates, Jan. 2000].

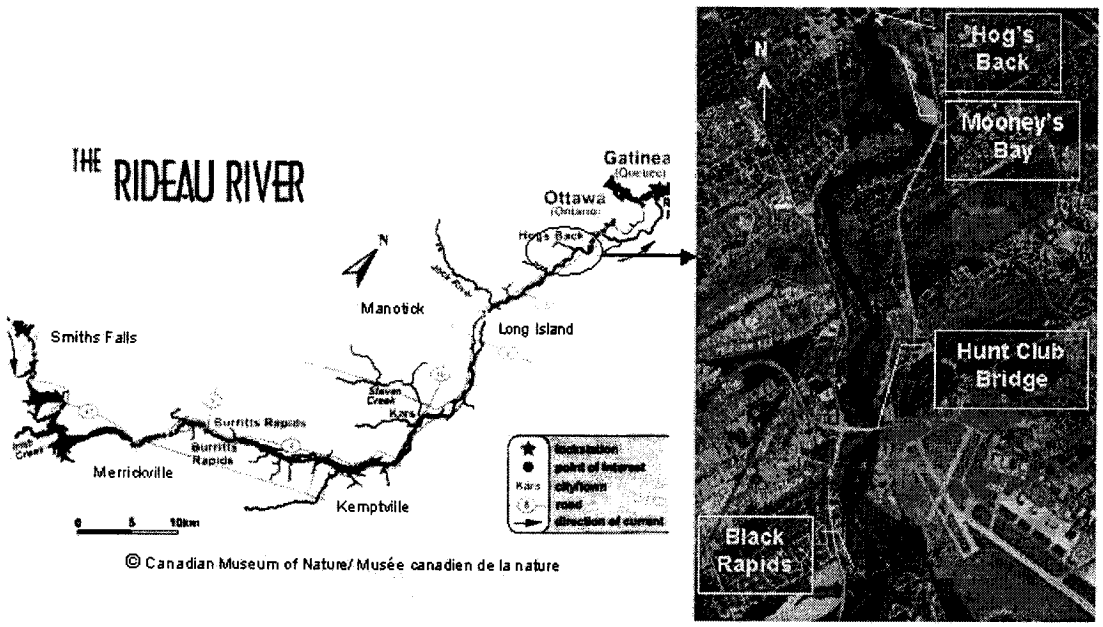

Figure 1.1 Layout Map [Ref.: Canadian Museum of Nature, City of Ottawa]

1.3 Objectives of the Study

The objectives of the present study are to model phytoplankton growth using a two-dimensional depth-averaged flow and transport model. The research aims at understanding the impact of flow and river geometry on phytoplankton growth in the Rideau River (Black Rapids to Hog's Back Reach). The study also aims at analyzing the impact of the controlling factors for phytoplankton growth such as light, temperature and nutrients.

1.4 Approach

Two-dimensional water quality hydrodynamic models are useful in the modelling of phytoplankton growth and the assessment of the relative responses of the river to various management options. These models can be used to assess a wide range of conditions that would otherwise be extremely expensive to evaluate in the field. The main objective of the present study is to model the flow and growth of phytoplankton using a two dimensional depth averaged model, MODELEUR. MODELEUR is a 2-D depth-averaged model, developed by INRS-EAU, a research center of University of Quebec [Secretan et al., 2000]. The program has three modules

- MODELEUR, a GIS based graphical users interface.
- HYDROSIM, based on the solution of Saint-Venant equations by finite-elements in steady or non-steady flow regimes.
- DISPERSIM, based on solution of advection-diffusion equation.

A phytoplankton growth element is not available in the present model. In order to model the phytoplankton growth the work has been conducted in the following steps: 1) A theoretical background study including previous studies was initially carried out. 2) Data including bathymetric data, water chemistry, physical parameters and Chl *a* were collected from various sources including the City of Ottawa, Parks Canada, Environment Canada, Baird and Associates and past studies carried out under the supervision of Frances Pick (Dept. of Biology, U. of Ottawa). 3) The next step was the development of the hydrodynamic model of the Rideau River (Black Rapids-Hog's Back Reach), its calibration, validation and sensitivity analysis for roughness selection. 4) In the last step, a model for phytoplankton growth was developed and a new element was coded in the DISPERSIM module. The phytoplankton growth model was calibrated and validated. Sensitivity analyses of important coefficients, constants and variable were also done.

1.5 Outline of the Report

Sections 1.2 and 1.3 of this introductory chapter address the background of the problem and the objectives and methodology. The fundamentals of hydrodynamic modelling and phytoplankton growth are discussed in Chapter 2. Various parameters governing phytoplankton growth are also discused in Chapter 2. A review of literature and past studies is also done in this chapter.

In Chapter 3, the methodology to achieve the objectives of phytoplankton growth modelling is described. Discussion and analyses of topographic, hydraulic and water quality data are done in this chapter. Modelling principles such as preparation of the model, calibration and validation are described in this chapter.

Chapter 4 includes the flow modelling of the Rideau River (Black Rapids-Hog's Back reach). A discussion of various aspects including grid generation, flow boundary conditions is presented in the early part of this chapter. The later part includes the flow simulation results, calibration and sensitivity analysis for bottom roughness was performed. Flow and numerical parameters used are also discussed in this chapter.

In the beginning of Chapter 5, the mathematical equations representing various components of the phytoplankton growth model are discussed. A discussion of rate constants and other coefficients governing growth along with their range are given in this chapter. Chapter 6 includes the phytoplankton modelling results. Calibration and validation of the model is also discussed in this chapter.

Chapter 7 presents conclusions regarding the flow and phytoplankton growth modelling. Finally, recommendations such as improvement in water quality monitoring and future studies for the continuation of the present study are also presented.

CHAPTER 2

2 THEORETICAL BACKGROUND

In this chapter flow and water quality modelling aspects are discussed. Discussion on relevant topics to hydrodynamic and water quality modelling and important factors considered in the selection of a water quality hydrodynamic model are given in the following paragraphs. Literature and previous studies regarding the subject are reviewed and important aspects are summarized in this chapter.

2.1 Shallow Water Equations

In MODELEUR the hydrodynamics are described by two-dimensional depth-averaged, St-Venant shallow water equations. The depth-averaged continuity equation is given by

$$\frac{\partial H}{\partial t}+\frac{\partial(HU_x)}{\partial x}+\frac{\partial(HU_y)}{\partial y}=0 \tag{2.1}$$

where H is the flow depth and U_x, U_y are the depth-averaged velocity fields.

The differential or non-conservative form of Shallow Water Equations for isotropic turbulence (disregarding the other external forces) is given by

$$\frac{dU_x}{dt}=\frac{\partial U_x}{\partial t}+U_x\frac{\partial U_x}{\partial x}+U_y\frac{\partial U_x}{\partial y}=-g\frac{\partial z_w}{\partial x}-\frac{\tau_{bx}}{\rho H}+\frac{1}{\rho}\left(\frac{\partial \sigma_x}{\partial x}+\frac{\partial \tau_{xy}}{\partial y}\right) \tag{2.2a}$$

$$\frac{dU_y}{dt}=\frac{\partial U_y}{\partial t}+U_x\frac{\partial U_y}{\partial x}+U_y\frac{\partial U_y}{\partial y}=-g\frac{\partial z_w}{\partial y}-\frac{\tau_{by}}{\rho H}+\frac{1}{\rho}\left(\frac{\partial \tau_{xy}}{\partial x}+\frac{\partial \sigma_y}{\partial y}\right) \tag{2.2b}$$

with:

$$\sigma_x = 2\mu_T \frac{\partial U_x}{\partial x} \tag{2.2c}$$

$$\sigma_y = 2\mu_T \frac{\partial U_y}{\partial y} \text{ and} \tag{2.2d}$$

$$\tau_{xy} = \mu_T \left(\frac{\partial U_x}{\partial y} + \frac{\partial U_y}{\partial x} \right) \tag{2.3}$$

where z_w is the free surface elevation; τ_{bx} and τ_{by} bed tangent shear stresses and p_a is the atmospheric pressure.

2.1.1 Turbulence and Reynold's Stresses

Turbulent flow occurs when inertial forces are greater than viscous forces, which is a frequent case in open channel flow. In turbulent flow, the particles of water follow an irregular path and there are fluctuating velocities present.

The Reynold's number is given by

$$\mathrm{Re} = \frac{Ul}{\upsilon} \tag{2.4}$$

where in case of open channels U is the norm $|\boldsymbol{U}|$ of the depth-averaged velocity vector $\boldsymbol{U}$ (U_x, U_y), l is a characteristic length scale (often taken to be the mean depth of flow), and $\upsilon = \mu/\rho$ is the kinematic viscosity. In rivers, turbulence is generated by velocity shear and hence originates where strong velocity gradients are present. Turbulent flows are not self-sustaining and in the absence of an external energy input the turbulence decays. In rivers, the energy input is mostly provided by gravity and sometimes by pressure gradients. Energy enters the flow at fairly large length scales but is transformed into smaller eddies. This gives a wide range of eddy sizes within

turbulent flow. Eddies are fluid volumes with a sense of rotation having various sizes. Eventually the energy reaches the smallest eddies and is dissipated as heat.

In the Navier Stokes equations, the terms for Reynold's stresses are also present. There are several ways to deal with these stresses. In practice, adjusting the turbulent viscosity is part of the calibration process. For simplified analysis, eddy viscosity can be a fixed constant in the domain, or it can also vary with space. When the problem centers on the use of the water level, the mixing length is not required. However in order to have a better representation of velocities, mixing length model is recommended [Heniche et al., 2000]. In 1925, Prandtl published a theory for predicting eddy viscosity in turbulent shear flow from an analogy between kinetic theory of gases and the behaviour of eddies in turbulent flow that has become known as the mixing length hypothesis. The turbulent shear stresses in one-dimensional flow can be related to the gradient in the mean velocity.

$$\tau_t = \upsilon_t \frac{\partial u}{\partial y} \tag{2.5}$$

where τ_t is turbulent shear stress, υ_t is turbulent viscosity.

The turbulent shear stress can also be written as

$$\tau_t = l_m{}^2 \left(\frac{\partial u}{\partial y} \right)^2 \tag{2.6}$$

where l_m is the Prandtl's mixing length. Equating the above two equations,

$$\upsilon_t = l_m{}^2 \left(\frac{\partial u}{\partial y} \right) \tag{2.7}$$

Although the above relation is empirical, the turbulence viscosity is often specified by the mixing length hypothesis of Prandtl. Prandtl's theory has two deficiencies: first, it is by no means certain that eddies interact in the same way as gas molecules; second, there is large range of eddy sizes

in turbulent flow so that it is not always easy to decide on a value of l_m. Nevertheless, it is a very useful equation and holds as a first approximation in many cases for suitably chosen value of turbulent viscosity.

The eddy viscosity terms in the governing equations actually represent the molecular viscosity and the effect of turbulence from the Reynold's stress terms.

$$E_{xx}\frac{\partial^2 y}{\partial x^2} = \mu\frac{\partial^2 y}{\partial x^2} + \frac{\partial}{\partial x}\frac{\overline{\partial u'v'}}{\partial x} \text{ [RMA2, 2001]} \tag{2.8}$$

where

μ = Molecular viscosity

u', v' = Turbulent deviations of the instantaneous velocity from the temporally averaged velocity u

$\overline{u'v'}$ =Time averaged of the velocity product over a time step

The effect of molecular viscosity is much smaller compared to eddy viscosity, E_{xx}. It is difficult to establish the value of E but analogy with physical conditions suggests that turbulence exchanges depends on the momentum and the distance over which that momentum is applied, i.e. length of the element. E should increase with the velocity and the size of spatial discretization of the domain. Turbulent exchanges are sensitive to changes in the direction of the velocity vector. Small values of the turbulent exchange coefficient allow the velocity vectors too much freedom to change their direction. This could make the numerical iterative solution unstable and by increasing E, convergence could be achieved. [RMA2, 2001]

One way to adjust the E is through the control of the Hydrodynamic Peclet number (Pe_H). Hydrodynamic Peclet number is defined as

$$Pe_H = \frac{\rho u \Delta x}{E} \tag{2.9}$$

where ρ is fluid density, u is average elemental velocity, Δx is length of element in streamwise direction and E is the eddy viscosity.

It is known from numerical analysis that for a problem to be numerically stable $P<P_c$ where P_c is the critical value, to ensure the numerical stability. The value of P_c is of the order of 1 and lower values would add numerical diffusion in the system. Based on provided Peclet number in a model the E can be automatically adjusted at each iteration.

2.1.1.1 Hydrostatic Pressure Distribution

The shallow water, long wave, or 2-D-depth-averaged equations are derived on the basis of a hydrostatic assumption in which the vertical accelerations are considered negligible compared to horizontal accelerations. The momentum equation in vertical direction is therefore reduced to a hydrostatic pressure equation.

The number of equations is often reduced by simplifying the third component of above equation to

$$\frac{dp}{dz} = -\rho g \tag{2.10}$$

by assuming that

- The gravity works only in the (negative) z-direction: $\mathbf{g} = (0,0,-g)$.
- No other external forces work in the z-direction (vertical accelerations are negligible).
- The flow is in good approximation horizontal (streamlines are straight and parallel).

These assumptions are often summarized as the *hydrostatic pressure assumption*. From the above equation (2.10) it can be concluded that

$$p(\mathbf{x}) = \rho g(z_w - z) + p_a \tag{2.11}$$

where z_w is the free surface elevation and p_a is the atmospheric pressure.

2.1.1.2 Averaging Over Depth

The vertical direction can be removed by integrating over the depth H from the bed $z_b(x,y)$ to the water level $z_w(x,y)$. The resulting three equations are given below, where H is z_w- z_b , U_x and U_y are the depth-averaged velocities in x- and y-directions.

From the mass conservation,

$$\frac{\partial H}{\partial t}+\frac{\partial (HU_x)}{\partial x}+\frac{\partial (HU_y)}{\partial y}=0 \tag{2.12}$$

or

$$\frac{dH}{dt}+H\frac{\partial U_x}{\partial x}+H\frac{\partial U_y}{\partial y}=0 \tag{2.13}$$

with

$$\frac{d}{dt}=\frac{\partial}{\partial t}+U_x\frac{\partial}{\partial x}+U_y\frac{\partial}{\partial y} \tag{2.14}$$

For integration of momentum conservation, an approximation is made such that the depth integrals of the non-linear velocity terms such as U^2 and U_xU_y, are included into the depth-averaged model, i.e. for all i, j and k.

$$\frac{\partial}{\partial x_i}\int_{z_b}^{z_w} u_j u_k dz \approx \frac{\partial HU_jU_k}{\partial x_i} \tag{2.15}$$

Disregarding the external forces and the lateral (turbulent) stresses except at the bottom, (the differential or non-conservative form of) the Shallow Water Equations can be written as

$$\frac{dU_x}{dt} = \frac{\partial U_x}{\partial t} + U_x \frac{\partial U_x}{\partial x} + U_y \frac{\partial U_x}{\partial y} = -g \frac{\partial z_w}{\partial x} - \frac{\tau_{bx}}{\rho H} + \frac{1}{\rho}\left(\frac{\partial \sigma_x}{\partial x} + \frac{\partial \tau_{xy}}{\partial y}\right) \tag{2.16a}$$

and

$$\frac{dU_y}{dt} = \frac{\partial U_y}{\partial t} + U_x \frac{\partial U_y}{\partial x} + U_y \frac{\partial U_y}{\partial y} = -g \frac{\partial z_w}{\partial y} - \frac{\tau_{by}}{\rho H} + \frac{1}{\rho}\left(\frac{\partial \tau_{xy}}{\partial x} + \frac{\partial \sigma_y}{\partial y}\right) \tag{2.16b}$$

where the components of bottom shear stress τ_b are given by

$$\tau_{bx} = U_x \frac{\rho g \sqrt{U_x^2 + U_y^2}}{C^2} \tag{2.17a}$$

$$\tau_{by} = U_y \frac{\rho g \sqrt{U_x^2 + U_y^2}}{C^2} \tag{2.17b}$$

with C the Chezy coefficient for bottom roughness.

2.2 Finite Element Method

2.2.1 Introduction

The shallow water equations can be solved using various techniques such as finite-element or finite-difference methods. The finite-element method has the ability to handle irregular boundaries and grid refinement [Chaudhry, 1994]. Refinements and smaller grid spacing around rapid variable changes such as edges or corners are more easily defined using the finite-element method. The computational grid for the finite-difference method is usually defined by parallel lines, which is not a limitation in the finite-element method. The following types of elements are used in HYDROSIM and DISPERSIM models.

2.2.2 T3 and T6 Element Types

Two-dimensional functions can be linear, quadratic or higher order. Figure 2.1 shows triangular T3 and T6 elements (Dhat, 1992). For rapidly changing variables higher order test functions are preferred. The linear approximation can be used if the element size is sufficiently small [Chaudhry, 1994]. T3 is used in DISPERSIM and T6 in HYDROSIM.

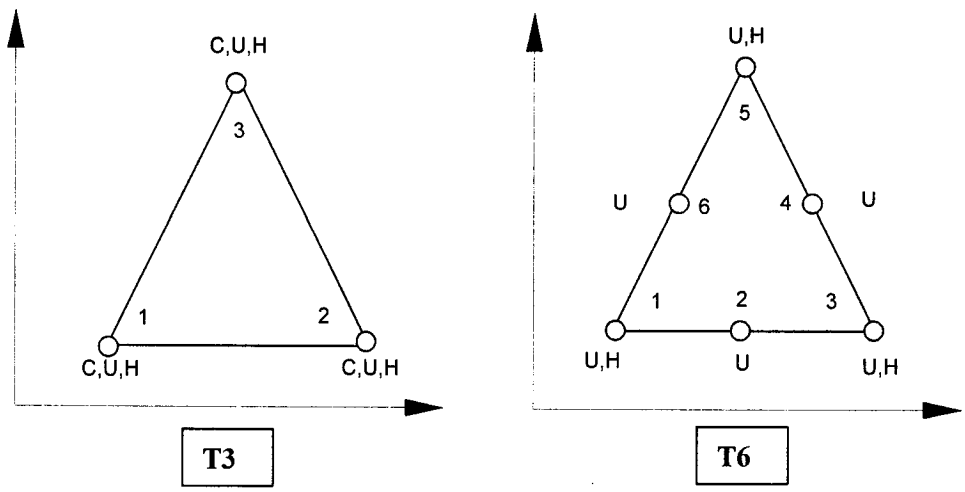

Figure 2.1 Two-Dimensional Triangular T3 and T6 Elements

2.3 Solution of Shallow Water Equations

Galerken method can be applied to the shallow water equations [Chaudhry, 1994]. The time-dependent terms in shallow water equations can be solved by either explicit or implicit finite-difference schemes. The rest of the terms are evaluated using finite-elements. The commonly used schemes for time derivatives are Euler, the trapezoidal rule, Adams-Moulten predictor-corrector, Runge-Kutta, and split-step schemes [Chaudhry, 1994].

In HYDROSIM, the solution method of the algebraic equation system is done by the iterative non-linear GMRES method, according to a "Newton-Inexact" scheme, with preconditioning [Heniche et al., 2000].

2.4 Transport Equation in Water Quality Models

Hydrodynamic surface water quality models are based on advection-diffusion equation, which expresses pollutant concentration as a function of flow (advective-transport) and mixing process (dispersive- transport). An additional source term to represent pollution loads and substance dependent water quality processes is also added in such models. From mass balance of constituents and state variables, we can write [SOBEK, 2001].

$$\frac{\partial Mass}{\partial t} = advection + dispersion + direct\ inputs + source\ or\ sink\ term \qquad (2.18)$$

If a mass balance in 1-D in an infinitesimally thin slice of a water body is carried out (Fig. 2.2).

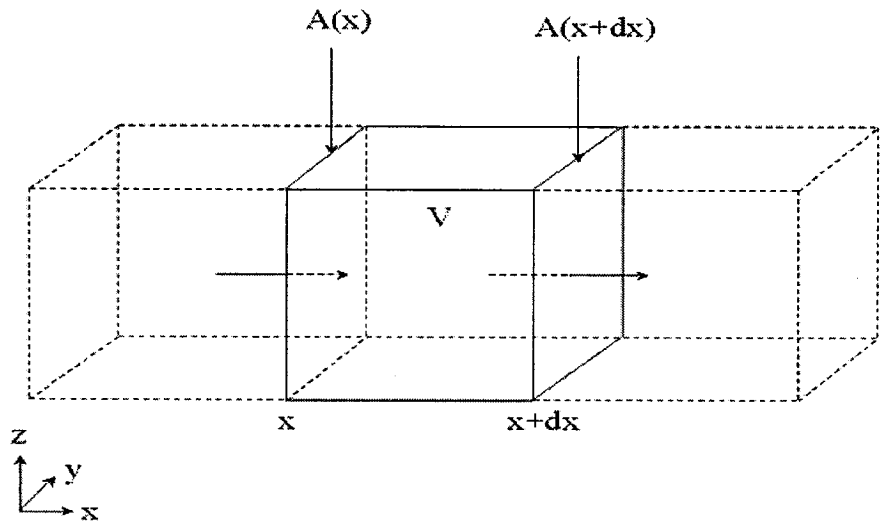

Figure 2.2 Schematic Overview of the Flow through a Slice [SOBEK, 2001]

The advective-transport can be computed as the flow through a surface, multiplied by the concentration at the surface. The flow is positive if it is directed into the positive x direction. For the upstream surface of the slice at position x, and the downstream surface of the slice at position x+Δx, the advective transport can be computed as follows:

$$T_a(x) = +Q(x)C(x)$$
$$T_a(x+\Delta x) = -Q(x+\Delta x)C(x+\Delta x) \quad \text{[SOBEK, 2001]} \qquad (2.19)$$

where T_a = advective transport [mg s^{-1}]; Q = flow [m^3 s^{-1}]; C = concentration [mg m^{-3}]

The minus sign in the second equation shows that there is outflow through the downstream side. The diffusive transport through a surface is computed according to Fick's Law [SOBEK, 2001]: it is inversely proportional to the concentration gradient in a direction perpendicular to the surface. The diffusive transport is proportional to the area of the surface, A. The constant of proportionality is called the "diffusion coefficient". For the upstream and the downstream surfaces of the slice the diffusive transport is computed as follows:

$$T_d(x) = -D(x)A(x)\left(\frac{\partial C}{\partial x}\right)_x$$
$$T_d(x+\Delta x) = D(x+\Delta x).A(x+\Delta x)\left(\frac{\partial C}{\partial x}\right)_{x+\Delta x} \quad \text{[SOBEK, 2001]} \qquad (2.20)$$

In this case, the minus sign is used at the upstream surface. The last term of the equation is a source term to represent pollution loads and substance dependent water quality processes. It is expressed as a "zero order" term, independent of the concentration and it is symbolized by the letter S.

Now the mass balance of a substance in the slice can be set up:

$$\frac{\partial M}{\partial t} = Q(x)C(x) - Q(x+\Delta x)C(x+\Delta x)$$
$$- D(x)A(x)\left(\frac{\partial C}{\partial x}\right)_x + D(x+\Delta x)A(x+\Delta x)\left(\frac{\partial C}{\partial x}\right)_{x+\Delta x} \quad \text{[SOBEK, 2001]} \qquad (2.21)$$
$$+ SV$$

If the thickness of the slice approaches zero, dividing by Δx, we obtain

$$\frac{\partial(AC)}{\partial t} = -\frac{\partial(QC)}{\partial x} + \frac{\partial}{\partial x}\left(DA\frac{\partial C}{\partial x}\right) + SA \qquad \text{[SOBEK, 2001]} \qquad (2.22)$$

This is the advection-diffusion equation in 1D. The above equation can also be written in the following form

$$\frac{\partial C}{\partial t} + \frac{\partial(UC)}{\partial x} = \frac{\partial}{\partial_x}\left(D\frac{\partial C}{\partial x}\right) + S \qquad (2.23)$$

2.4.1 Advection Diffusion Equation in 2-D

After depth integration the equation in 2-D may be written in the form [INRS-EAU, 2000]

$$H\frac{\partial C}{\partial t} + U_x H\frac{\partial C}{\partial x} + U_y H\frac{\partial C}{\partial y} - \frac{\partial}{\partial x}H(D_{xx}\frac{\partial C}{\partial x} + D_{xy}\frac{\partial C}{\partial y}) - \frac{\partial}{\partial y}H(D_{yx}\frac{\partial C}{\partial x} + D_{yy}\frac{\partial C}{\partial y}) - \Delta S = 0 \qquad (2.24)$$

C [kg m^{-3}] : concentration;

H [m]: depth ;

U_x, U_y [m s^{-1}] : depth-integrated velocity components in x and y direction ;

D_{ij} [m^2 s^{-1}] : components of dispersion tensor;

ΔS [kg m^{-2} s^{-1}]: Source or sink term over the whole flow depth

2.4.2 Background on Dispersion Coefficient

It is useful at this point to discuss briefly the difference between diffusion and dispersion. Both diffusion and dispersion tend to spread out pollutants (Fig. 2.3) but diffusion is due to the random motion of water in time, whereas dispersion is due to the differential movement of water in space (Chapra, 1997). From this point onward diffusion and dispersion are used as analogous terms. The selection of diffusion coefficients in transport equations is not very straightforward. The process of molecular diffusion is usually insignificant for surface water transport modelling ($D \approx 10^{-9}$ m^2/s). Turbulence is also responsible for diffusion. Generally, velocity differences or advection cause more diffusion than turbulence. Selection of the diffusion coefficient also depends upon schematization in the model. In 1D models 'D' has a higher value than 2- or 3D models. In 1D models, the velocity distribution along lateral and vertical directions is also averaged so the overall mixing effect is greater. A typical range of coefficient of diffusion is shown in Fig. 2.4.

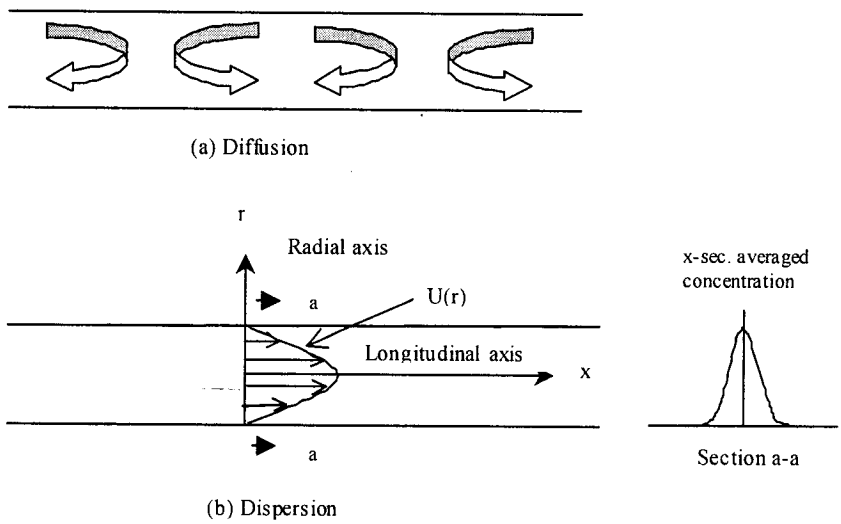

Figure 2.3 Contrast between Diffusion and Dispersion [Chapra, 1997]

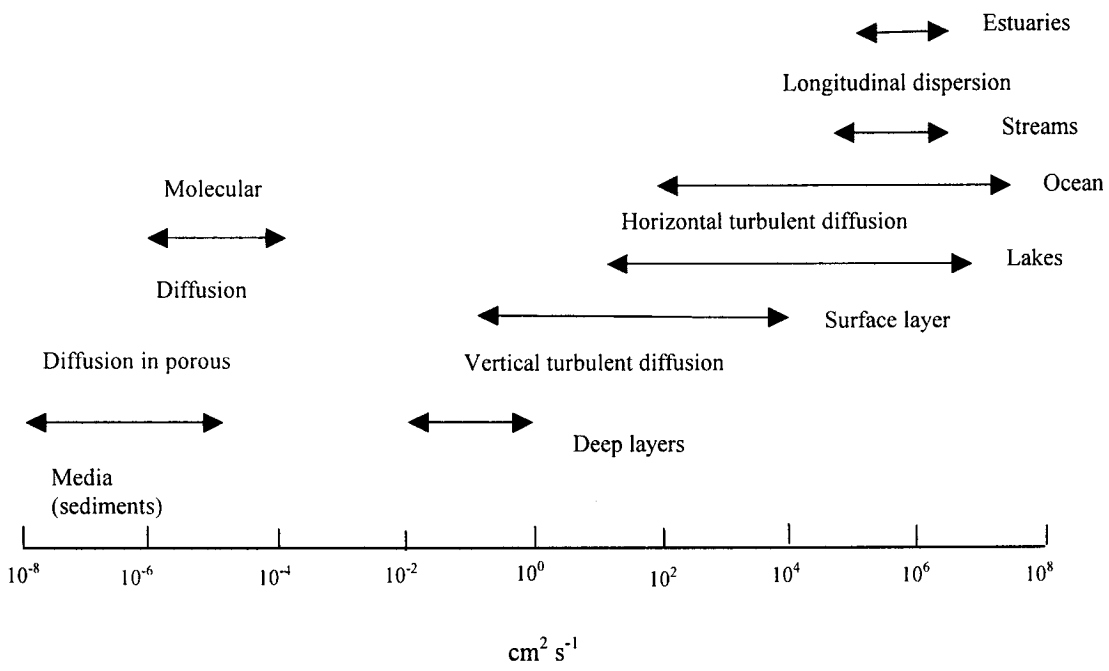

Figure 2.4 Typical ranges of the diffusion coefficient in natural waters and sediments. (Chapra, 1997)

Dispersion around bends, groynes and dead zones is a relatively complex phenomenon. Velocity gradients in the longitudinal direction such as present around groynes and dead zone interfaces can produce mass transport in the lateral direction and vice versa [Fischer et al., 1979]. In some depth-averaged two-dimensional models, the effect of secondary flow is incorporated in the transport equation to account for the spiral mixing along these interfaces. The geometry of dead zones and their connection to the main flow determines the exchange properties in a natural stream with dead zones [Fischer et. al., 1979]. The dispersive mixing results from the averaging process in modelling and the magnitude of dispersive mixing depends on the degree of uniformity in the velocity distributions, various processes controlling mixing are shown in Fig. 2.5 [Martin et al., 1999].

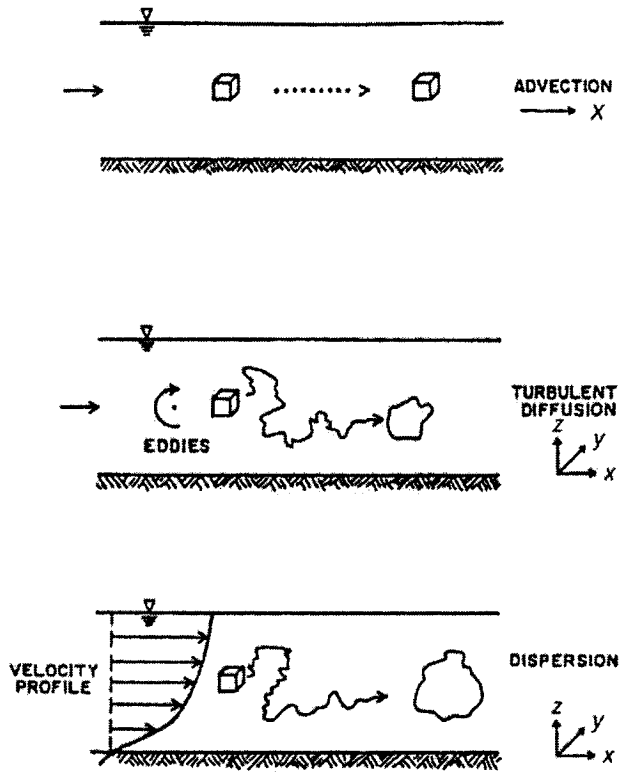

Figure 2.5 Transport due to Advection, Turbulent Diffusion and Dispersion [Martin et al., 1999]

2.5 Peclet Numbers for Transport and Flow Phenomena

The Peclet number 'Pe' is a dimensionless number and can be used to estimate whether a given system is advection or turbulent-diffusion dominated. Peclet number for transport (Pe_T) is the ratio of advective flux to the turbulent diffusivity flux.

$$Pe_T = \frac{U\Delta x}{D} \tag{2.25}$$

where U is average velocity; Δx is the spatial step; D is the coefficient of diffusion.

The Peclet number for hydrodynamics (Pe_H) is defined as

$$Pe_H = \frac{\rho U \Delta x}{E} \tag{2.26}$$

where ρ is fluid density [gcm^{-1}], U is average elemental velocity; Δx is length of element in longitudinal direction; and E is eddy viscosity [Pa-s].

2.6 Available Models for Hydrodynamic and Water Quality Modelling

Some of the models available commercially are listed below. The source and processes, which these models can simulate, are also highlighted.

2.6.1 MODELEUR

MODELEUR is a 2-D model, developed by INRS-EAU, a research center of University of Quebec. The program has three modules

1. MODELEUR is a GIS based graphical users interface.
2. HYDROSIM is based on the solution of Saint-Venant equations by finite-elements in steady or non-steady flow regimes.
3. DISPERSIM is based on solution of advection-diffusion equation. The following processes can be simulated in DISPERSIM.

    - Conservative and non-conservative sources
    - Bacterial pollution
    - BOD modelling
    - Thermal modelling

2.6.2 QUAL2E

The QUAL2E model was developed by the United States Environmental Protection Agency (EPA). It is a 1D model and basically designed for computations of total maximum daily loads (TMDL) in waterways. It can simulate flow and transport phenomena such as

- Nutrient cycles
- Algal production
- Non-point sources

QUAL2E for WINDOWS interface runs under WINDOWS 3.1, WINDOWS 95 and WINDOWS 98. It does not run under WINDOWS NT. QUAL2E-UNCAS is an enhancement to QUAL2E that allows the user to perform uncertainty analysis. Three uncertainty options are employed in QUAL2E-UNCAS: sensitivity analysis, first order error analysis and Monte Carlo simulation.

2.6.3 RMA Suite of Models

RMA was developed by Resource Management Associates and United States Army Corps of Engineers-Waterways Experiment Station (WES). They have developed a series of models for hydrodynamic and water quality modelling. The following are some of the models used in water resources.

2.6.3.1 RMA 2

RMA 2 is a 2-D depth-averaged hydrodynamic Finite Element (FEM) model. It can be used for steady and unsteady simulations. Elements consist of curved triangles and quadrilaterals. An implicit solution scheme is used for time-dependent systems.

2.6.3.2 RMA 10

RMA 10 is a 3D hydrodynamic Finite Element (FEM) model for stratified flow. It can be used for steady and unsteady simulations. Elements consist of curved bricks, tetrahedra and other complex shapes [King, 2002]. An implicit solution scheme is used for time dependent systems.

RMA 2 and RMA 10 models are capable of simulating a system using mixed approximation using two-dimensional approximation in the area of interest and one-dimensional approximations in other areas where the system is mostly linear. This helps to ensure cost effective model applications.

2.6.3.3 RMA 11

RMA-11 is a finite element water quality model for simulation of three dimensional estuaries, bays, lakes, rivers and coastal regions. It is also capable of simulating one- and two-dimensional approximations of systems, either separately or in combined form. It is designed to accept input of velocity fields from the three-dimensional stratified flow model, RMA-10, and these are used in the solution of the advection diffusion constituent transport equations. Additional inputs of constituent sources and sinks are required along with parameters for each constituent. The model was originally developed under contract to the Corps of Engineers, and in its earlier version (RMA-4) has been established as an integral part of the Corps' TABS-2 modelling system. Consulting firms, universities and government agencies in Europe, Asia and Australia, have used RMA-11.

Constituents that may be represented are:

- Temperature with a full atmospheric heat budget at the water surface
- BOD/DO
- The nitrogen cycle (including organic nitrogen, ammonia, nitrite and nitrates)
- The phosphorus cycle (including organic phosphorus and phosphates)
- Algal growth and decay

- Cohesive suspended sediment
- Non-cohesive suspended sediment such as sand
- Conservative constituents
- Coliform bacteria

2.6.4 WL|Delft Hydraulics Models

Delft models include SOBEK, Delft2-D and Delft 3D. SOBEK is a 1D hydrodynamic and water quality model and was developed by Delft Hydraulics in the Netherlands. Some of the processes that can be simulated by SOBEK are

- Dissolved oxygen
- Nutrients and eutrophication
- Pollution by toxic substances
- Coliform Bacteria, microbiological pollution, etc.

2.6.5 HEC5Q

HEC5Q was developed by the United States Army Corp of Engineers (USACE). The following processes can be simulated in HEC5Q. It is appropriate particularly for reservoir simulations.

- Reservoir simulations and water quality downstream
- Temperatures
- BOD etc.
- Nitrogen & phosphorus cycle
- Algal growth
- Coliform bacteria

2.6.6 TELEMAC

TELEMAC is a modeling system for hydrodynamics, sediment transport and water quality in the natural environment. The TELEMAC system was developed by Electricité de France-Laboratoire National d'Hydraulique. Modules such as WQ-2D, WQ-3D and SUBIEF are available with the TELEMAC modelling system.

2.6.7 WASP

WASP 6.1 is a water quality simulation programme. It was developed by US EPA for TMDL analysis. It can be linked to various flow models such as EFDC (3D hydrodynamic model) and SWMM, etc.

There are many other models available for flow and water quality modelling. Some of the models are discussed in Table 2.1 along with their important features and characteristics [modified from Palmer, 2001].

		QUAL2E	MODE-LEUR	TELEMAC/ WQ-2-D & WQ-3D	WASP	HEC5Q	MIKE MODELS	DELFT MODELS	RMA SUITE OF MODELS	CE-QUL-W2
1	**Author**	USEPA	INRS-Eau	Electricité de France	USEPA	USACE	Danish Hydraulic Laborat-ories	WL| Delft Hydraulics	RMA & USACE	USACE
2	**Water Body**									
	Rivers	X	X	X	X		X	X	X	
	Reservoirs & Lakes		X	X		X	X	X	X	X
	Estuaries & Coastal Areas		X	X				X	X	X
3	**Attributes**									
	Dynamic		X	X	X		X	X	X	X
	Stochastic	X				X				
	Stormwater Flow				X		X			
4	**Spatial Characteri-stics**									
	1D	X			X		X	X	X	
	2-D		X	X			X	X	X	X
	3D			X			X	X	X	

Table 2.1 Characteristics of Some of the Water Quality Models *Cont....*

		QUAL2E	MODE-LEUR	TELEMAC/ WQ2-D & WQ3D	WASP	HEC5Q	MIKE MODELS	DELFT MODELS	RMA SUITE OF MODELS	CE-QUL-W2
5	**Water Quality**									
	Dissolved Oxygen	X	X	X		X	X	X	X	X
	Nitrogen & Phosphorus Cycles	X		X	X	X	X	X	X	X
	Algae Growth & Decay	X			X	X	X	X	X	
	Indicator Bacteria	X	X	X	X	X	X	X	X	X
	Suspended Solids		X	X			X	X	X	X
	Heavy metals		X		X		X			
	Dissolved Substances	X				X	X	X		X
	Acidity									
	Temperature	X	X	X	X	X	X	X	X	X
	Oils, grease, PAHs						X			

Note: *X: Available/Simulated*

***Cont*.....Table 2.1 Characteristics of Some of the Water Quality Models**

2.7 Eutrophication and Phytoplankton Abundance

The planktonic community of aquatic ecosystems includes both plant and animals [Reynolds, 1984]. Phytoplankton are microscopic floating plants, mainly algae, that live suspended in bodies of water and drift with the currents as they cannot move about themselves or because they are too

small or weak to effectively swim against a current. In food chains, phytoplankton are grazed mainly by zooplankton.

Eutrophication is the excessive growth of aquatic plants due to over-fertilization of the aquatic system. The over-fertilization occurs due to abundance of nutrients in the waters [Thomann et al., 1987]. Increased nutrient loading increases the capacity of a water body to support a greater production of phytoplankton [Reynolds, 1984].

When algae grow so thick that they make water visibly green, the condition is termed as an algal 'bloom'. Algal blooms have many deleterious effects in freshwaters, including reduced aesthetic appeal and recreational use, and taste and odour problems in drinking water. Algal blooms can also have adverse ecological effects, including shading of aquatic plants, and depletion of oxygen as algae decay, which reduces habitat available to fish.

Three hundred and fourteen species of phytoplankton have been found in Rideau River [The Rideau River Round Table, 2001]. The most diverse group of algae was the green algae (chlorophytes) with 172 species. However, the most common algae in the Rideau were cryptophytes, bi-flagellated algae that are typically found in clean waters. In lower section of the Rideau, diatom species can be found that are more typical of nutrient-enriched systems such as in highly eutrophic European rivers [Yang et al. 1997].

2.7.1 Nutrients

Inorganic nutrients are the basic elements for life in aquatic system. Some are required in large quantities for cell development and hence are referred to as macronutrients. Macronutrients such as carbon, oxygen, nitrogen, phosphorus, sulfur, silica, and iron are required in large quantities for growth. Smaller quantities of micronutrients such as magnesium, copper, and zinc are also necessary [Chapra, 1997]. Phytoplankton growth primarily depends on the availability of nitrogen and phosphorus in aquatic systems as they are critical in transfer and storage of cell energy.

2.7.1.1 Phosphorus

From a water quality modelling point of view, phosphorus is a critical nutrient as it is usually in short supply compared to other macronutrients [Chapra, 1997]. Phosphorus does not exist in a gaseous form in the atmosphere, it is not abundant in the earth's crust and the phosphate minerals that do exist are not very soluble. In addition, phosphate tends to sorb strongly to fine grained particles [Chapra, 1997]. Phosphorus is removed from the water through sedimentation of fine grained particles. For cases where the water is in contact with sediments containing oxygen, sediment phosphorus becomes chemically trapped [Chapra, 1997].

Human and animal wastes contain substantial amounts of phosphorus and can be a source of pollution in natural waters. Non-point sources from agricultural and urban runoff also contain excess phosphorus. Soil erosion also leads to phosphorus transport into water [Chapra, 1997].

Phosphorus in natural waters may be subdivided into the following fractions [Chapra, 1997]:

- Soluble reactive phosphorus (SRP). This is the form readily available to plants. It consists mainly of the species $H_2PO_4^-$, HPO_4^{2-}, and PO_4^{3-}.
- Particulate organic phosphorus. This consists of living plants, animals and bacteria as well as organic detritus.
- Non-particulate organic phosphorus. These are dissolved or colloidal organic compounds containing phosphorus. Their primary origin is the decomposition of particulate organic phosphorus.
- Particulate inorganic phosphorus. This category consists of phosphate minerals such as apatite, sorbed orthophosphate and phosphates complexed with solid matter.
- Non-particulate inorganic phosphorus. This includes condensed phosphates such as those found in detergents.

Some researchers have worked on the discrepancy between SRP and PO_4-P [Stephen, 1981]. It has been shown through radiotracer techniques that the molybdenum blue method can overestimate orthophosphorus concentration in lakes and that is why analytical orthophosphorus (PO_4-P) determinations in filtered lake water samples are termed as SRP [Stephen, 1981].

2.7.1.2 Nitrogen

Nitrogen is an essential nutrient for plant growth and can act as a fertilizer that stimulates plant growth. The primary forms of nitrogen are [Chapra, 1997]

- Free nitrogen (N_2)
- Ammonium (NH_4^+)/ammonia (NH_3)
- Nitrite (NO_2^-)/nitrate (NO_3^-)
- Organic nitrogen.

The major processes governing the dynamics of these groups are [Chapra, 1997]

- Ammonia and nitrate assimilation, which includes the uptake of inorganic nitrogen by phytoplankton and bacteria.
- Ammonification, that is the transformation of organic nitrogen to ammonia. This is a complicated process involving several mechanisms such as bacterial decomposition, zooplankton excretion and direct destruction or autolysis after cell death.
- Nitrification, which is the oxidation of ammonia to nitrite at a temperature and oxygen dependent rate [Chapra, 1997], and nitrite to nitrate through the action of aerobic bacteria. This process utilizes oxygen and is generally modelled as a first-order reaction.
- Denitrification, whereby under anaerobic conditions nitrate can serve as an electron acceptor for certain bacteria. Nitrite is formed as an intermediate with the end product being free nitrogen.
- Nitrogen fixation. Free N_2 is unavailable for use by most organisms because of the triple bond between the two nitrogen atoms and thus making the molecule almost inert. Only a few algae have the ability to fix elemental nitrogen. Blue-green algae possessing heterocysts can fix free nitrogen giving them a competitive advantage in waters with high phosphorus loadings where other non-fixing algae would be potentially nitrogen limited [Chapra, 1997].

As is the case for phosphorus, human and animal waste both contain substantial amounts of nitrogen. In addition, non-point sources from agricultural land also contribute excess nitrogen. Species of nitrogen such as nitrate do not sorb to particulate matter so they are easily transported to surface water along with ground water flow [Chapra, 1997].

Apart from phosphorus and nitrogen other nutrients such as carbon and silicon are also required for algal growth. The reason for not discussing those nutrients is discussed in following section.

2.7.1.3 Limiting Nutrients

In order to understand the importance of each nutrient for plant growth, the concept of limiting nutrient is generally used [Chapra, 1997]. Generally the ratio of nitrogen to phosphorus in algal biomass is 7.2 (by atomic weight), which is also referred to as the Redfield ratio [Kalff, 2002]. Hence an N:P ratio in water that is less than 7.2 suggests that water is nitrogen limited and ratios greater than 7.2 indicate that water is phosphorus limited [Chapra, 1997]. Table 2.2 gives an idea of N:P ratio for various sources of waters.

Sr. No.	Source type	TN/TP	IN/IP	Limiting Nutrient
1	Raw sewage	4	3.6	Nitrogen
2	Activated sludge	3.4	4.4	Nitrogen
3	Activated sludge plus nitrification	3.7	4.4	Nitrogen
4	Activated sludge plus phosphorus removal	27.0	22.0	Phosphorus
5	Activated sludge plus nitrogen removal	0.4	0.4	Nitrogen
6	Activated sludge plus nitrogen and phosphorus removal	3.0	2.0	Nitrogen
7	Non-point sources	28	25	Phosphorus
8	Marine waters	-	2	Nitrogen

IN: Inorganic nitrogen; IP: Inorganic phosphorus; TN: Total nitrogen; TP: Total phosphorus

Table 2.2 N:P Ratios for Point, Non-Point, and Marine Waters [Chapra, 1997]

Phosphorus is generally considered the primary controllable nutrient governing the eutrophication process in fresh waters, however, productive estuaries have a tendency to be nitrogen-limited as they are deficient in nitrogen [Chapra, 1997]. Systems subject to phosphorus removal and non-point source input are generally phosphorus limited [Chapra, 1997].

2.7.1.4 Modelling Phytoplankton-Nutrient Interactions

The growth of phytoplankton including photosynthesis and respiration processes depends on a number of factors but the major factors which influence growth are as follows:

- availability of nutrients;
- diurnal light variation and light attenuation;
- temperature
- algal self-shading;
- benthic reactions;
- settling rate of algae

Figure 2.6 shows the nutrient and plant interaction as modelled in QUAL2E model [Chapra, 1997].

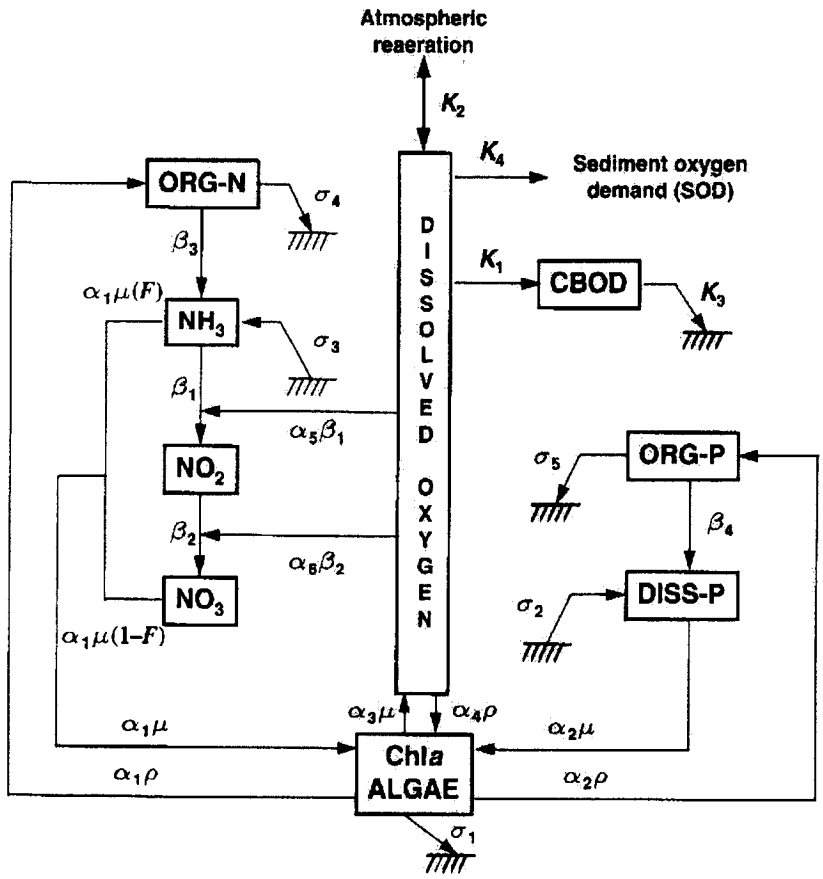

Figure 2.6 QUAL2E Kinetics Showing Nutrient/Plant Interactions. [Chapra, 1997]

2.8 Residence Time and Phytoplankton Growth

Hydraulic residence time or hydraulic retention time is the average time that a particle of water resides within a lake or impoundment [Martin, 1999]. The substance residence time is the time that a particle or substance would stay or reside in a system (Chapra, 1997). If the residence time is greater, the net increase in biomass is also proportionately greater [Reynolds, 1984]. A study carried out on 31 rivers in Ontario [Basu and Pick, 1996] found no relationship between Chl *a* and residence time. The residence time in the latter study was computed using an empirical relationship given by Leopold et al, (1964).

$$R = 0.08A_d^{0.6} / Q^{0.1} \qquad (2.27)$$

Where R is the water residence time at the sampling site (days), A_d is the watershed area upstream of the sampling site (km^2) and Q is the river discharge ($m^3 s^{-1}$). It was also concluded that the lack of relationship could be a result of algal biomass not being equivalent to algal abundance [Basu and Pick, 1996]. More recently, Walks et al., (2001) concluded, "it does not make sense to use Leopold's hydrological relationships that are based on mean flow to understand river plankton dynamics".

Rivers do not have storage like lakes but they do store water in hydraulic dead zones such as area between groynes, oxbow lakes, embayments along the shore, and areas behind islands or river bends. These areas may be totally disconnected from the main channel or may be mixing through secondary flow. Current velocity in these areas can be almost negligible to a small percentage of the main channel velocity.

One of the primary interests in water quality modelling is not only to estimate the average residence time at a location but also to compute the age of a particle at different locations in a river such as dead zones. Research on the transport equation of air age was done and the diffusion of tracer gas is given as follows [Li Xianting et al., 1999]

$$\frac{\partial C}{\partial t}+\frac{\partial}{\partial x_j}\left(u_j C\right)=\frac{\partial}{\partial x_j}\left(D\frac{\partial C}{\partial x_j}\right)+S \qquad (2.28)$$

where C is the concentration of tracer gas, u is velocity, D is the diffusive coefficient, S is the source term, subscript j can be 1, 2 or 3, which indicates the three space coordinates x, y or z.

After depth integration and substitution, the transport equation of water age in steady state is given as follows [after Li Xianting et al., 1999]

$$U_x H\frac{\partial A_w}{\partial x}+U_y H\frac{\partial A_w}{\partial y}-\frac{\partial}{\partial x}\left(H\left(D_{xx}\frac{\partial A_w}{\partial x}+D_{xy}\frac{\partial A_w}{\partial y}\right)\right)-\frac{\partial}{\partial y}\left(H\left(D_{xy}\frac{\partial A_w}{\partial x}+D_{yy}\frac{\partial A_w}{\partial y}\right)\right)=H(1) \qquad (2.29)$$

Where A_w is the water age and D is the diffusion coefficient. The source term 1 represent the aging process of 1 s s^{-1}. This analogy can be applied to the transport equation for water flow and water particle age at any arbitrary location in the river could be computed.

2.9 Previous Studies on the Rideau River

Some of the previous studies carried out on the Rideau River are outlined below.

Storm Water Management Study (1990-91)

A Rideau River stormwater management study was carried out in 1990-91 [RMOC, 1992]. QUAL2E was used to model the Manotick-Mooney's Bay reach of the Rideau River. The effect of various stormwater discharges on fecal coliform loadings in the Rideau River was studied.

Development of a Numerical Model of Mooney's Bay (1997)

A numerical model of Mooney's Bay was developed to study the 3D circulation in the Bay [Baird & Associates, 1997]. In this study MIKE3D was used to model the circulation process in Mooney's Bay.

Phytoplankton and Zooplankton Development in a Lowland, Temperate River (1997)

A study on the Rideau River was carried out by F.R. Pick and B. K. Basu, University of Ottawa in 1994-95. It was concluded that due to shallow depths (3-5m) in the river, often the entire column was within the euphotic zone and hence light limitation of phytoplankton growth in Rideau River was unlikely. They did not observe a negative relationship between Chl *a* and river discharge but the sampling period was May until October when the flows were relatively low in the Rideau River.

Numerical Modelling of the Rideau River (1998)

Two-dimensional numerical modeling of the Rideau River (Manotick-Mooney's Bay) was carried out [Baird & Associates, 1998] to study the hydrodynamics and bacterial pollution in the river. TELEMAC-2-D was used to model hydraulic and bacterial (Escherichia Coli) processes.

Numerical Modelling of Bacterial Dispersion in Mooney's Bay (2001)

This study [Baird & Associates, 2001] was based on the circulation model of Mooney's Bay carried out in 1997. For the period of 2000-2001 the same model was extended for bacterial contamination and various pathways for bacterial plumes and circulation patterns in the Mooney's Bay were studied.

CHAPTER 3

3 METHODOLOGY AND MODELLING ASPECTS

3.1 Introduction

The main objective of the present study was to model the phytoplankton dynamics in a reach of the Rideau River (Black Rapids-Hog's Back Reach). In the first part of the study a 2-D depth-averaged hydrodynamic model of the selected reach was developed. Later on, a phytoplankton growth element was incorporated in the DISPERSIM module.

3.2 Selection of Modelling Reach and Simulation Period

The present study includes Black Rapid's to Hog's Back Reach which is about 6 km in length. In the year 1998, 2-D modelling was carried out [Baird & Associates, 1998] to simulate bacterial contamination in the Rideau River (Long Island-Hog's Back). Long Island-Hog's Back Reach is about 14 km in length and bathymetric surveys were carried out during previous modelling studies [Baird & Associates, 1998].

The Year 2000 was selected for the simulation of phytoplankton growth in the Rideau River. The year 2000 was a relatively wet year (Fig. 3.1) but an intensive water quality monitoring programme was initiated in this year for which data were available from Canadian Museum of Nature.

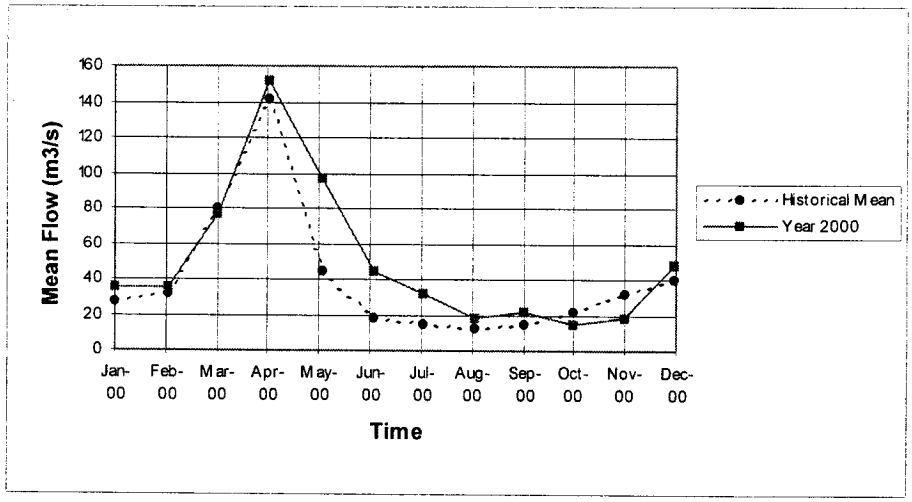

Figure 3.1 Year 2000 Versus Historical Mean: 1933 to 1990 [Preece, 2001]

3.3 Data Collection

Data collection is the basic and vital task for any modelling project. Generally two sets of data are required for modelling: one set of measured data for calibration and one set of measured data for validation.

Water quality monitoring in the Rideau River has been evaluated by several organizations. These include the Ontario Ministry of the Environment (MOE), the City of Ottawa, the Canadian Museum of Nature (CMN), Rideau Valley Conservation Authority (RVCA). Several research projects conducted by researchers at the University of Ottawa have focused on water quality in the Rideau River over the last decade [The Rideau River Round Table, 2001].

The data collection has been classified into the following main categories:

3.3.1 Bathymetric Data

Bathymetric data of Black Rapids to Hog's Back of Rideau River, about 6.5 km reach, was collected from Baird and Associates. The Z-values were fixed to Geodetic Survey of Canada (GSC) Datum and horizontal datum was reported to be NAD 27. The projection used for conversion from geographical coordinate system to rectangular coordinate system is based on Zone 9, MTM 3 degrees zones.

3.3.2 Hydrological and Hydraulic Data

Parks Canada and Environment Canada are responsible for most of the flow and water level measurements in the Rideau River.

Data collected from Parks Canada and Environment Canada are shown in Table 3.1.

Sr. No.	Location	Source	Period	Flow Measurements	Water Levels	Data Type
1	Long Island	P.C	June-Aug. 2000	Available	Available d/s of	Daily maximum
2	Jock River	P.C	June-Aug. 2000	Available		Daily maximum
3	Black Rapids	P.C	June-Aug. 2000	Not available	Available u/s of	Daily maximum
4	Carleton	P.C	June-Aug. 2000	Available		Daily maximum
5	Carleton	E.C	June-Aug. 2000	Available	Available	Daily average
6	Hog's Back	P.C	June-Aug. 2000	Not available	Available u/s of	Daily maximum

P.C : Parks Canada; E.C : Environment Canada

Table 3.1 Source and Type of Flow and Water Level Data

The downstream water level at Black Rapids is not measured; the difference in the water level between the upper and lower pools at Black rapids is reported to be approximately 2.9 m [Baird & Associates, 1998].

Figure 3.2 shows the water level as a function of time from June 2000 to August 2000, upstream of Hog's Back. Precipitation data for the study period are given in Table 3.2.

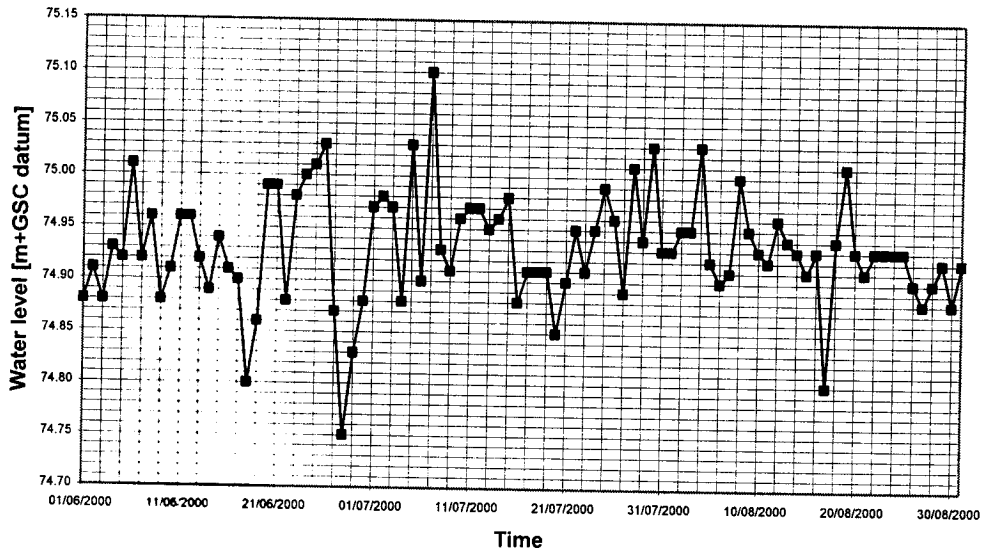

Figure 3.2 Water Level vs Time (Year 2000) at U/S of Hog's Back [Source: Parks Canada]

Year 2000 Month	Rainfall [mm]			
	May	June	July	August
1	0.4	-	2.6	5.4
2	-	1.6	16.8	3
3	-	0.2	Trace	2.2
4	4	2.2	-	-
5	1.6	0.4	-	-
6	Trace	2.6	-	0.2
7	4.4	-	Trace	14
8	26.8	2.0	1	-
9	18.4	7.4	9.2	19.8
10	14.8	15.2	0.2	Trace
11	0.2	10.8	-	9.8
12	0.6	-	-	2.4
13	1.6	0.4	-	-
14	1.4	2.6	1.6	-
15	Trace	3.6	9.3	2
16	-	0.4	5.2	1.2
17	-	-	Trace	-
18	22.8	3.2	-	-
19	-	2.4	-	-
20	-	-	-	-
21	-	16.4	11.2	-
22	1	6.2	7.6	Trace
23	7	-	-	16
24	8.2	0.2	-	-
25	9.4	46.4	-	-
26	0.2	0.2	-	Trace
27	-	4.4	Trace	Trace
28	-	-	-	-
29	-	1.8	3.6	Trace
30	-	0.4	-	-
31	Trace		1.8	-

Lat: 45° 19'N; Long: 75° 40'W (WMO ID: 71628)

Table 3.2 Rainfall Data at Ottawa-Cartier Macdonald Int'l Airport

[Environment Canada, 2001]

3.3.2.1 Water Balances

Water balances for the Rideau River between the Jock River entrance and Hog's Back for the period June 2000 to August 2000 were carried out. A number of small tributaries and stormwater outfalls join the Rideau River between the Jock River and Carleton Station. However, flow data for these tributaries and stormwater outfalls were not available and were not included in the water balance computations.

Water balance computations show average increase of flows at Carleton Station on the order of 7, 13 and 25 % for June, July and August 2000, respectively (refer to Table 3.3).

Period	Volume d/s Jock River Entrance [m^3]	Volume at Hog's Back (Carleton Station) [m^3]	Percent Difference [%]
June 2000	107,069,472	114,454,080	7
July 2000	68,948,064	78,174,720	13
August 2000	39,546,058	49,429,440	25

Table 3.3 Water Balances between Jock River Entrance and Hog's Back

3.3.3 Point Load Sources

A number of point sources of stormwater effluent discharge directly into the Rideau River (Black Rapids-Hog's Back Reach). The area surrounding the Rideau River in this reach is mainly urban. These facilities discharge directly into the Rideau River without treatment, although implementation of future facilities is being considered [Baird & Associates, 2000]. Some of the major point load sources are tabulated in Table 3.4 and plotted in Fig. 3.4.

Sr. No.	Description	Type of Treatment/Facility	Catchment Area [ha]	Distance from Hog's Back (km)
1	Nesbitt Outfall	None	110	0.35
2	Walkley Outfall	None	80	1.41
3	Southmore Outfall	None	35	1.45
4	Prince of Wales Drive	None	45	2.68
5	Nepean Creek	Tributary		3.11
6	Colonnade Catchment (Merivale Trunk Storm Sewer-MTSS)	Pipe storage	530	3.57
7	Uplands creek	Tributary		3.80
8	Riverwalk Park	Wetland	26	4.48
9	Bentley	Wet pond	20	4.69
10	Rideau Heights Business Park	None	90	5.35
11	Hunt Club Bridge	Infiltration	44	5.38
12	Black Rapids Creek	Tributary		6.85

Table 3.4 Tributaries and Existing Point Source Discharges [Baird & Associates, 2000]

Tributaries and Point Source Discharges (Source: Baird & Associates, Jan. 2000)

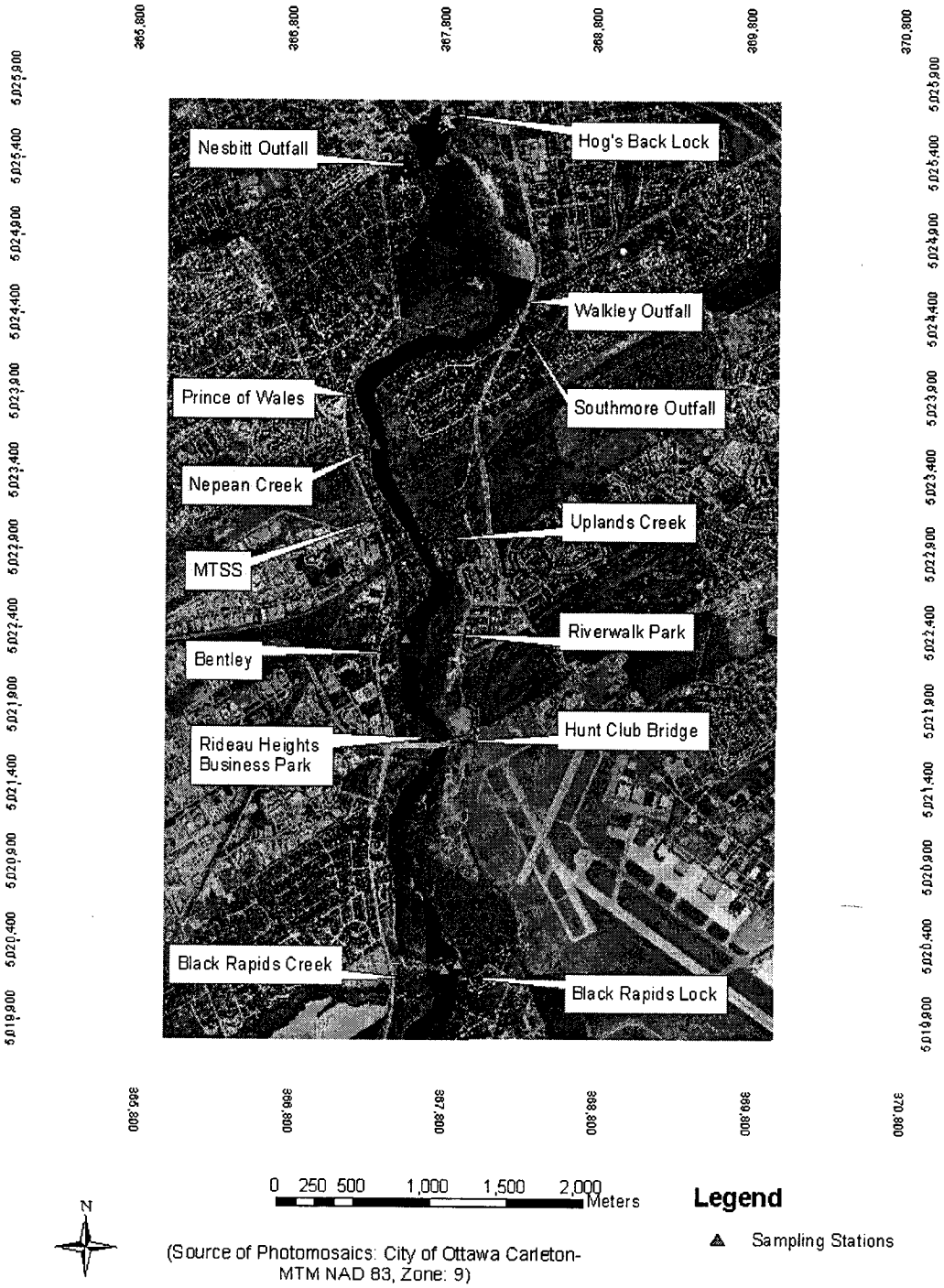

Figure 3.3 Tributaries and Point Sources

3.3.4 Water Quality Data

Water quality data for year 2000 were obtained from Canadian Museum of Nature (CMN). Data for the following parameters were acquired from CMN for water quality modelling of Rideau River

- Nutrients such as phosphorus (TP and SRP) and nitrogen.
- Measurements of Chl *a*.
- Dissolved oxygen (DO).
- Temperatures, conductivity, pH, Eh

The location of the sampling sites is shown in Fig. 3.5. The sampling was carried out from March 15, 2000 to October 25, 2000. Figure 3.6 shows water chemistry and chlorophyll-a samples and their collection dates. It can be observed from Fig. 3.6 that due to the limitation of availability of resources, there is not a single day where samples at all stations along Black Rapids-Mooney's Back reach were taken. TP data were available at each station and SRP data were available at all stations except for stations DH317 and DH318.

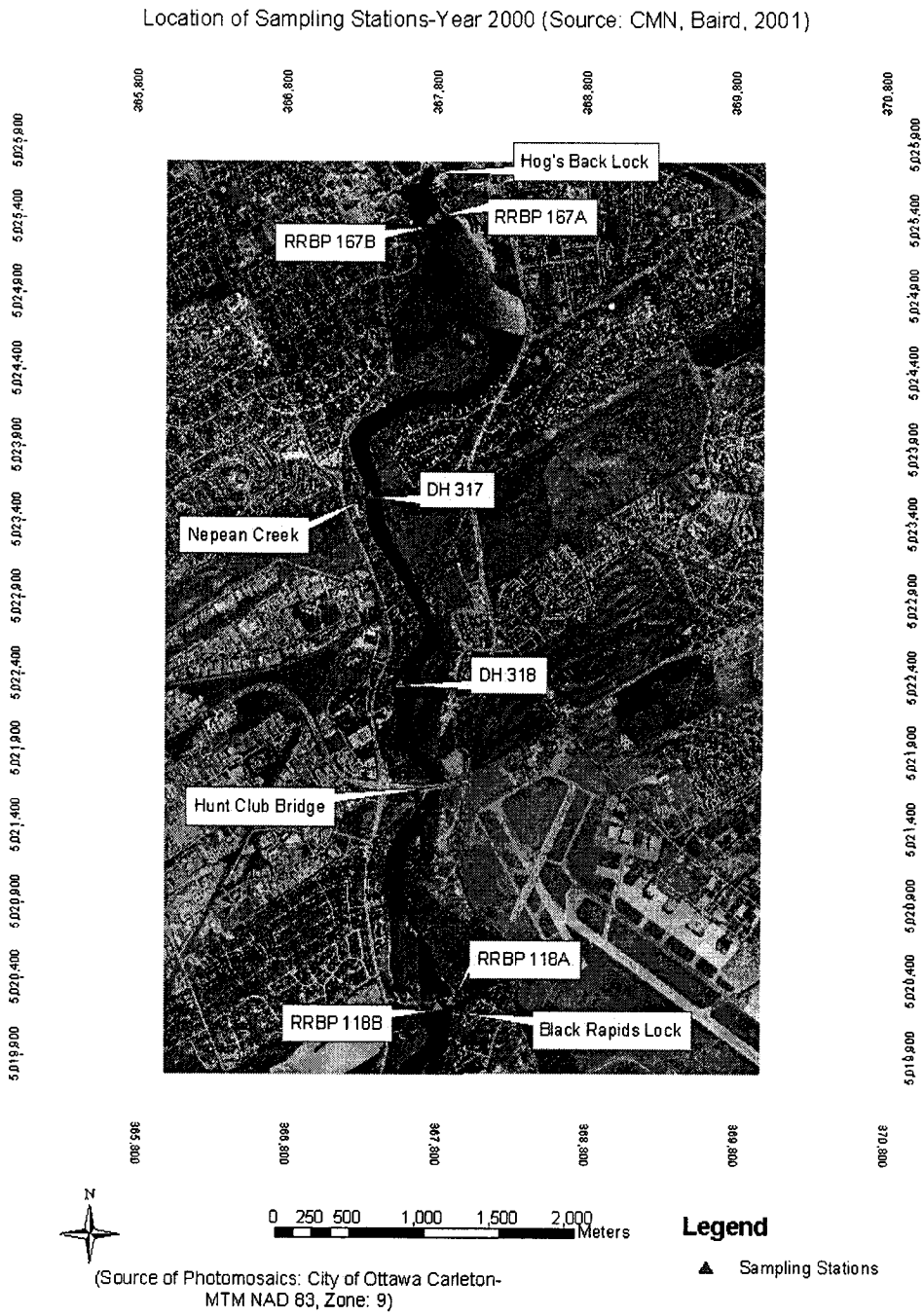

Figure 3.4 Location of Sampling Stations

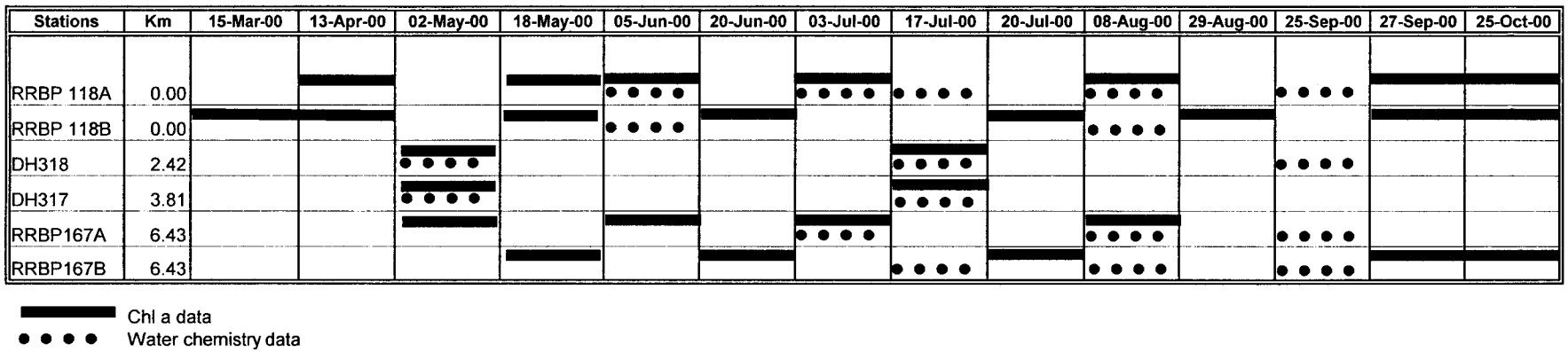

Figure 3.5 Data Availability Periods for Year 2000 for Water Chemistry and Chlorophyll a (Source: CMN)

Temperature and DO profiles were plotted at all sampling stations to locate any zones where anoxic conditions might develop over the sampling period. The plots for the stations RRBP167A and RRBP 167B in Mooney's Bay are shown in Figs. 3.6 to 3.7. When the oxygen content of water near the sediment interface decreases, the oxidized microzone barrier is weakened [Wetzel, 1983]. According to the experiments of Mortimer, the release of phosphorus increases markedly as the redox potential decreases [Wetzel, 1983]. A study in Esthwaite Water, England [Wetzel, 1983] found a sudden release of ferrous iron and phosphate into the water when the E_7 (E_h at pH 7) was equal to +200 mV at the interface surface.

Anoxic conditions at station 167B develop close to bottom of Mooney's Bay on August 08, 2000 as shown in Fig. 3.7 and it is worth mentioning here that this station is located in the deepest zones in Mooney's Bay. Internal loading of phosphates could be a source of food for phytoplankton under such conditions.

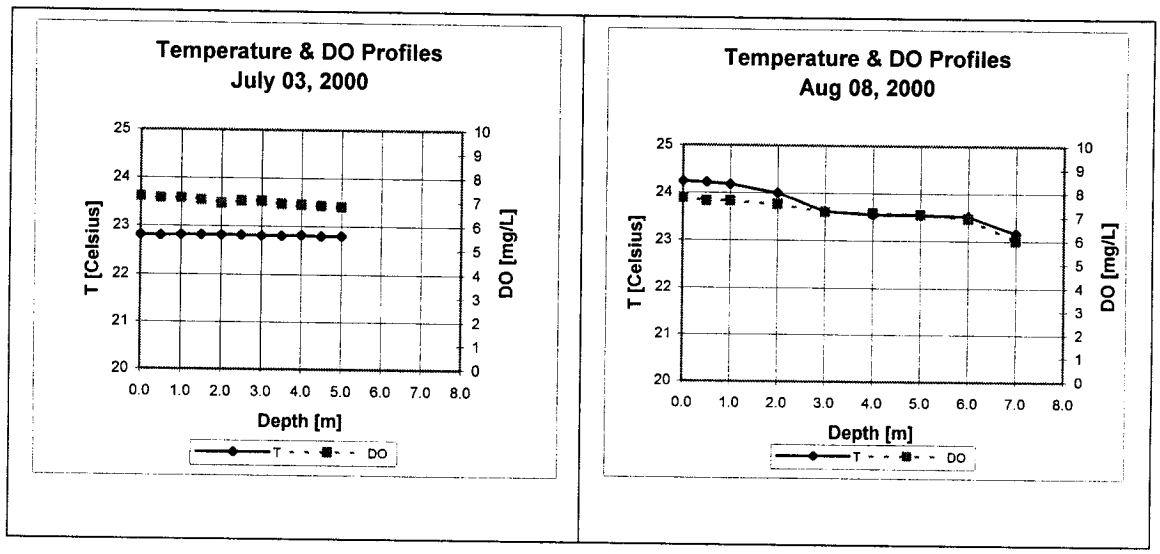

Figure 3.6 Temperature and DO Profiles at Station RRBP 167A

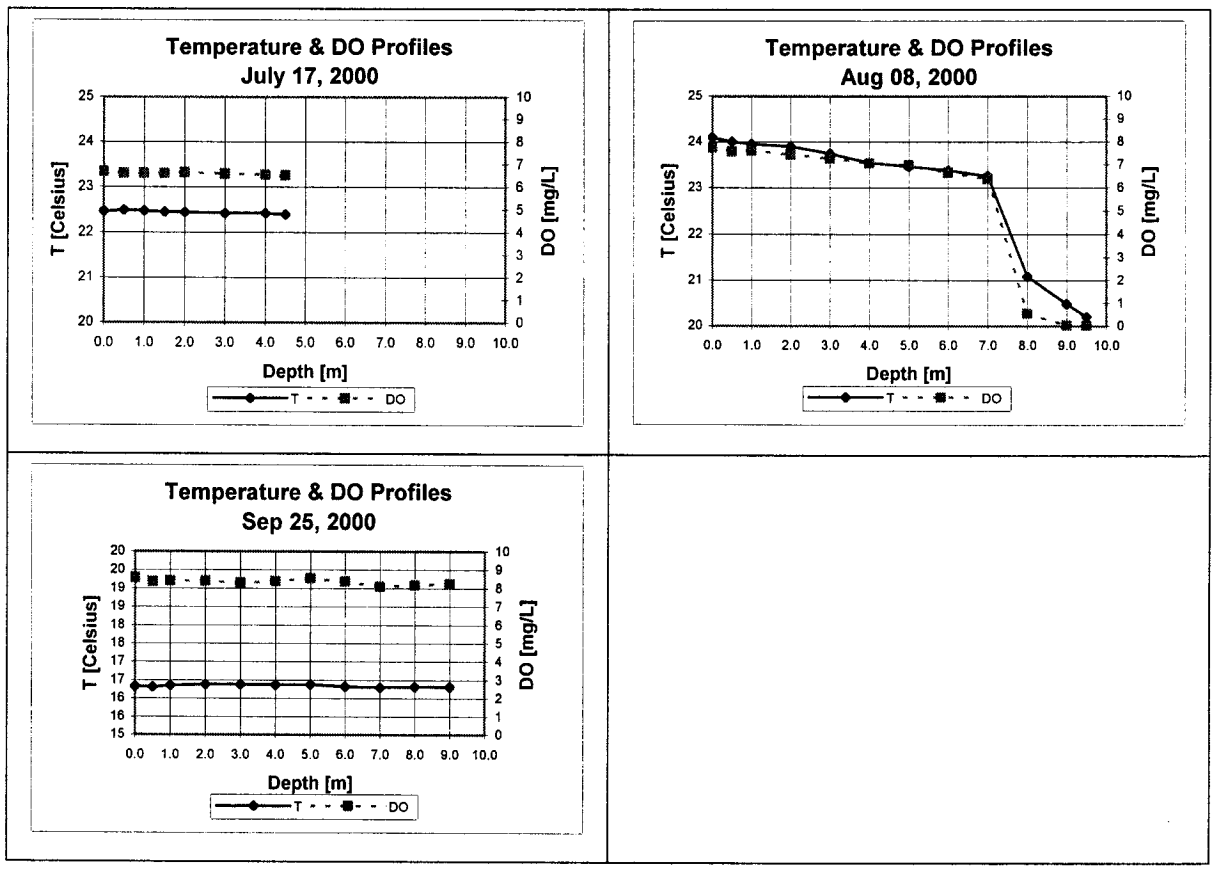

Figure 3.7 Temperature and DO Profiles at Station RRBP 167B

Figure 3.8 shows a plot of various water quality parameters versus depth at sampling station RRBP 167B. It can be observed that E_h, *DO* and *T* show a sudden drop in the measurements.

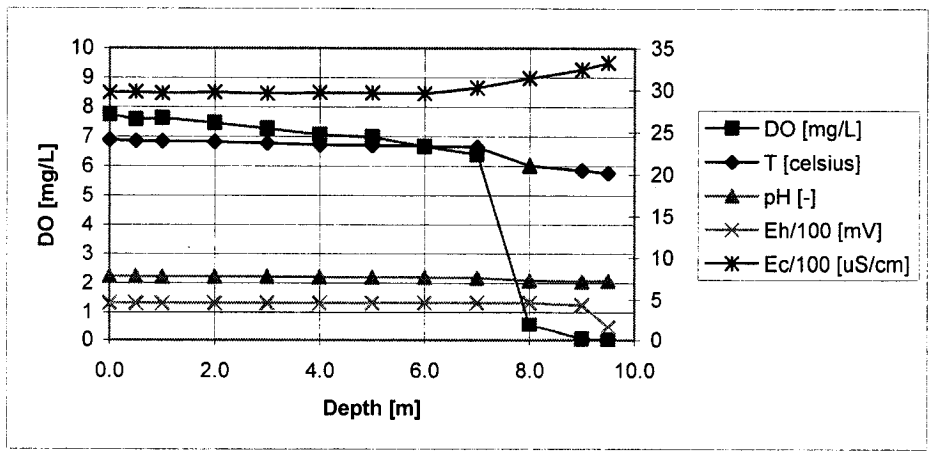

Figure 3.8 T, DO, pH, E_h & Ec Profiles at RRBP 167B, Aug. 08, 2000

Figure 3.9 shows a plot of Chl *a*, TP and SRP at various stations over the sampling period. There is no correlation can be observed from the plots shown in Fig. 3.9. It can be seen that in August the Chl *a* at stations RRBP 167B and RRBP 118A continue to increase whereas the TP and RP concentrations decline.

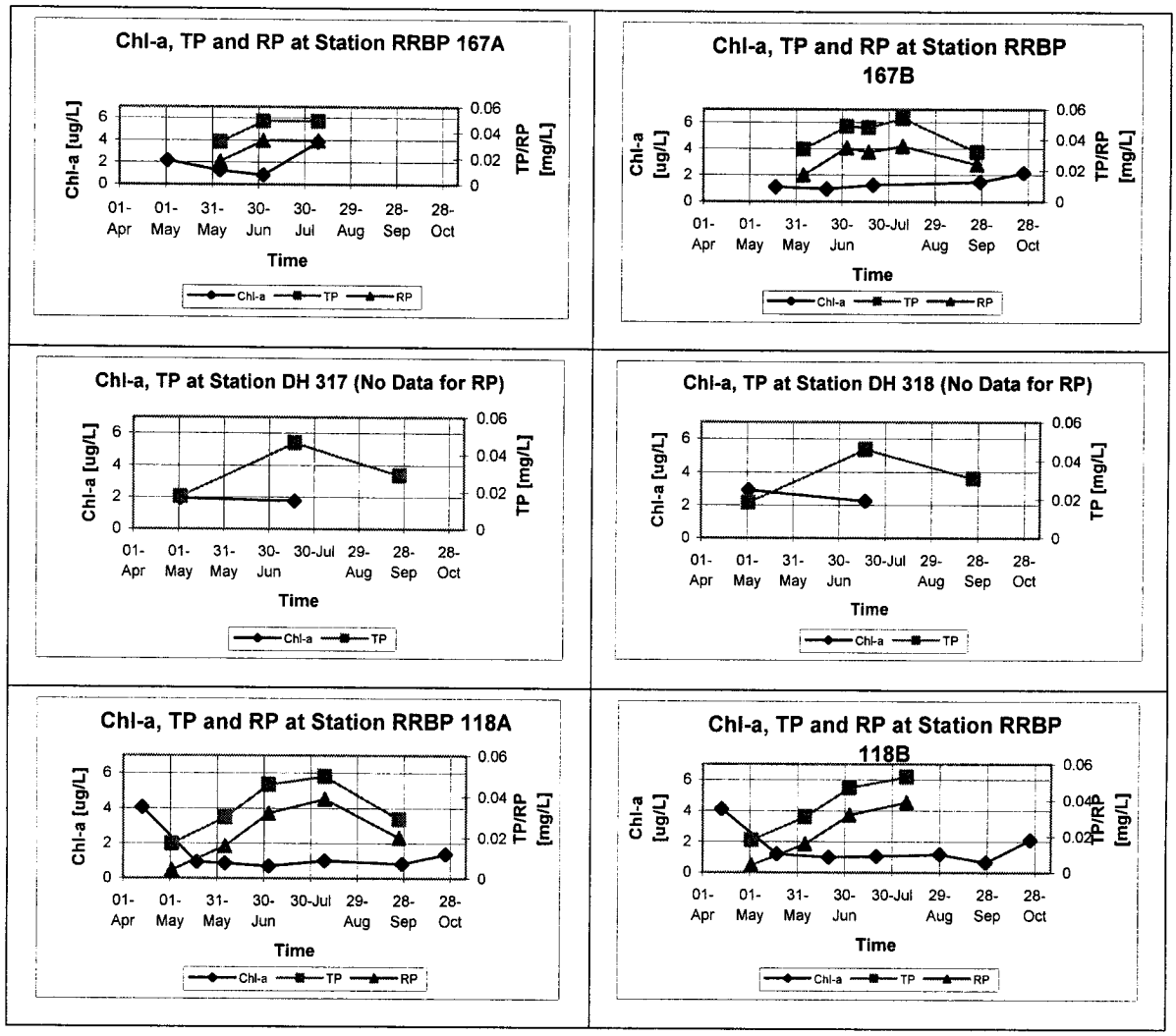

Figure 3.9 Time variation of Chl-a, TP and RP at Sampling Stations

Longitudinal profiles of measured Chl *a* are difficult to plot for the reason that, there was no single day when measurements were available at all stations. Averaging of Chl *a* over a month is not appropriate as the order of longitudinal variation is small. Figure 3.10 shows the longitudinal plot of measured data points of Chl *a* at various sampling stations.

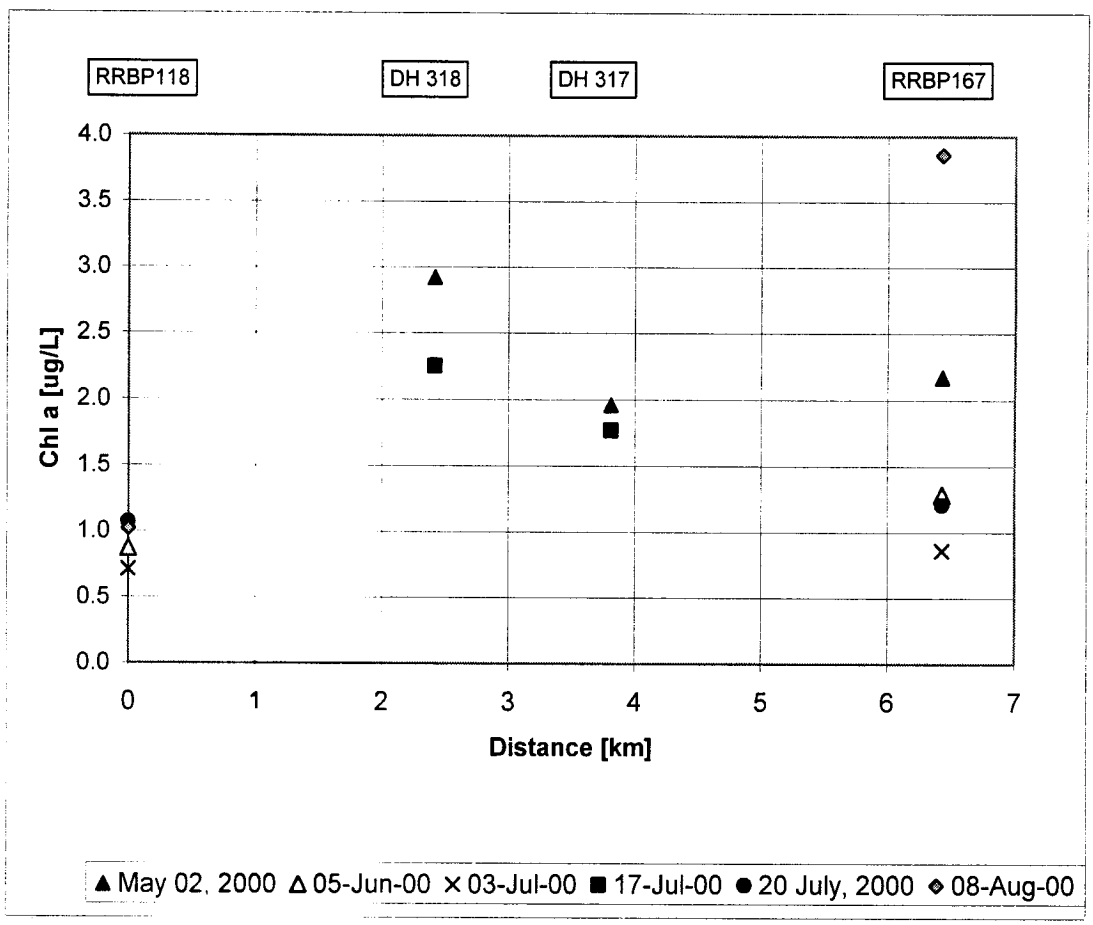

Figure 3.10 Longitudinal Profile of Measured Data Points of Chl *a*

It is interesting to note that Chl *a* concentrations are higher at station DH318 than station DH 317 for May 02 and July 17, 2000. Station DH 317 is downstream at about 1.4 km of station DH 318.

No Chl *a* data were available for upstream stations at RRBP 118A and RRBP 118B on the dates for which Chl *a* data were available for DH317 and DH318.

3.4 Selection of Hydrodynamic and Water Quality Model

The selection of a hydrodynamic water quality model is very important in the representation of actual processes, simulation and predictions. The selection of a model depends on the availability of resources such as computational time and money. In most cases, the actual process is simulated in the model by using a simplified schematization, which represents the actual model and gives good desired results as well.

Generally, the selection of a specific water quality model for a research project is based on four main factors:

1. *The selection between one, two or three-dimensional hydrodynamic models:* One of the factors in the selection of a model is the interest and nature of the problem. If the flowing water is well-mixed in the lateral and vertical directions then a one dimensional model may be appropriate and would save a lot of modelling and computational time and resources. The nature of existing measurements and data also plays a vital role in model selection.

2. *Selection of model also depends upon the state of flow i.e. steady or unsteady:* For steady state simulations, simple models can be used although hydrodynamic models have the capability of simulating both steady and unsteady states of flow.

3. *Simulation of specific water quality parameters, processes and model applications:* The model should have a powerful process library including all the variables, processes and forcing functions, which are relevant to the specific nature of the problem.

4. *Availability and authorization to modify the code:* Another factor, which may be important in a research project, is the availability of the code and the authorization to modify it.

One-dimensional analogy applies if the modelling interests are only in the mixing far from the source of pollution. With two-dimensional models, prediction of the mixing relatively close to a source, which may be concentrated at one bank, or distributed over only part of the cross section, could be done. Two-dimensional models can be useful in the study of hydraulic dead zones and dynamics of phytoplankton between main flow and dead zones.

Two-dimensional models require extensive and accurate information on geometry and boundary conditions and take more resources in terms of setting-up of the model and computational time for simulations. Generally, they are applied for specific area/reach problems.

Section 2.7 lists some of the commercially available models. In the present study, MODELEUR has been used which is comprised of two modules, HYDROSIM and DISPERSIM. Support on the use of the model was available through this study and the code for DISPERSIM was available for modifications and addition of phytoplankton growth element.

DISPERSIM is also not directly linked with MODELEUR and results have to be imported to view in MODELEUR. The algal growth element in DISPERSIM was not available and was developed during this study as a new component.

3.4.1 Solution Method in HYDROSIM

In HYDROSIM, the solution method of the algebraic equation system is done by the iterative non-linear GMRES method, according to a "Newton-Inexact" scheme, with preconditioning [Heniche et al., June 2000]. The GMRES solution algorithm works on three loops. The first loop is driven by the variable NPREC, the second by the variable NRDEM and the third by NITER, which cannot exceed the value of TNDF.

The first loop is dedicated to the calculation of the pre-conditioning matrix, the second to the solution update and the third to the calculation of the solution sub-space of the type Krylov by the GMRES method [Heniche et. al., 2000].

3.5 Phytoplankton Growth Modelling

Algae vary in size from one micrometer, as unicellular organisms to large seaweeds, which can grow to over 50 metres in length [Darley, 1982].

Phytoplankton are microscopic floating plants mainly algae that live suspended in bodies of water as they drift about with the currents as they can not move themselves or because they are too small or weak to effectively swim against a current.

Photosynthesis is the process in which plants use the energy of the sun to make sugars by combining carbon dioxide from air and water. The plant then stores these sugars as carbohydrates, which are used as energy for growth. The other process by which the energy is released is called respiration. Chlorophyll is the green pigment in plants used to capture the energy in light during photosynthesis. The process of photosynthesis can be described by following equation whereas respiration is the reverse of this equation.

$$6CO_2 + 6H_2O \longrightarrow C_6H_{12}O_6 + 6O_2 \qquad \text{[Thomann, 1987]} \qquad (3.1)$$

Important factors controlling growth and decay rate of algae and their modelling are discussed in the following sections.

3.5.1 Growth

The total biomass of phytoplankton can be correlated to the measured Chl *a*. The advantages of measuring Chl *a* are that the measurement is direct, it integrates different cell types and ages and it accounts for cell viability [WASP 6.0]. We can write

$$a = \alpha_0 A \qquad \text{[QUAL2E, 1987]} \qquad (3.2)$$

where a is the chlorophyll-a concentration [ug-Chl a L^{-1}], A is the algal biomass concentration [mg-A L^{-1}], α_0 is a conversion factor [ug-Chl a mgA^{-1}]

For a batch system (zero-dimensional and transient), a mass balance for phytoplankton growth can be written as [Chapra, 1997]

$$\frac{da}{dt} = k_g a \qquad (3.3)$$

where k_g is the first order growth rate [d^{-1}]. If the initial condition is $a_0 = 0$, then above equation can be solved by integrating as

$$a = a_0 e^{k_g t} \qquad (3.4)$$

The phytoplankton growth (k_g) is known to be on the order of 2 d^{-1} [Chapra, 1997]. The solution of above equation yields an exponential growth of phytoplankton whereas because of number of loss processes in nature, exponentially high rates of growth are rarely reached [Chapra, 1997].

Quantifying the growth rate of phytoplankton could be done through the classical approach in which it is assumed that the effect of factors affecting the growth is multiplicative [Thomann, 1987]

$$k_g = k_{g\max} \phi_T \phi_L \phi_N \qquad (3.5)$$

where k_{gmax} = maximum specific growth rate of phytoplankton, ϕ_T = algal growth limitation factor for temperature [-], ϕ_L = algal growth limitation factor for light [-] and ϕ_p = algal growth limitation factor for nutrient [-].

The factors affecting growth are discussed in more detail in the following sections.

3.5.1.1 Temperature

Although temperature, light and nutrients stimulate algal growth, experiments have shown that light and temperature show a suppression of growth at high levels [Chapra, 1997]. Various models are available to represent the effect of temperature on plant growth. One of the methods to calculate the effect of temperature on growth is a simple linear model with some minimum temperature below which growth does not occur,

$$k_{g,T} = 0 \qquad T \le T_{\min} \tag{3.6}$$

$$k_{g,T} = k_{g,ref} \frac{\mathrm{T} - \mathrm{T}_{\min}}{\mathrm{T}_{\mathrm{ref}} - T_{\min}} \qquad T > T_{\min} \tag{3.7}$$

where $k_{g,T}$= growth rate [d^{-1}] at temperature T [°C]

$k_{g,ref}$= growth rate [d^{-1}] at reference temperature T_{ref} [°C]

T_{min} = temperature below which growth stops.

Another model, which is more commonly used, is the theta model based on Van't Hoff-Arrehnius equation [Chapra, 1997],

$$k_{g,T} = k_{g,20}\theta^{\mathrm{T}-20} \tag{3.8}$$

A value of θ on the order of 1.066 is proposed to be used based on a large number of studies involving many species of phytoplankton [Chapra, 1997].

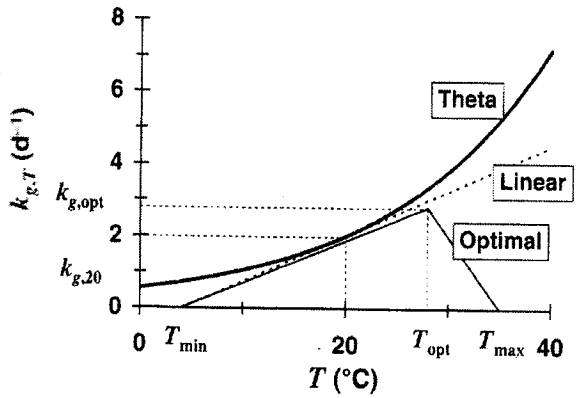

Figure 3.11 Some of the Models Used to Characterize the Effect of Temperature on Phytoplankton Growth [Chapra, 1997]

In some models the dependence is zero at a minimum temperature and it increases to a peak growth rate at an optimal temperature, and then decreases at higher temperature. A simple linear approach to this method is as follows [Chapra, 1997].

$$k_{g,T} = 0 \qquad T \le T_{\min} \tag{3.9}$$

$$k_{g,T} = k_{g,opt} \frac{T\text{-}T_{\min}}{T_{opt} - T_{\min}} \qquad T_{\min} \le T \le T_{opt} \tag{3.10}$$

$$k_{g,T} = k_{g,opt} \frac{T_{\max}\text{-}T}{T_{\max} - T_{opt}} \qquad T > T_{opt} \tag{3.11}$$

The theta model is typically used when phytoplankton are simulated as a single state variable [Chapra, 1997]. This implies that there will always be species that grow at any particular temperature. When several individual species or groups are modelled, the optimal temperature approach can be used [Chapra, 1997]. Experiments have shown that major algal groups have differing sensitivity to temperature (Fig. 3.12). Groups such as diatoms grow at lower temperatures and blue green algae grow faster at higher temperatures [Chapra, 1997].

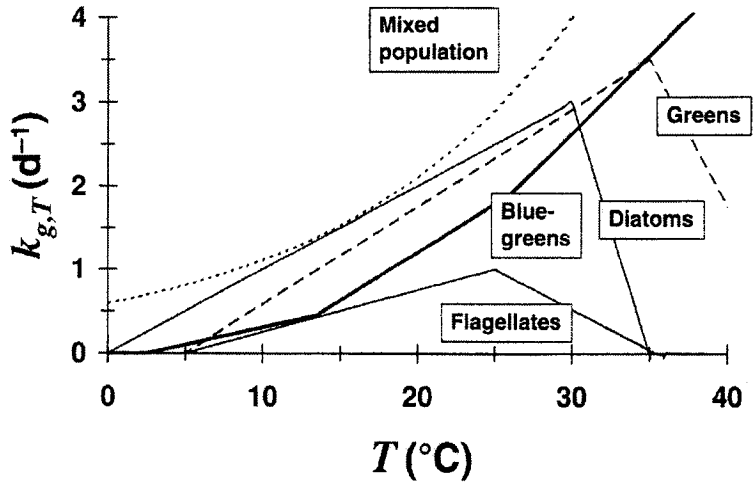

Figure 3.12 Temperature Dependence for Several Algal Groups [Chapra, 1997]

A comparison of temperature correction coefficients is given in Table 3.5. Equation 3.8 can be used for applying corrections to rate coefficients and other water quality variables as given below.

Rate Coefficient	QUAL2E, 1987	Chapra, 1997
Algal growth, k_g [d^{-1}]	1.047	1.066
Algal respiration, k_r [d^{-1}]	1.047	1.066
Algal settling, k_s [d^{-1}]	1.024	-
Rate constant for the mineralization/decay of organic phosphorus to dissolved phosphorus, β_4 [d^{-1}]	1.047	-
Benthos source rate of dissolved phosphorus, σ_2 [mg-P m^{-2} d^{-1}]	1.074	-
Organic phosphorus settling rate, σ_5 [d^{-1}]	1.024	-

Table 3.5 Temperature Corrections for Coefficients

3.5.1.2 Light

One of the important factors for phytoplankton growth is the light energy. Light is often a limiting factor for the phytoplankton growth, the light fluctuates tremendously in both space (depth and latitude) and time (daily and seasonally). The widely used term " light" refers to radiation visible to humans. The wavelength visible to humans is 380-770 nm and the photosynthetically available radiation (PAR) are in the range of approximately 380-710 nm [Kalff, 2002].

Assuming that rate of photosynthesis is directly proportional to the light energy [Chapra, 1997]

$$P(t) \infty I(t) \tag{3.12}$$

where $I(t)$ is available light [ly d^{-1}], where 1 langley [ly] is 1 cal cm^{-2}.

The variation of light over a diurnal cycle can be idealized by a half-sinusoid function (Fig. 3.13) and can be written as [Chapra, 1997]

$$\begin{aligned} P(t) &= P_m \sin[\omega(t - t_r)] \quad & t_r < t < t_s \\ P(t) &= 0 & \text{otherwise} \end{aligned} \tag{3.13}$$

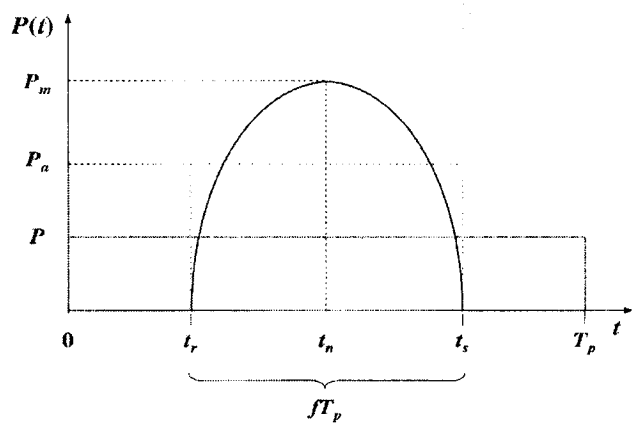

Figure 3.13 Schematization of Photosynthesis Over the Diurnal [Chapra, 1997]

where P_m = maximum rate [g m^{-3} d^{-1}]

ω = angular frequency [$= \pi/(fT_p)$]

t_r = time of sunrise [d]

t_s = time of sunset [d]

f = fraction of day subject to sunlight (the photoperiod)

T_p = daily period (1 d or 24 hr etc. depending on units of time)

The photoperiod is related to other parameters by

$$f = \frac{t_s - t_r}{T_p} \tag{3.14}$$

The average daylight rate can be determined by [Chapra, 1997]

$$P_a = \frac{\int_0^{T_p} P(t)dt}{fT_p} = P_m \frac{2}{\pi} \tag{3.15}$$

The effect of light on phytoplankton growth is complicated by the fact that three main factors have to be combined to come up with the total effect. These factors are the diurnal surface light variation, light attenuation with depth, and the dependence of growth rate on light (refer to Fig. 3.14). The dependence of growth rate on light has been quantified by experiment and the growth rate peaks at an optimal level for which various models have been developed [Chapra, 1997].

According to the Michaelis-Menten formulation [Chapra, 1997]

$$F(I) = \frac{I}{k_{si} + I} \tag{3.16}$$

which is a saturation-type reaction and k_{si} is a half saturation constant for light [ly d^{-1}]. This model does not capture growth attenuation at high intensity, but such an expression might be justified when the phytoplankton are simulated as a single group [Chapra, 1997].

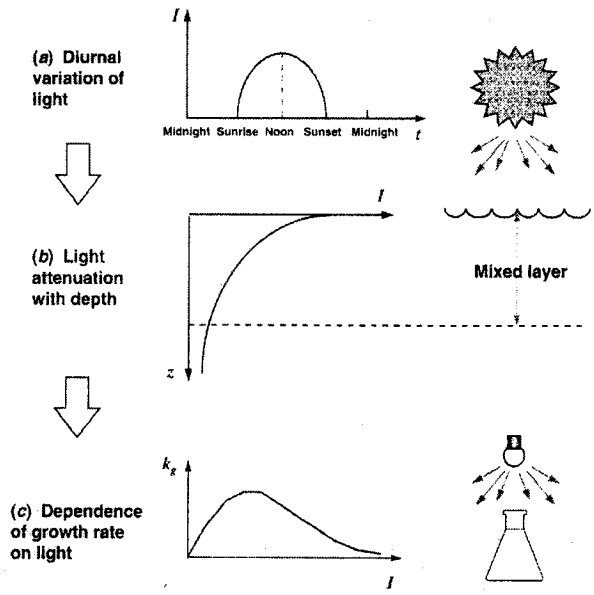

Figure 3.14 Incorporating Light into the Phytoplankton Growth Model [Chapra, 1997]

A different approach was taken by Steele [Chapra, 1997], who included the growth-inhibition at high light levels

$$F(I) = \frac{I}{I_s} e^{-\frac{I}{I_s}+1} \tag{3.17}$$

where I is the light level and I_s is the optimal light level at which growth rate is equal to maximum growth rate. I_s ranges from about 100 to 400 ly d^{-1} and lower values are used for species, which adapt to low light and higher values are for high light adapted species. [Chapra, 1997]. I_s values for mixed population of phytoplankton are about 100-400 ly d^{-1} with 300 ly d^{-1} as an approximate average [Thomann et. al., 1987]

The temporal variation in light can be characterized by a half sinusoid as derived in Eq. 3.15

$$I_a = I_m\left(\frac{2}{\pi}\right) \tag{3.18}$$

where I_m = maximum light intensity, thus the average daylight value is about 2/3 of the maximum [Chapra, 1997].

In reference to Fig. 3.15, if total daily solar radiation (I_t) as reported by meteorological stations is available, then the incoming solar radiation can be computed from the following simplified assumption [Thomann, 1987]

$$I_0 = I_a = \frac{I_t}{f} \qquad 0 < t < f$$

$$I_0 = 0 \qquad f < t < 1 \tag{3.19}$$

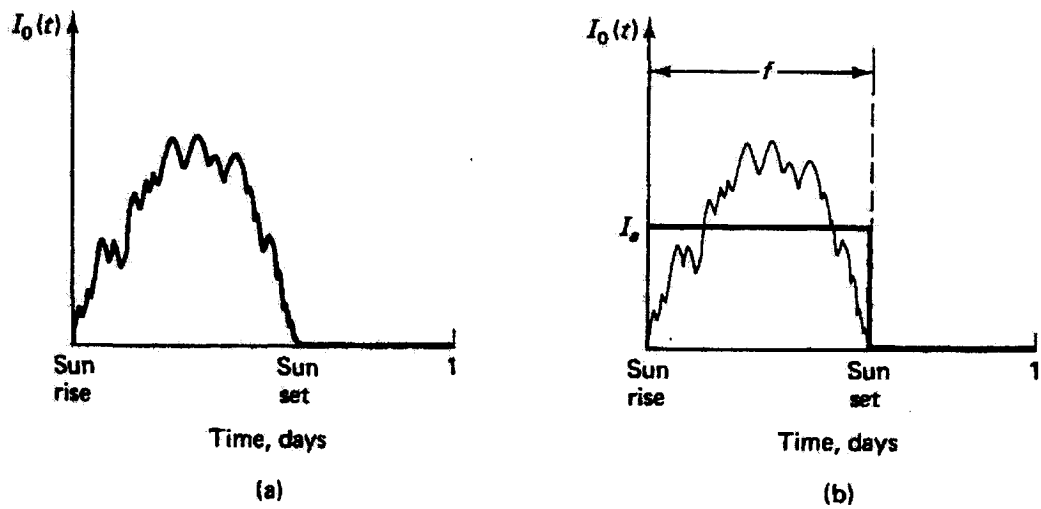

Figure 3.15 (a) Variation of Solar Radiation on a Clear Day. (b) Approximation for Averaging [Thomann, 1987]

The spatial variation of light through a column of water can be modelled by the Beer-Lambert Law [Chapra, 1997]

$$I(z) = I_0 e^{-k_e z} \tag{3.20}$$

where I_0 is solar radiation at surface and k_e = light extinction coefficient. k_e can be related to other factors by [Chapra, 1997]

$$k_e = k_e' + 0.0088a + 0.054a^{2/3} \tag{3.21}$$

where a = Chl a concentration [ug L^{-1}], k_e' = light extinction due to factors other than phytoplankton, which can be either measured directly or calculated through following equation [Chapra, 1997]

$$k_e' = k_{ew} + 0.052N + 0.174D \tag{3.22}$$

where k_{ew} is light extinction due to particle-free water and colour [m^{-1}]; N = nonvolatile suspended solids [mg L^{-1}]; D = detritus [nonliving organic suspended solids, mg L^{-1}]. For comparison, k_e for Lake Ontario is of the order of 0.5 m^{-1} [Thomann et. al., 1987].

All the above formulas can be applied to compute the mean light limitation for a well-mixed layer (Fig. 3.16). Using the Steele model, substitute Eq. 3.20 into Eq. 3.17 to give an equation for growth limitation at depth z,

$$F(I) = \frac{I_a e^{-k_e z}}{I_s} e^{-\frac{I_a e^{-k_e z}}{I_s}+1} \tag{3.23}$$

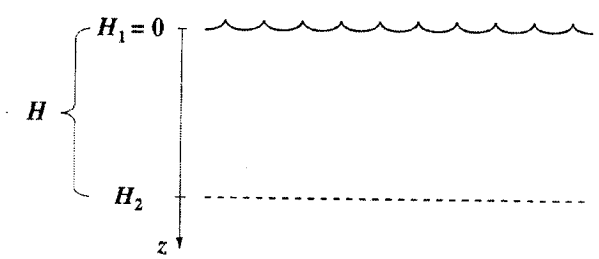

Figure 3.16 A Column of Water of Thickness H= H_2-H_1. For the Particular Case, the Surface Layer is Depicted, H_1 = 0 [Chapra, 1997]

Equation 3.23 can be integrated over depth and over one day to get the mean value as follows [Chapra, 1997]

$$\phi_L = \frac{1}{H}\int_{H_1}^{H_2}\frac{1}{T_p}\int_{0}^{fT_p}\frac{I_a e^{-k_e z}}{I_s} e^{-\frac{I_a e^{-k_e z}}{I_s}+1}\, dt dz \tag{3.24}$$

Evaluating this double integral results in [Chapra, 1997]

$$\phi_L = \frac{2.718 f}{k_e H}\left(e^{-\alpha_1} - e^{-\alpha_0}\right) \tag{3.25}$$

where

$$\alpha_0 = \frac{I_a}{I_s} e^{-k_e H_1} \tag{3.26}$$

and

$$\alpha_1 = \frac{I_a}{I_s} e^{-k_e H_2} \tag{3.27}$$

where I_a is the average incident light intensity during day light hours just below surface [ly d^{-1}]

For typical range of I_a of 500-1000 ly d^{-1}, the value of light attenuation factor ranges from 0.1 to 0.5 [Thomann et. al., 1987]. It should be remembered that the light value used in above equations is visible, photosynthetically available light radiation [PAR]. This value is about 40-50% of the energy in the complete standard spectrum used for such calculations as heat budgets or photolysis [Chapra, 1997]. It is also to be noted that all the radiation outside the visible range is absorbed in the first meter below the surface [Chapra, 1997].

3.5.1.3 Nutrients

The most common approach for modelling nutrients is the Michaelis-Menten equation [Chapra, 1997] and is described as follows

$$\phi_N = \frac{N}{k_{sN} + N} \tag{3.28}$$

where ϕ_N is the algal growth limitation factor for nutrients [-], N = concentration of limiting nutrient [mg-nutrient L^{-1}]and k_{sN} is half saturation constant [mg-nutrient L^{-1}]. This is a variable order equation and depending on the value of N, it varies from zero order to first order as shown in Fig. 3.17.

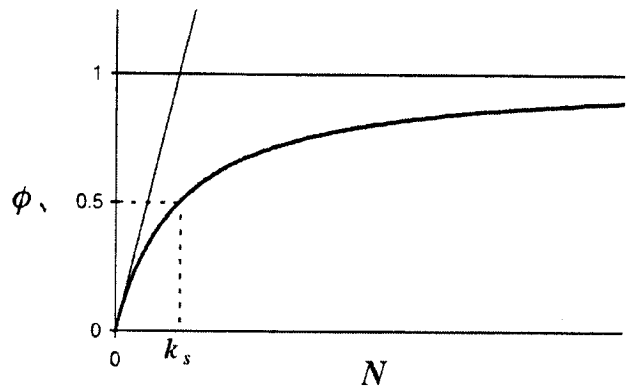

Figure 3.17 The Michaelis-Menten (or Monod) Model of Nutrient Limitation [Chapra, 1997]

As discussed in Section 2.8.1, phosphorus and nitrogen are essential nutrients for phytoplankton growth. Three approaches are discussed below to determine the combined effect of these nutrients [Chapra, 1997]:

1. **Multiplicative:** In this approach the two nutrients are multiplied as follows.

$$\phi_N = \phi_p \phi_n \tag{3.29}$$

where ϕ_p is the algal growth limitation factor for phosphorus [-] and ϕ_n is the algal growth limitation factor for nitrogen [-]

According to the above approach both nutrients in short supply will more severely limit growth than a single nutrient. The disadvantage of the multiplicative approach is that it gives a low value when both nutrients are considered [Chapra, 1997].

2. **Minimum:** According to this approach the nutrient in shortest supply controls the growth

$$\phi_N = \min(\phi_p, \phi_n) \tag{3.30}$$

This type of approach is most commonly used and accepted formulation and is based on Liebig's law of the minimum [Chapra, 1997]. This approach was used in the present study.

3. **Harmonic mean:** In this approach the reciprocals of the limitation terms are combined as follows

$$\phi_N = \frac{2}{\frac{1}{\phi_p} + \frac{1}{\phi_n}} \tag{3.31}$$

The above approach also takes into effect many nutrients but not as severe as in the multiplicative approach. This approach has been criticized in cases where one nutrient is limiting. For example if phosphorus is limiting (near zero) and nitrogen is in excess (near one), ϕ_N approaches $2\phi_p$ rather than ϕ_p [Chapra, 1997].

3.5.1.4 Limiting Nutrient in Black Rapids-Hog's Back Reach

Sampling of various water quality parameters in the study area was carried out from May 02, 2000 to Sep. 25, 2000 by the Canadian Museum of Nature. Analysis of nitrogen and phosphorus data show that TKN:TP ratios during this period were in the range of 11.9 to 35 in Black Rapids-Hog's Back Reach. In other study [Basu and Pick, 1996] various parameters including Chl *a*, zooplankton biomass, nutrient concentrations and water residence time were measured in 31 rivers in eastern Canada. In that study TN:TP ratio for the Rideau River was 23.59. This indicates that the river is phosphorus limited.

3.5.1.5 Modelling of Phosphorus Cycle

As discussed in the preceding section, phosphorus is the limiting nutrient in the Black Rapids-Hog's Back Reach of Rideau River. Phosphorus in the form of orthophosphates or dissolved inorganic phosphorus is consumed by phytoplankton [Chapra, 1997]. Phosphorus discharged from sewage treatment plants is generally in the dissolved inorganic form and is readily taken up by algae. [Bowie et al., 1985].

The following differential equations describe the phosphorus cycle and its transformations from one form to the other [Chapra, 1997], the equations have been modified to standard notations.

Organic Phosphorus (P_1)

$$\frac{dP_1}{dt} = \alpha_2 k_r A - \beta_4 P_1 - \sigma_5 P_1 \qquad (3.32)$$

(Accumulation = Respiration - Mineralization - Settling)

where P_1 is concentration of organic phosphorus [mg-P L^{-1}]; α_2 is fraction of phytoplankton biomass that is phosphorus [mg P mg-A^{-1}]; k_r is the algal respiration rate [day^{-1}]; A is the algal

biomass concentration [mg-A L^{-1}]; β_4 is the rate constant for the mineralization/decay of organic phosphorus to phosphate [d^{-1}]; σ_5 is the organic phosphorus settling rate [d^{-1}]

Bowie et. al. (1985) present rate constants for particulate organic phosphorus to phosphate directly while eliminating the in between transformation of dissolved organic phosphorus.

Inorganic Phosphorus or Orthophosphates (P_2)

The mineralization of organic phosphorus into dissolved inorganic phosphorus is a temperature dependent phenomenon.

$$\frac{dP_2}{dt} = \beta_4 P_1 + \frac{\sigma_2}{H} - \alpha_2 k_g A \qquad (3.33)$$

(Accumulation = Mineralization + Benthic loading - Growth)

where P_2 is concentration of inorganic or dissolved phosphorus [mg-P L^{-1}]; σ_2 is the benthos source rate of dissolved phosphorus [mg-P m^{-2} d^{-1}]; H is mean depth [m]; k_g is algal growth rate [d^{-1}]

The selection of a half saturation growth constant (as opposed to the uptake constant) for phosphorus was based on previous studies and the calibration. In a dynamic modelling study carried out on the Belgian part of River Meuse (Everbecq et.al, 2001), the value for four categories of phytoplamkton, namely, 1.*Stephanodiscus hantzschii* (centric diatom), 2. Small centric diatoms (up to 15 μm in diameter), 3. Non-siliceous algae (primarily Chlorophytes) and 4. *Aulacoseira* (a colonial filamentous centric diatom genus) was taken as 0.01 mg-P L^{-1}.

Table 3.6 shows the monthly variation of TP and RP at all sampling stations. The variation of TP and RP over time is very small. The data points are plotted in Fig. 3.18. In order to model the phosphorus cycle, measurements on particulate organic phosphorus are required. RP measurements at intermediate stations, DH 318 and DH 317 were also not available. Unless data

Date	Station	RP [mg/L]	TP [mg/L]
05-Jun-00	RRBP 118A	0.016	0.030
05-Jun-00	RRBP 118B	0.016	0.031
05-Jun-00	RRBP 167A	0.018	0.033
05-Jun-00	RRBP 167B	0.017	0.034
Mean		*0.017*	*0.032*
Maximum		*0.018*	*0.034*
Minimum		*0.016*	*0.030*
Standard Dev.		*0.0010*	*0.0018*
03-Jul-00	RRBP 118A	0.032	0.046
03-Jul-00	RRBP 118B	0.032	0.047
03-Jul-00	RRBP 167A	0.034	0.049
03-Jul-00	RRBP 167B	0.035	0.049
Mean		*0.033*	*0.048*
Maximum		*0.035*	*0.049*
Minimum		*0.032*	*0.046*
Standard Dev.		*0.0015*	*0.0015*
17-Jul-00	DH 317	-	0.046
17-Jul-00	DH 318	-	0.046
17-Jul-00	RRBP 167B	0.032	0.048
Mean		-	*0.047*
Maximum		-	*0.048*
Minimum		-	*0.046*
Standard Dev.		-	*0.0011*
08-Aug-00	RRBP 118A	0.039	0.050
08-Aug-00	RRBP 118B	0.039	0.053
08-Aug-00	RRBP 167A	0.034	0.049
08-Aug-00	RRBP 167B	0.036	0.054
Mean		*0.037*	*0.052*
Maximum		*0.039*	*0.054*
Minimum		*0.034*	*0.049*
Standard Dev.		*0.0024*	*0.0024*
25-Sep-00	DH 317	-	0.029
25-Sep-00	DH 318	-	0.031
25-Sep-00	RRBP 118A	0.020	0.029
25-Sep-00	RRBP 167B	0.024	0.032
Mean		*0.022*	*0.030*
Maximum		*0.024*	*0.032*
Minimum		*0.020*	*0.029*
Standard Dev.		*0.0028*	*0.0015*

Table 3.6 Monthly Variation of TP and RP

for particulate organic phosphorus and RP are available, it is not possible to model and calibrate the phosphorus cycle.

Since the variation of phosphorus over time was small, in the present study, it was found appropriate to use the measured reactive phosphorus at the sampling stations in order to model the phosphorus limitation on growth in Michaelis-Menten equation.

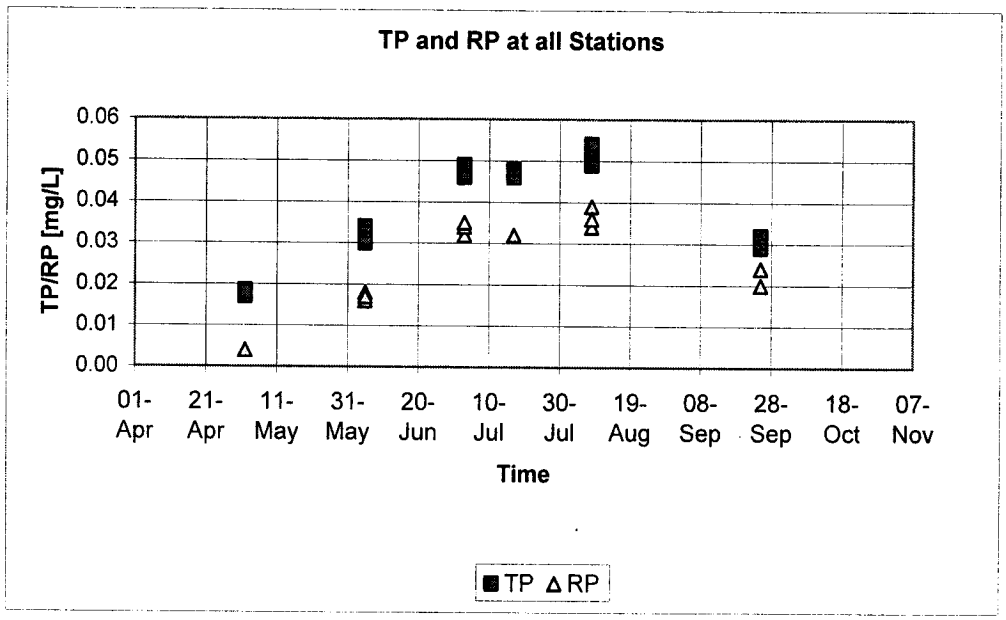

Figure 3.18 TP and RP at all Stations

Since the variation over month in TP and RP was small, monthly averages were computed and longitudinal profiles for TP and RP are shown in Figs. 3.19 and 3.20.

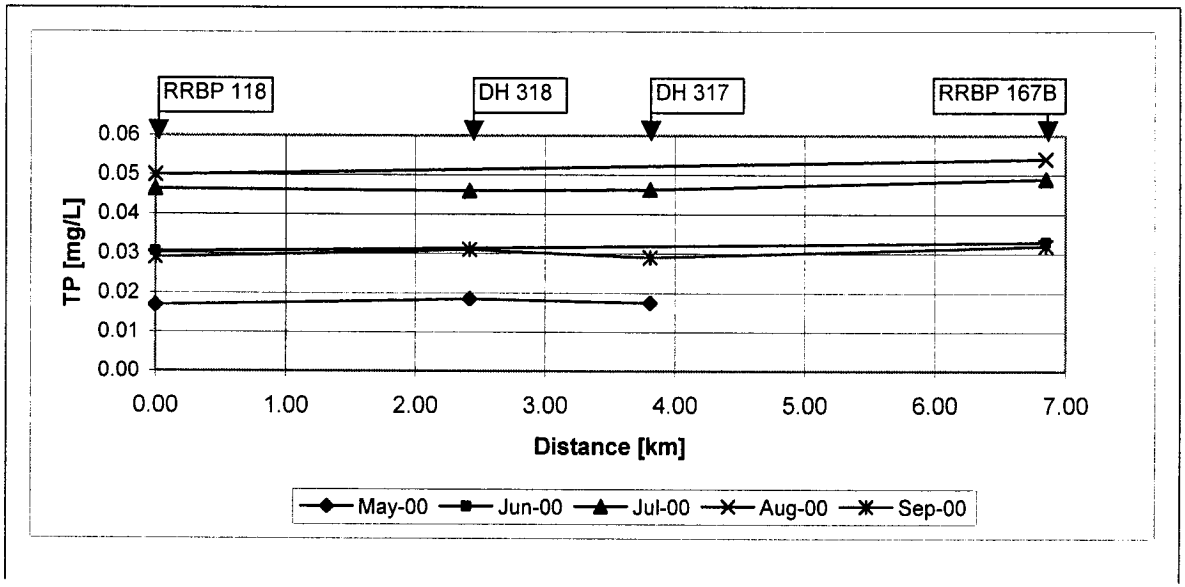

Figure 3.19 Longitudinal Profiles at Stations DH 317 and DH 318

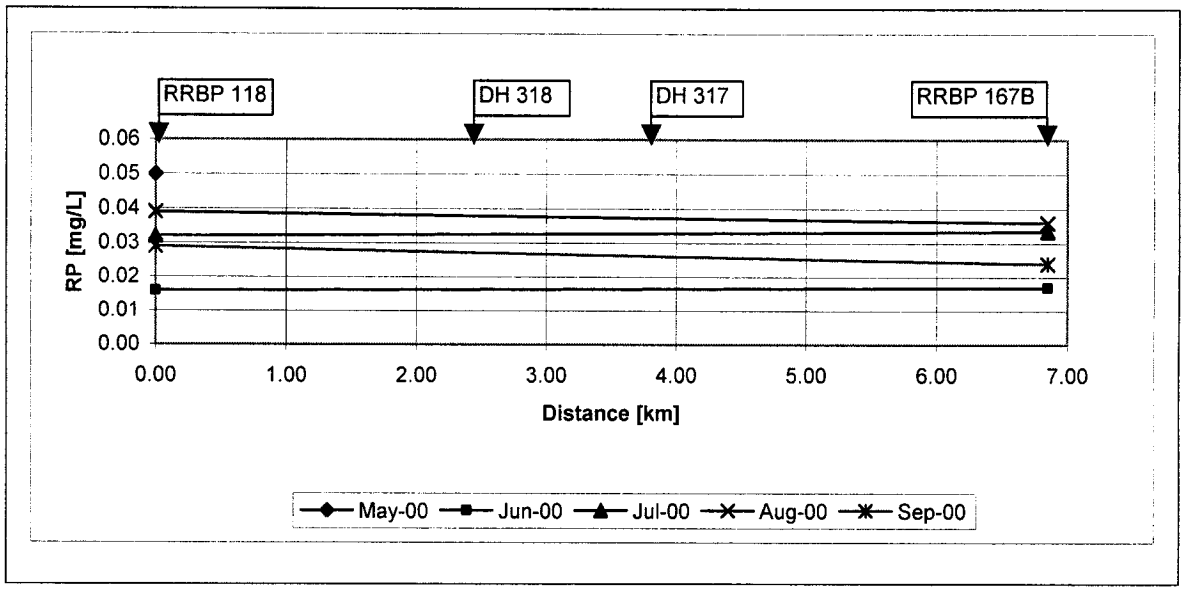

Figure 3.20 Longitudinal Profiles of TP and RP based on Monthly Averages

3.5.2 Losses

In order to model the loss rate of phytoplankton, the following losses may be considered important in water quality modelling [Chapra, 1997].

Respiration: In respiration phytoplankton release energy in the form of CO_2 by breaking down sugar and other organic compounds. Part of CO_2 is used in growth and maintenance of the cells. [Chapra, 1997]

Excretion: In this process mainly nutrients are considered to be released; however, organic carbon can also be released as a byproduct [Chapra, 1997].

The above processes can be defined by following equation

$$C_6H_{12}O_6 + 6O_2 = 6CO_2 + 6H_2O + \text{released energy} \qquad (3.34)$$

It is difficult to measure respiration and excretion losses separately therefore, generally they are modelled as single first order decay, k_r [Chapra, 1997]. Values of k_r range between 0.01 and 0.5 d^{-1} with typical values of the order of 0.1 to 0.2 d^{-1} [Chapra, 1997]. A theta model is usually used to correct the respiration/excretion rate for temperature [Chapra, 1997].

Predatory losses: Death of algae due to filtration and grazing by zooplankton and benthic organisms (e.g. zebra mussels) is possible. When predators are not explicitly modelled, the dynamics cannot be simulated so the loss due to grazing could be handled by a constant grazing loss coefficient. Simulation of growth of zooplankton is a dynamic process and in order to simulate the grazing of phytoplankton by zooplankton a first order grazing constant is used where grazing rates are assumed proportional to phytoplankton levels. Reported grazing rates vary from 0.1 to 1.5 L mgC^{-1} d^{-1} [WASP 6.0]. These are the grazing rates on phytoplankton per unit zooplankton population. These grazing rates when multiplied with the zooplankton population [mgC L^{-1}] give the biomass reduction rate in days [WASP 6.0].

In a different approach [Everbecq et al., 2001] two types of zooplankton are considered in modelling of phytoplankton dynamics and zooplankton's filtration rate along with their names is as follows: 1) *Brachionus*-like (at 20°C) : 1.6 L mgC^{-1} d^{-1} and 2) *Keratella*-like (at 20°C) : 1.35 L mgC^{-1} d^{-1}. Total phytoplankton carbon biomass could be calculated from Chl *a*, using C: Chl *a* ratio of 37 [Descy and Gosselain, 1994].

A study was carried out in the Rideau River on data for years 1994 and 1995. For a mean density of 65 individuals L^{-1} and a mean infiltration rate of 1 ml $individual^{-1}$ d^{-1}, crustacean zooplankton can filter 6.5% of the water column per day. Rotifiers with mean density of 500 individuals L^{-1} and a mean filtration rate of 60 µL $individual^{-1}$ d^{-1}, can filter 3% of the water column per day [Basu & Pick, 1997].

In the present study, the phytoplankton-predator dynamics is not modelled as data on all sampling stations on zooplankton population are required to do that.

Settling losses: Losses due to settling of algae can be modelled using Stokes' law. The settling velocity of a particle can be estimated using Stokes' law [Chapra, 1997],

$$v_s = \alpha \frac{g}{18} \frac{(\rho_s - \rho_w)}{\mu} d^2 \qquad (3.35)$$

where v_s= settling velocity [cm s^{-1}]; α = a dimensionless form factor reflecting the effect of particle shape on settling velocity (for a sphere it is 1.0); g = acceleration due to gravity; ρ_s and ρ_w = densities of the particle and water respectively [g cm^{-3}]; μ = dynamic viscosity [g cm^{-1} s^{-1}] and d = an effective particle diameter [cm].

Stokes' law provides a useful theoretical reference but it may not provide good results of actual settling velocity. Stokes' law is based on the assumption that flow is laminar whereas flow in most natural systems is turbulent. Further more phytoplankton can become buoyant due to internal gases and there settling velocity would also depend on their physiological state.

Generally, the phytoplankton have complex shape (which would lead to α lower than 1.0) and thus the settling velocity would also be less. Table 3.7 shows measured values for phytoplankton and other particles.

Particle type	Diameter [μm]	Settling velocity [m d^{-1}]*
Phytoplankton:		
Thalassiosira nana	4.3-5.2	0.1-0.28
Scenedesmus quadricauda	8.4	0.27(0.89)
Asterionella formosa	25	0.2(1.48)
Thalassiosira rotula	19-34	0.39-2.1
Coscinodiscus lineatus	50	1.9(6.8)
Melosira agassizii	54.8	0.67(1.87)
Rhizosolenia robusta	84	1.1(4.7)

*Figures in parenthesis are for stationary growth phase.

Table 3.7 Settling Velocities of Particles Found in Natural Waters [Chapra, 1997]

Reynolds (1984) compiled data from an earlier research carried out by Smayda, 1970 and plotted average sinking rate as a function of average cell diameter. According to that data the average sinking rate for 10 μm is of the order of 0.75 m d^{-1}.

The loss due to settling is incorporated in the model as following [QUAL2E, 1987]

$$k_s = \frac{v_s}{H} \tag{3.36}$$

where k_s is phytoplankton settling loss rate [d^{-1}] and H is depth [m] at a particular node

Mortality due to non-predatory effects such as bacterial decomposition of cell, extreme environmental conditions or toxic substances, etc. are not included currently in the model approach.

The equation for the growth rate coefficient is given hereunder

$$k_g = k_{g,20}\theta^{T-20}\left[\frac{2.718f}{k_e H}\left(e^{-\alpha_1} - e^{-\alpha_0}\right)\right]\left[\frac{p}{k_{sp}+p}\right] \tag{3.37}$$

Now, we can develop an equation for phytoplankton growth

$$\Delta S = H(k_g a - k_r a - k_p a - k_s a) \tag{3.38}$$

where ΔS term is the source/sink term in Equation 2.24 [kg m^{-2} s^{-1}], H is the water depth [m], a is algal biomass concentration [kg-Chl a m^{-3}], t is time [sec], k_g is growth rate which is temperature dependent [sec^{-1}], k_r is respiration rate of phytoplankton [sec^{-1}], k_p is predatory loss coefficient [sec^{-1}], v_s is settling velocity [m sec^{-1}], k_s is phytoplankton settling loss rate [sec^{-1}] , d is depth [m]. It is worth noting that the units in the Equation 3.38 have been modified in order to be consistent with Equation 2.24.

3.5.3 Rate Coefficients and other Parameters

Most of the rate coefficients are temperature dependent and corrections for ambient temperature have to be applied to the rate coefficients. Table 3.8 gives a comparison of various coefficients used in some of the water quality models.

Description	QUAL2E	CHAPRA	WASP 6.0
Ratio of chlorophyll-a to algal biomass, α_0 [μg-Chl *a* mg-A^{-1}]	10-100		
Maximum algal growth rate, k_{gmax} [d^{-1}][1]	1-3		2
Algal respiration rate, k_r [d^{-1}][1]	0.05-0.5		0.05-0.2[2]
Steele's model optimum light level coefficient, I_s [ly d^{-1}]	352.78	-	
Saturating Light Intensity, I_s [ly d^{-1}] in saturation model			200-500
Half saturation constant for Phosphorus growth limitation, k_{sp} [mg-P L^{-1}]	0.001-0.05	0.001-0.05	0.001
Half saturation constant for Nitrogen growth limitation, k_{sn} [mg-N L^{-1}]	0.01-0.30	0.005-0.02	0.025
Fraction of day that is day light, f [-]			0.3-0.7
Average daily surface solar radiation, I_a [ly d^{-1}]			200-750
Extinction Coefficient, k_e [m^{-1}]			0.1-5
Carbon-Chl *a* ratio			20-50
Settling velocity, v_s [m d^{-1}][1]	0.15-1.8		0.1
Fraction of phytoplankton biomass that is phosphorus, α_2 [mg-P mg-A^{-1}]	0.01-0.02		
Rate constant for the mineralization of particulate organic phosphorus to phosphate, β_4 [d^{-1}][1,2]	0.01-0.7		
Benthos source rate of dissolved phosphorus, σ_2 [mg-P m^{-2} d^{-1}][1]	Variable		
Organic phosphorus settling rate, σ_5 [d^{-1}]	0.001-0.1[1]		

[1] *Temperature dependent; 2 Bowie et al., 1985*

Table 3.8 Typical Value for Coefficients Used in Phytoplankton Modelling

CHAPTER 4

4 FLOW MODELLING OF RIDEAU RIVER

4.1 Introduction

In the first part of the study, flow modelling was carried out using 2-D depth averaged model, HYDROSIM. Black Rapids to Hog's Back Reach of the Rideau River is about 6.5 km and is between two water control structures (refer to Fig. 3.3). Water levels in the summer are raised to facilitate navigation between Kingston and Ottawa.

At the Black Rapids Locks there are number of structures that pass flow including a navigation lock. A broad crested weir is constructed to control the water level upstream and two sluice gates are used in periods of high flow. The difference in the water level between upstream and downstream pool is approximately 2.9 m [Baird & Associates, 1998]. No water level measurements were available at downstream of the Black Rapids Lock.

Hog's Back is a gated weir structure with a navigation lock facility. Water levels at Mooney's Bay are raised through a gated weir at the North end of the Bay. The target elevation for the Mooney's Bay reach is 74.9 m GSC datum in summer [Baird & Associates, 1994]. Actual water levels are within few centimeters of this elevation.

4.2 Grid generation

HYDROSIM is based on the finite element method in which the grid is composed of T6 type elements, triangular in shape [Secretan et al., 2000]. The governing equations for fluid flow are approximated on this grid. One of the advantages of the finite element method is that complex geometries and boundaries can be readily defined by adjusting the size and number of the elements. A finite element grid was generated with isotropic elements in longitudinal and lateral

direction. The resolution of the grid was between 5 to 20 m depending upon the width of the River and refinements near the boundaries (Fig. 4.1).

The bathymetric data covered the area of the waterway at normal summer water levels. The bathymetric data were interpolated over this grid, the digital elevation model is given in Fig. 4.2. Figures A.1 and A.2 (Appendix-A) show the digital terrain model maps on large scale. Figure 4.3 shows flow simulation results for the water depth on July 20, 2000 for a flow of 28.6 $m^3 s^{-1}$. Figures A.3 and A.4 (Appendix-A) show the water depth maps on large scale.

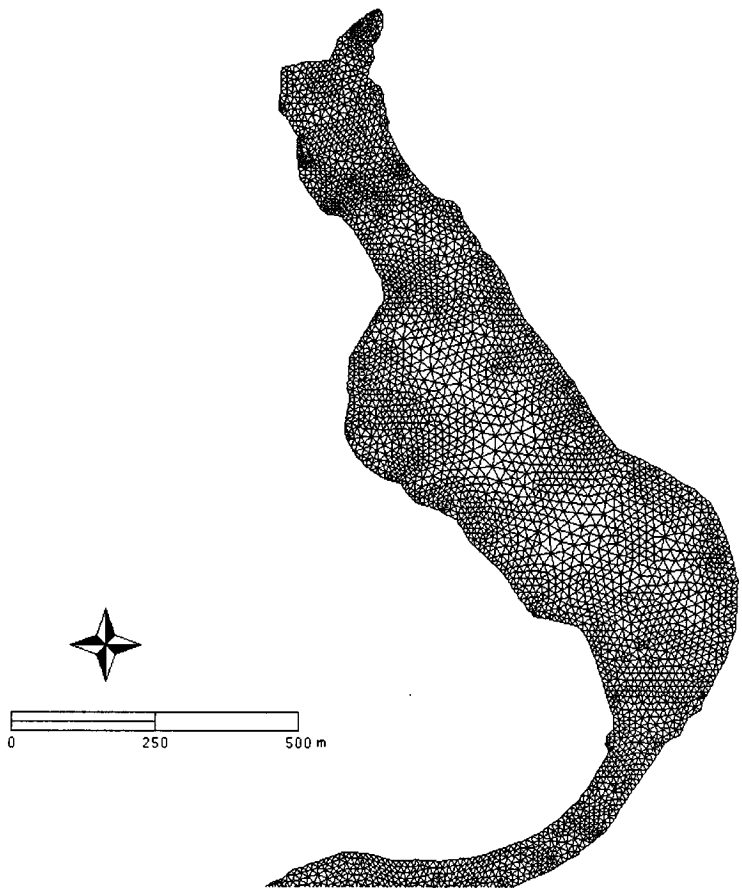

Figure 4.1 Hydrodynamic Mesh for Mooney's Bay

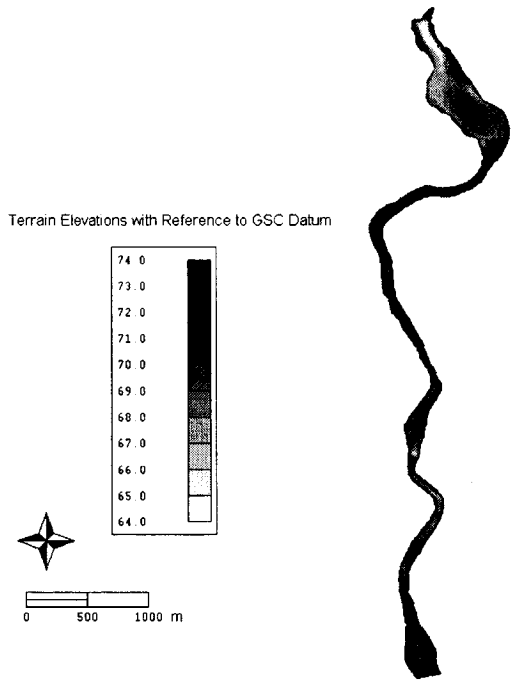

Figure 4.2 Digital Elevation Model of Black Rapids-Hog's Back Reach

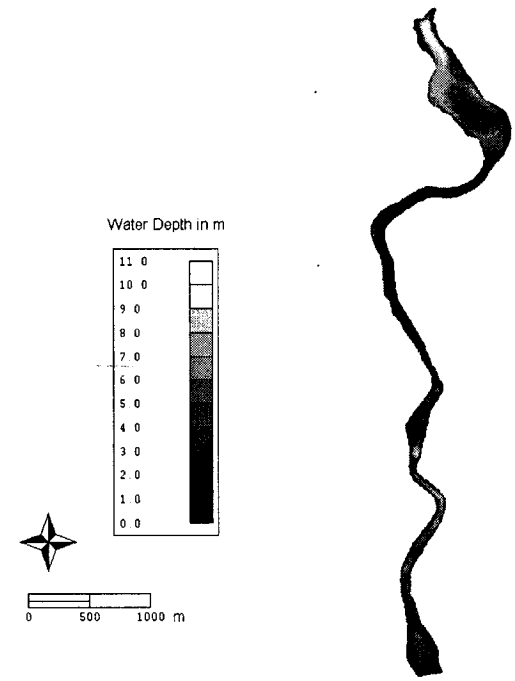

Figure 4.3 Water Depth for Flow of 28.6 $m^3 s^{-1}$ (July 20, 2000)

4.3 Flow Boundary Conditions

Steady state simulations were carried out for flows in the range of 10 m^3/s to 40 m^3/s. The upstream boundary was steady discharge with normal-discharge solicitation-type boundary in HYDROSIM. The downstream boundary at Hog's Back was fixed as water level-type. The side or solid boundaries were simulated as no flux types.

4.4 Flow and Numerical Parameters

As discussed earlier in Sec. 2.5, Peclet Number for flow 'Pe_H' is defined as

$$Pe_H = \frac{\rho U \Delta x}{\mu} \tag{4.1}$$

where ρ is fluid density [g cm^{-1}], U is average elemental velocity; Δx is length of element in longitudinal direction; and μ is eddy viscosity [Pa-s]

The way viscosity is managed in HYDROSIM is as follows:

$$\mu_{global} = \mu_M + \mu_T + \mu_N \tag{4.2}$$

where μ_{global} is the global viscosity; μ_M is the molecular viscosity; μ_T is the eddy viscosity; μ_N is the numerical viscosity.

It is known from numerical analysis that for a problem to be numerically stable $P<P_c$ where P_c is the critical value. Various simulations were carried out and the final value for P_c equal to 0.5 was selected. Better mass conservation was achieved with this value. A value of μ equal to 0.001 Pa-s also gave better mass conservation results. During initial simulations a convection coefficient of 0.5 was used, which gave stability to the model but produced mass conservation errors. In later simulations a convection coefficient of 1.0 was used which gave better accuracy and convergence to the model and thus producing good mass conservation.

The lower bound viscosity was chosen as 1e-06 and upper bound viscosity as 20. These values define the upper and lower eddy viscosity limits in the model. Sometime increasing the upper limit stabilize the model but not necessarily produce good mass conservation. For low flows, convergence was not easy to achieve and for that revising pre-conditioning criterion 'NPREC' as 40 helps to reduce the mass conservation errors in the flow model.

In practice, adjusting the turbulent viscosity is part of the calibration process. For simplified analysis, eddy viscosity can be a fixed constant in the domain and it could be spatially varied also. When the problem centers on the use of the water level, the mixing length is not required. However in order to have a better representation of velocities, a mixing length model is recommended [Heniche et al., 2000].

4.5 Calibration of Model and Sensitivity Analysis

In the flow model calibration process, specific model parameters are adjusted until the simulation results match the available measurements. Once the final parameters have been selected, the model is then validated against an independent data set. The two basic calibration parameters in a 2-D depth-averaged model are 1) bottom friction and 2) horizontal turbulence coefficient. Bottom friction affects water levels and velocities whereas horizontal turbulence coefficient is used to model circulation patterns and eddies. Both of these calibration parameters can be varied within a narrow range.

In the Rideau River, average river current velocities were measured using AFFRA (Acoustic Flowmeter For Remote Areas) acoustic pulse system at locations shown in Fig. 4.4 in years 1994, 1995 and 1996. The AFFRA gave an average current velocity based on the time of travel of the sound pulses along a predetermined path between the two posts. The depth of measurements at locations BACD was 2.5 m, BLIK at 4.5 m and GEFH at 2.5 m [Baird & Associates, June 1994]. Measurement at Hog's Back was taken at approximately 2 m below the surface. In 1997 3-D modelling of Mooney's Bay was carried out using MIKE3 model. Effects of thermal stratification and wind-induced currents were simulated in MIKE3.

It was concluded in that study [Baird & Associates, Sep. 1997] that the current speeds predicted at Hog's Back matched well with the field data (Fig. 4.5), whereas the results at station GEFH showed poor correlation with AFFRA measurements. It was reported to be due to inaccuracy in AFFRA measurements at this location [Baird & Associates, Sep. 1997]. The data from BLIK and BACD showed the trend (Figs. 4.6 & 4.7), but were typically about 60 percent of the magnitude of the recorded data for BACD, and less than half for BLIK [Baird & Associates, 1997]. It was concluded [Baird & Associates, 1997] that this difference was due to accuracy of the measured currents.

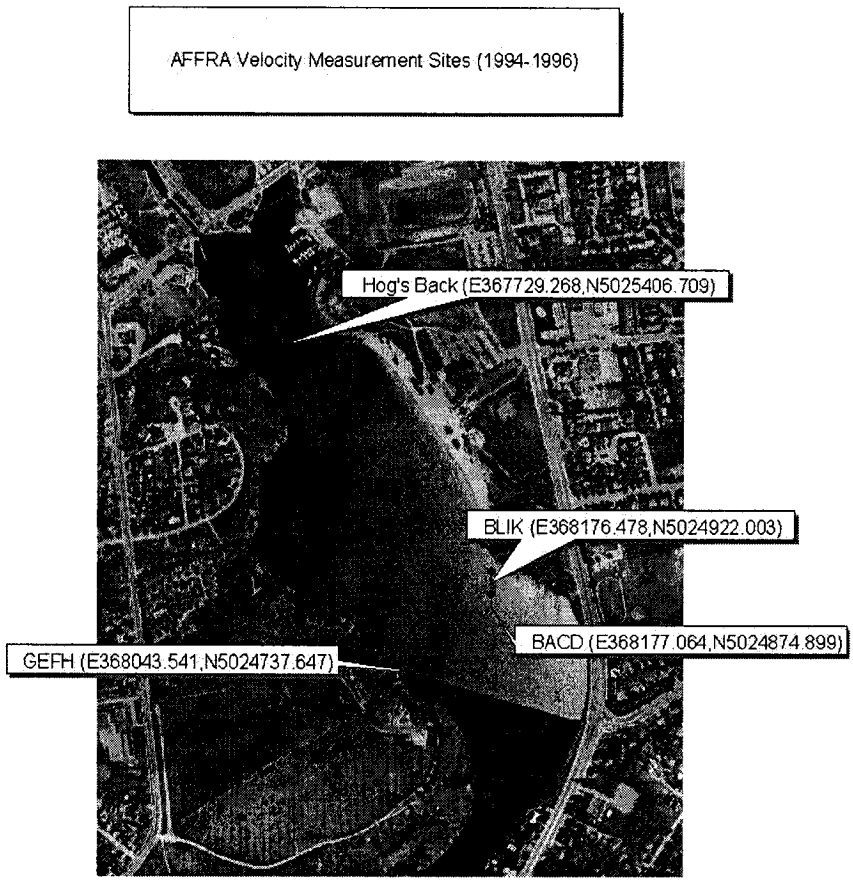

Source of Photomosaics: City of Ottawa-Carleton, MTM NAD83, Zone 9

Figure 4.4 AFFRA Velocity Measurement Sites (1994-1996)

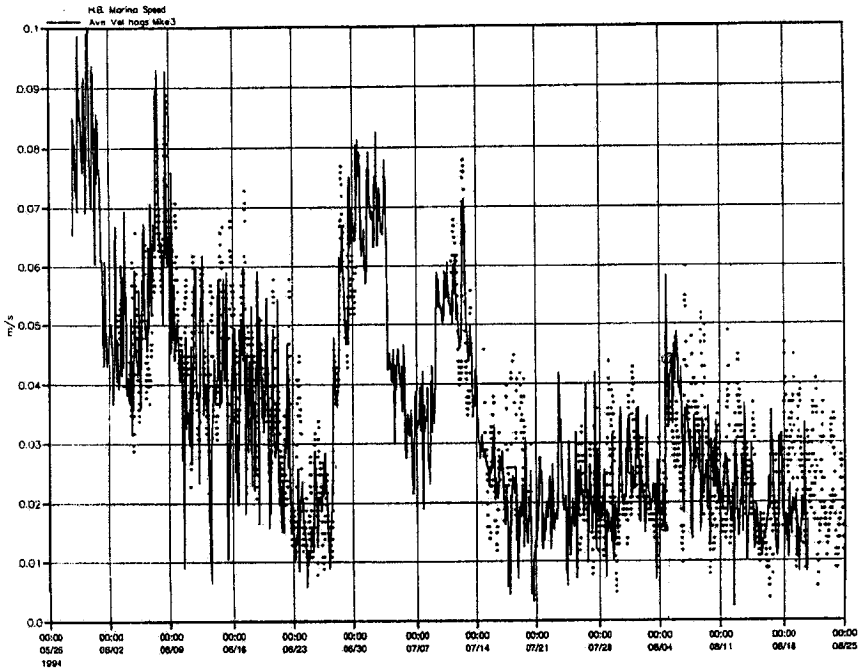

Figure 4.5 MIKE3 Model Results vs

AFFRA Measurements at Hog's Back [Baird & Associates, 1997]

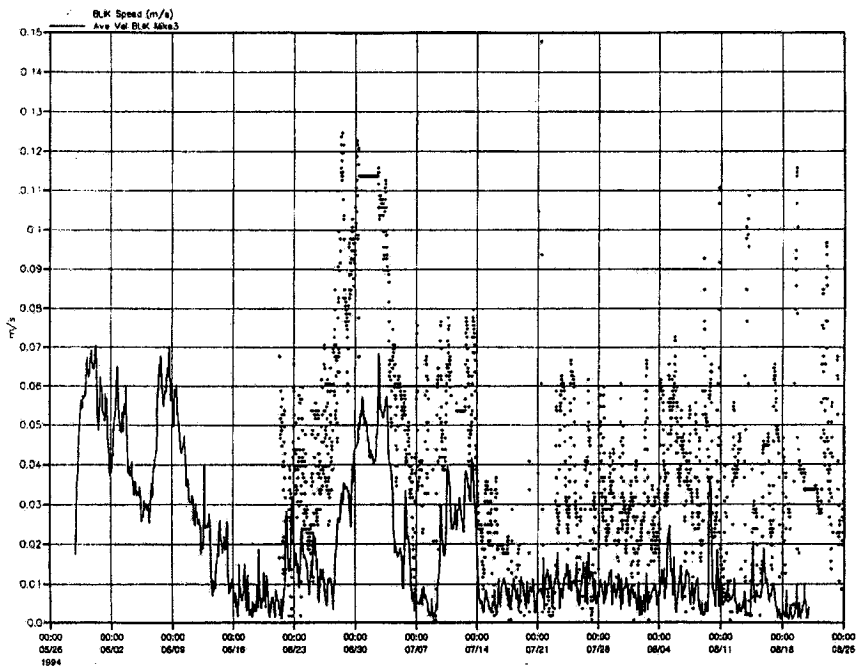

Figure 4.6 MIKE3 Model Results vs AFFRA Measurements at Station BLIK [Baird & Associates, 1997]

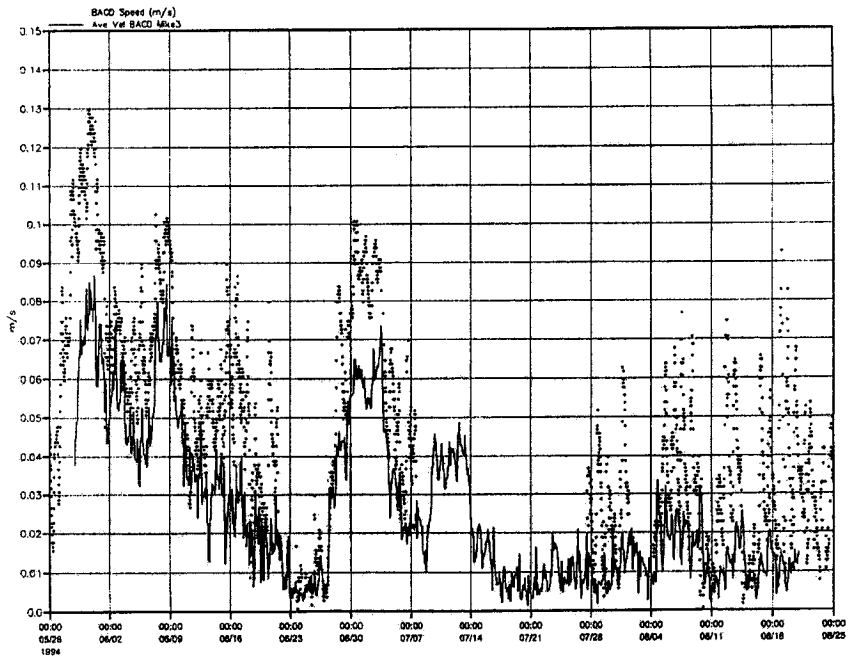

Figure 4.7 MIKE3 Model Results vs AFFRA Measurements at Station BACD [Baird & Associates, 1997]

In the present study, initial attempts were made to calibrate the model per AFFRA measurements. Simulation for flows of 10.3 m^3s^{-1} and 33.6 m^3s^{-1} were carried out. These flows were chosen based on the flows in summer and availability of current velocity data in electronic version for these flows. The value of Manning's roughness coefficient '*N*' selected was 0.022 and was based on the following reasons

- Value of Strickler coefficient selected during Rideau River modelling [Baird & Associates, December 1998] was 45, which is equivalent to *N* value of 0.022.
- From information on selection of *N* by Chow [Ven Te Chow, 1973], value of 0.025 is the minimum value recommended by Chow for rivers like the Rideau.
- Calculations were carried out to compute Chezy's roughness coefficient 'C' and then converting it into Manning's roughness *'N'*. Current-related form-roughness was ignored in the computations, as no bed form data are available. The Manning's roughness *'N'* came out to be in the range of 0.015 to 0.018.

- During a sensitivity analysis for a range of N (discussed in following sections), it was found that for low flow there is minor change in water surface elevation and current velocities for various values of N.

The comparison of simulation results from the present study with available AFFRA measurements are given in Tables 4.1 to 4.3. Better calibration at stations Hog's Back and BLIK was achieved with N= 0.022. Station BLIK is towards the east of Mooney's Bay and by lowering the Eddy Viscosity (increasing Peclet Number), higher velocities were observed during simulations.

Time	Mean Daily Flow [$m^3 s^{-1}$]	AFFRA's 'V' at Hog's Back [$cm\ s^{-1}$]				Computed 'V' [$cm\ s^{-1}$]
		Mean	Maximum	Minimum	Std. Dev.	
June 04, 1994	33.6	4.7	6.6	2.9	0.95	4.01
July 16, 1994	10.3	2.1	3.2	1.2	0.64	1.20

Table 4.1 Comparison of Simulated and Measured Current Velocity at Hog's Back

Time	Mean Daily Flow [$m^3 s^{-1}$]	AFFRA's 'V' at Station BLIK [$cm\ s^{-1}$]				Computed 'V' [$cm\ s^{-1}$]
		Mean	Maximum	Minimum	Std. Dev.	
July 16, 1994	10.3	2.3	3.7	1.7	0.56	1.86

Table 4.2 Comparison of Simulated and Measured Current Velocity at Station BLIK

Time	Mean Daily Flow [$m^3 s^{-1}$]	AFFRA's 'V' at Station BACD [$cm\ s^{-1}$]				Computed 'V' [$cm\ s^{-1}$]
		Mean	Maximum	Minimum	Std. Dev.	
June 04, 1994	33.6	6.1	7.6	4.9	0.81	5.01

Table 4.3 Comparison of Simulated and Measured Current Velocity at Station BACD

It is worth mentioning here that the simulated velocity was depth-averaged velocity whereas the AAFRA measurements were taken at different depths as discussed in the preceding paragraphs.

The change in river surface elevation in Black Rapids to Hog's Back Reach is below detectable limits under average summer flow conditions [Baird & Associates, December 1998]. No water level measurements were available downstream of Black Rapids Lock. The only water level measurements available in the study reach were at upstream of Hog's Back. Therefore direct calibration of the flow model in summer conditions is difficult to achieve.

A sensitivity analysis was, therefore, carried out by varying the bottom roughness (Manning's *N*) for a flow range of 10 $m^3 s^{-1}$ to 40 $m^3 s^{-1}$. Table 4.4 gives the water level difference between Black Rapids and Hog's Back under varying flows and roughness. For low flows such as 10 $m^3 s^{-1}$, the maximum water level difference was only 5 mm. The maximum water level difference observed for flow of 40 $m^3 s^{-1}$ is 67 mm. Variation in current velocity for the above analysis is given in Table 4.5.

Manning's N	10 m^3/s	20 m^3/s	30 m^3/s	40 m^3/s
0.017	2 mm	-	-	-
0.020	2 mm	8 mm	19 mm	33 mm
0.022	2 mm	9 mm	20 mm	35 mm
0.025	2 mm	10 mm	22 mm	39 mm
0.030	3 mm	12 mm	26 mm	46 mm
0.040	5 mm	19 mm	39 mm	67 mm

Table 4.4 Water Level Difference between Black Rapids & Hog's Back (E367530.476, N5020874.411)

Manning's N	10 $m^3 s^{-1}$	20 $m^3 s^{-1}$	30 $m^3 s^{-1}$	40 $m^3 s^{-1}$
0.017	2.58 cm s^{-1}	-	-	-
0.020	2.57 cm s^{-1}	5.16 cm s^{-1}	7.70 cm s^{-1}	10.24 cm s^{-1}
0.022	2.59 cm s^{-1}	5.15 cm s^{-1}	7.72 cm s^{-1}	10.26 cm s^{-1}
0.025	2.58 cm s^{-1}	5.16 cm s^{-1}	7.71 cm s^{-1}	10.25 cm s^{-1}
0.030	2.59 cm s^{-1}	5.16 cm s^{-1}	7.69 cm s^{-1}	10.24 cm s^{-1}
0.040	2.59 cm s^{-1}	5.14 cm s^{-1}	7.69 cm s^{-1}	10.19 cm s^{-1}

Table 4.5 Current Velocity at Black Rapids (E367530.476, N5020874.411)

The friction coefficient had negligible effect on current velocities. Above results show that under low flow conditions in summer, the current velocity and water level are rather insensitive to the

bottom friction parameter. Figure 4.8 shows the effect of N on water level difference between Black Rapids and Hog's Back under various flow conditions. For flow equal to 30 m^3 s^{-1} and Manning's N of 0.022, the maximum water level difference is 20 mm in the study reach, which is about 6.5 km in length.

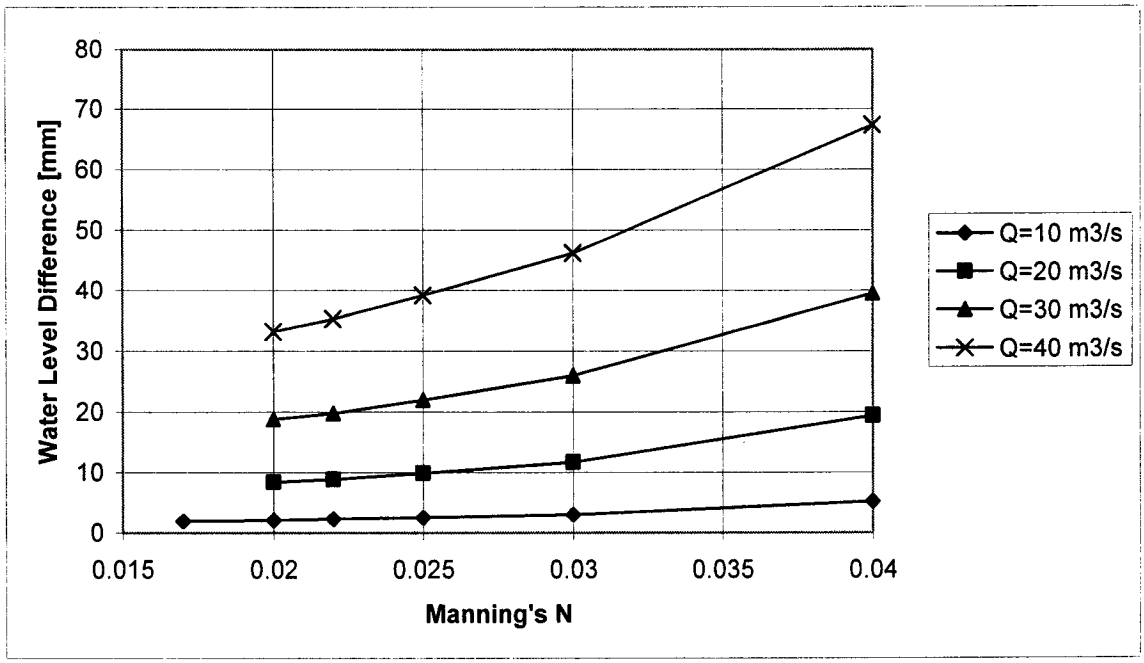

Figure 4.8 Water Level Difference between Black Rapids and Hog's Back

Velocity vectors are plotted in Fig. 4.9 for flow of 28.6 m^3 s^{-1} corresponding to July 20, 2000 average daily flow. Figures A.5 and A.6 in Appendix-A show the velocity maps for July 20, 2000 simulation. Two recirculation zones in Mooney's Bay are shown in Fig 4.10 on the western bank, the main recirculation zone is along north-west of the Bay. Most of the flow is concentrated towards the eastern bank.

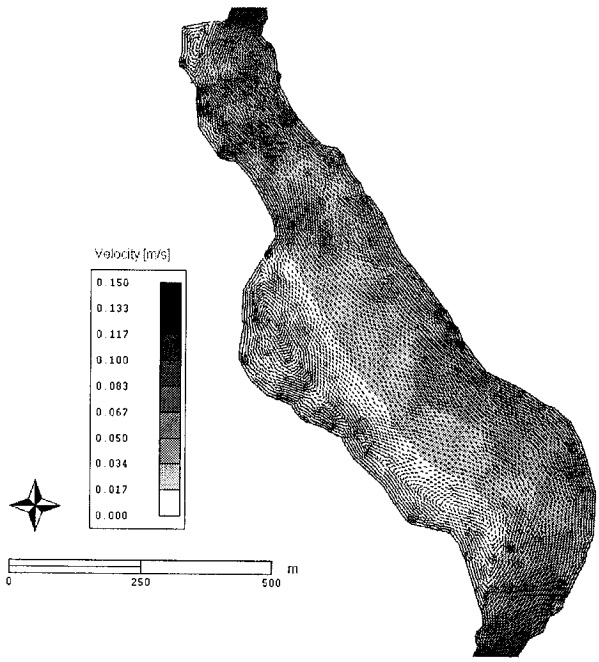

Figure 4.9 Velocity Vectors in Mooney's Bay for Flow of 28.6 $m^3 s^{-1}$ (July 20, 2000)

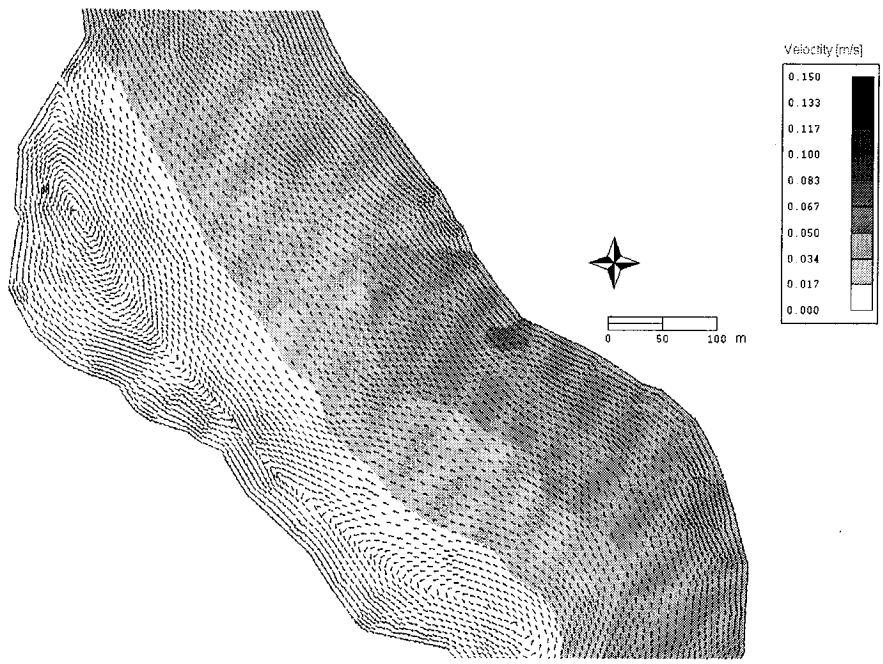

Figure 4.10 Dead Zones in Mooney's Bay for Flow of 28.6 $m^3 s^{-1}$ (July 20, 2000)

CHAPTER 5

5 VALIDATION AND RESULTS OF PHYTOPLANKTON GROWTH AND WATER AGE MODELLING

5.1 Introduction

After completion of the flow modelling the next step in the study was water quality modelling. As discussed before, the phytoplankton element was not initially included in the DISPERSIM, which is an advection-diffusion or transport module. The methodology for the phytoplankton growth and the mathematical model are discussed in detail in Section 3.5. The phytoplankton growth model developed in the present study is given in Equations 3.37 and 3.38. The validation and results of phytoplankton and water age modelling are given in the following sections.

5.2 Validation of the Growth Model with 1-D Analytical/Numerical Solutions

In this section, the phytoplankton growth model was validated with analytical/numerical solutions of the equations. The steady state 1-D transport equation including only losses due to respiration and settling can be written as following.

$$U_x H \frac{\partial C}{\partial x} = H(-k_r C - k_s C) \tag{5.1}$$

where H is the water depth [m] and U_x is the depth-averaged velocity in x-direction.

The analytical solution of above equation is as following.

$$C(x) = C_{ent} \exp\left(-\frac{k_r x}{q}\left[H_{ent} + \frac{S_b x}{2} \right] - \frac{v_s x}{q} \right) \tag{5.2}$$

where $H = H_{ent} + S_b x$ [m] (with a linear variation); $q=Q/b$[m^2 s^{-1}]; $k_s=v_s/H$ [s^{-1}]; Q is the flow [m^3 s^{-1}]; H_{ent} is the depth at entrance [m]; b is the width of channel [m]; S_b is the bed slope [-] and x is the distance [m]; C_{ent} is the concentration at entrance [kg m^{-3}].

The steady state transport equation including growth and losses due to respiration and settling can be written as following.

$$U_x H \frac{\partial C}{\partial x} = H\left(k_g C - k_r C - k_s C\right) \tag{5.3}$$

where k_g is defined in Equation 3.37 and includes a term, α_I, which itself is an exponential function of $H(x)$ making k_g difficult to integrate analytically. Maple 7 [Waterloo Maple, 2001] was used to find numerical solutions of Equation 5.3 [Appendix-C].

Simulation in DISPERSIM were carried out using the growth model developed in the present study. As the validation of the simulated results were to be done with 1-D equation, the growth of phytoplankton was simulated in a rectangular channel of 10 m width and 50 m length. The number of elements used were 3,448. The velocity in y-direction was zero and the velocity in x-direction was incorporated as following.

$$U_x(x) = \frac{Q}{bH(x)} \tag{5.4}$$

The coefficients, physical and numerical parameters used in DISPERSIM simulation are given in Table 5.1.

Constants and Coefficients		Physical and Numerical Parameters			
k_{gmax} [d^{-1}]	1.70	T [°C]	23.78	B_L [-]	0
k_r [d^{-1}]	0.20	I_a[ly d^{-1}]	485	B_H [-]	0
I_s [ly d^{-1}]	300 v	f [-]	0.6	B_F [-]	0
k_e [m^{-1}]	0.5	SRP [mg P L^{-1}]	0.034	D_{mol} [m s^{-2}]	0
k_{sp} [mg-P L^{-1}]	0.01	C_{ent} [mg Chl *a* L^{-1}]	1.0	Sb [-]	0.1
θ [-]	1.047			H_{ent} [m]	1.0
v_s [m d^{-1}]	0.75			q [m^2 s^{-1}]	1.0

Table 5.1 List of Coefficients, Physical and Numerical Parameters

The comparison of analytical solution with simulated results is given in Table 5.2.

Location	Chl *a* Concentration [µg L^{-1}]	
X [m]	Analytical Solution	Simulated Solution
25.0	1.0002191	1.0002193
37.5	1.0004438	1.0004439
50.0	1.0006931	1.0006934

Table 5.2 Comparison of 1-D Analytical and Simulated Results for Growth Model

5.3 Validation of the Water Age Model with 1-D Analytical Solution

In this section the water age model was validated against the analytical solution of the water age equation. The 1-D steady state transport equation including aging process of 1 s s^{-1} can be written as follows.

$$U_x H \frac{\partial C}{\partial x} = H \tag{5.5}$$

The analytical solution of above equation is as follows.

$$C(x) = C_{ent} + \frac{x}{q}\left[H_{ent} + \frac{S_h x}{2}\right] \tag{5.6}$$

Simulation in DISPERSIM were carried out using the growth model developed in the present study. The schemetization for the channel and grid for this simulation are same as for the channel described in Section 5.8. The coefficients, physical and numerical parameters used in DISPERSIM simulation are given in Table 5.3.

Constants and Coefficients		Physical and Numerical Parameters			
k_{gmax} [d^{-1}]	0	ΔS [$s\ s^{-1}$]	1.0	B_L [-]	0
k_r [d^{-1}]	0	Sb [-]	0.1	B_H [-]	0
k_s [d^{-1}]	0	H_{ent} [m]	1.0	B_F [-]	0
		q [$m^2\ s^{-1}$]	1.0	D_{mol} [$m\ s^{-2}$]	0

Table 5.3 List of Coefficients, Physical and Numerical Parameters for Water Age Validation

The comparison of analytical solution with simulated results is given in Table 5.4.

Location	Water Age [s]	
X [m]	Analytical Solution	Simulated Solution
25.0	56.25	56.245016
37.5	107.8125	107.82736
50.0	175.0	175.15181

Table 5.4 Comparison of 1-D Analytical and Simulated Results for Growth Model

5.4 Simulation Periods

In Section 3.3.4, limitations of the year 2000 data are discussed. The water quality measurements were done in such a way that limited continuous temporal and spatial water quality data were available for year 2000. This limited the simulations to steady state and for the days on which data at upstream station and downstream station were available.

Table 5.5 shows the monthly flow data for June, July and August for the years 1994, 1995, 1996, and 2000. Due to large variance in monthly flows, steady state daily flow simulations were carried out for use in the DISPERSIM model. Figure 5.1 shows the flow variation from May to August 2000 in the Rideau River at Ottawa.

Period	Flows ($m^3 s^{-1}$) Mean	Maximum	Minimum
1994			
June	29.30	58.30	7.99
July	19.50	50.20	7.27
August	11.10	25.10	6.26
1995			
June	16.50	73.80	3.18
July	4.79	14.70	2.50
August	15.00	94.40	2.75
1996			
June	18.10	27.30	10.50
July	9.54	12.40	6.49
August	10.50	22.20	6.40
2000			
June	43.79	99.60	18.90
July	28.24	55.20	13.90
August	18.32	35.80	8.08
1994,1995,1996, 2000			
June	26.92	99.60	3.18
July	15.52	55.20	2.50
August	13.73	94.40	2.75
Historical Mean (Ref: Water Survey of Canada, 1990)			
June	18.20	-	-
July	12.73	-	-
August	9.97	-	-

Source: Environment Canada, 1998

Table 5.5 Monthly Flow Data for June, July and August for the Rideau River at Ottawa

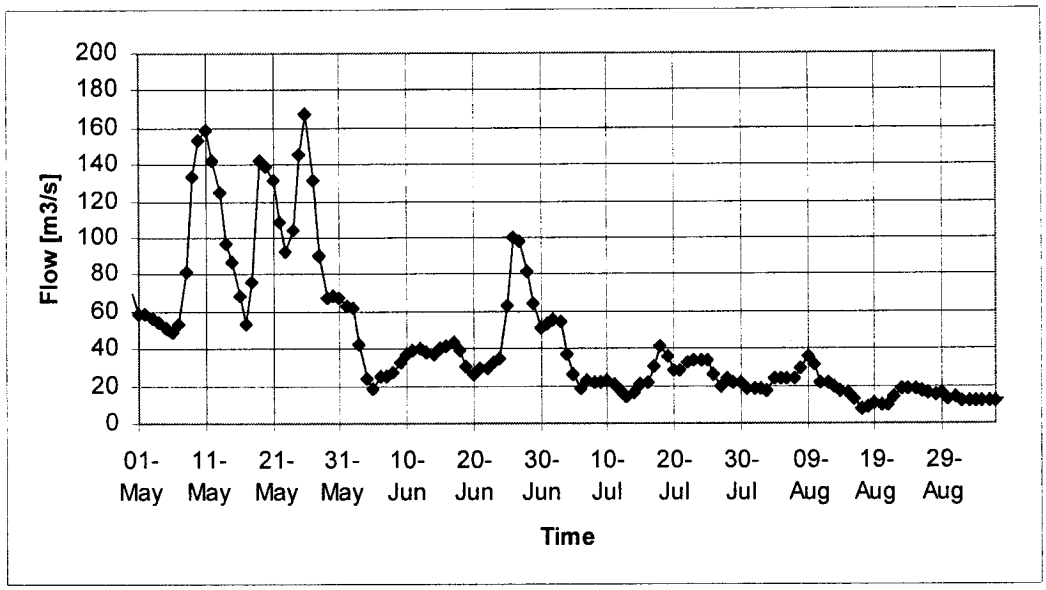

**Mean daily flows for year 2000 at the Rideau River at Ottawa-02LA004, Source: Environment Canada, 2001*

Figure 5.1 Flows at Hog's Back*- May-August 2000

5.5 Boundary Conditions

The upstream boundary was selected as a concentration-type Dirichlet boundary condition, which is one of the available options for the boundary conditions in the DISPERSIM. The downstream boundary was selected as an open-type boundary condition. On closed boundaries, Neumann-type was imposed according to which no flux could come in or out of the sides or closed boundaries. These boundaries were selected as they gave good results with no negative concentration values in the domain.

5.6 Selection of Dispersion Coefficients

In DISPERSIM, the diffusion coefficients are handled in such a way that the user is allowed to enter the multiplier factors for molecular diffusivity, vertical, horizontal and longitudinal diffusion.

As discussed before, dispersion around bends, groynes and dead zones is a relatively complex phenomenon. During initial simulations of phytoplankton growth, negative concentrations were observed in dead zones in Mooney's Bay. In order to remove these numerical oscillations the multiplier factor for longitudinal dispersion was selected as 2 whereas the horizontal factor was selected as 50. Dispersion coefficients are incorporated in DISPERSIM in such a way that assigning a value of 2.0 to the longitudinal dispersion weighting factor doubles the value of the longitudinal dispersion coefficient. The numerical oscillation, which cause negative values in dead zones and interface of main flow and dead zones in the Mooney's Bay could be solved by refining the mesh in those areas, which would require more modelling effort and computational time.

5.7 Calibration and Validation of Phytoplankton Growth Model

The calibration of the model was done for June 05, 2000, July 3, 2000 and July 20, 2000 and August 08, 2000 at stations RRBP 167A and RRBP 167B. Chl *a* data for DH 317 and DH318 were available for July 17, 2000 only and for that day Chl *a* data for the upstream station (RRBP 118A and RRBP 118B) were not available.

Table 5.6 gives the comparison of Chl *a* concentrations at the upstream station (RRBP 118) and station RRBP 167 in Mooney's Bay. The difference between the concentrations is large for August 08, 2000 as can be observed in Table 5.6. In all periods there is a general increase in Chl *a* as the water flows to the downstream station RRBP167.

Period	Measured Chl *a* at Black Rapids [ug L^{-1}]	Measured Chl *a* in Mooney's Bay [ug L^{-1}]
June 05, 2000	0.87	1.29
July 03, 2000	0.71	0.86
July 20, 2000	1.07	1.21
August 08, 2000	1.02	3.86

Table 5.6 Comparison of Measured Chl *a* Concentrations

Table 5.7 gives a list of constants, coefficients, and physical and numerical parameters used in the four simulations discussed above.

Constants and Coefficients		**Physical and Numerical Parameters**			
June 05, 2000					
k_{gmax} [d^{-1}]	1.70	T [°C]	17.73	B_L [-]	2
k_r [d^{-1}]	0.20	I_a[ly d^{-1}]	551	B_H [-]	50
I_s [ly d^{-1}]	300	f [-]	0.65	B_F [-]	0.01
k_e [m^{-1}]	0.5			D_{mol} [m s^{-2}]	1e-06
k_{sp} [mg-P L^{-1}]	0.01			Q [m^3 s^{-1}]	18.9
θ [-]	1.047				
v_s [m d^{-1}]	0.75				
July 03, 2000					
k_{gmax} [d^{-1}]	1.70	T [°C]	22.86	B_L [-]	2
k_r [d^{-1}]	0.20	I_a[ly d^{-1}]	516	B_H [-]	50
I_s [ly d^{-1}]	300	f [-]	0.65	B_F [-]	0.01
k_e [m^{-1}]	0.5			D_{mol} [m s^{-2}]	1e-06
k_{sp} [mg-P L^{-1}]	0.01			Q [m^3 s^{-1}]	54.7
θ [-]	1.047				
v_s [m d^{-1}]	0.75				
July 20, 2000					
k_{gmax} [d^{-1}]	1.70	T [°C]	22.49	B_L [-]	2
k_r [d^{-1}]	0.20	I_a[ly d^{-1}]	533	B_H [-]	50
I_s [ly d^{-1}]	300	f [-]	0.63	B_F [-]	0.01
k_e [m^{-1}]	0.5			D_{mol} [m s^{-2}]	1e-06
k_{sp} [mg-P L^{-1}]	0.01			Q [m^3 s^{-1}]	28.6
θ [-]	1.047				
v_s [m d^{-1}]	0.75				
August 08, 2000					
k_{gmax} [d^{-1}]	1.70	T [°C]	23.78	B_L [-]	2
k_r [d^{-1}]	0.20	I_a[ly d^{-1}]	485	B_H [-]	50
I_s [ly d^{-1}]	300	f [-]	0.60	B_F [-]	0.01
k_e [m^{-1}]	0.5			D_{mol} [m s^{-2}]	1e-06
k_{sp} [mg-P L^{-1}]	0.01			Q [m^3 s^{-1}]	29.4
θ [-]	1.047				
v_s [m d^{-1}]	0.75				

Table 5.7 List of Coefficients, Physical and Numerical Parameters

Figures 5.2 and 5.3 show the map of Chl *a* concentration for July 02, 2000. For large scale maps of Chl *a* concentrations for the four simulations, please refer to Appendix-B. The maximum concentrations are observed in the dead zone along the west bank of the Rideau River. Measurements in the dead zones are not available for year 2000 but limited data available in the Mooney's Bay for the year 1995 [Duffe et al., 1995] showed a similar trend.

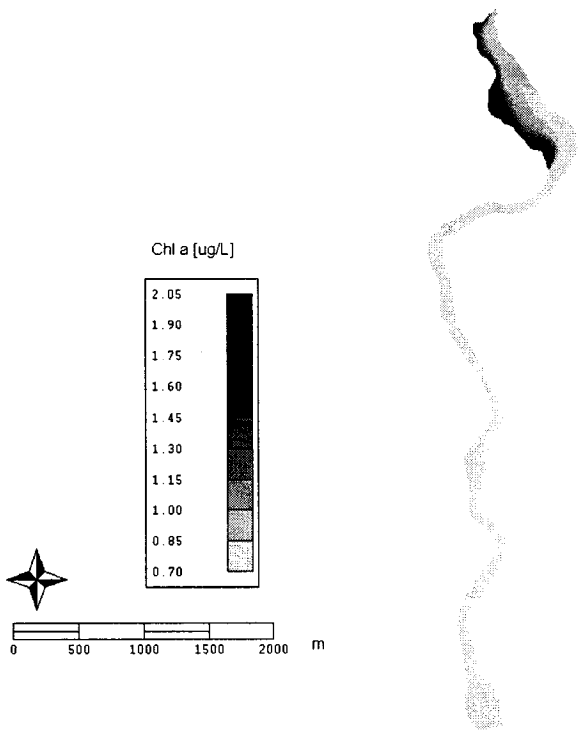

Figure 5.2 Simulated Chl *a* Concentrations in Black Rapids-Hog's Back Reach for July 03, 2000

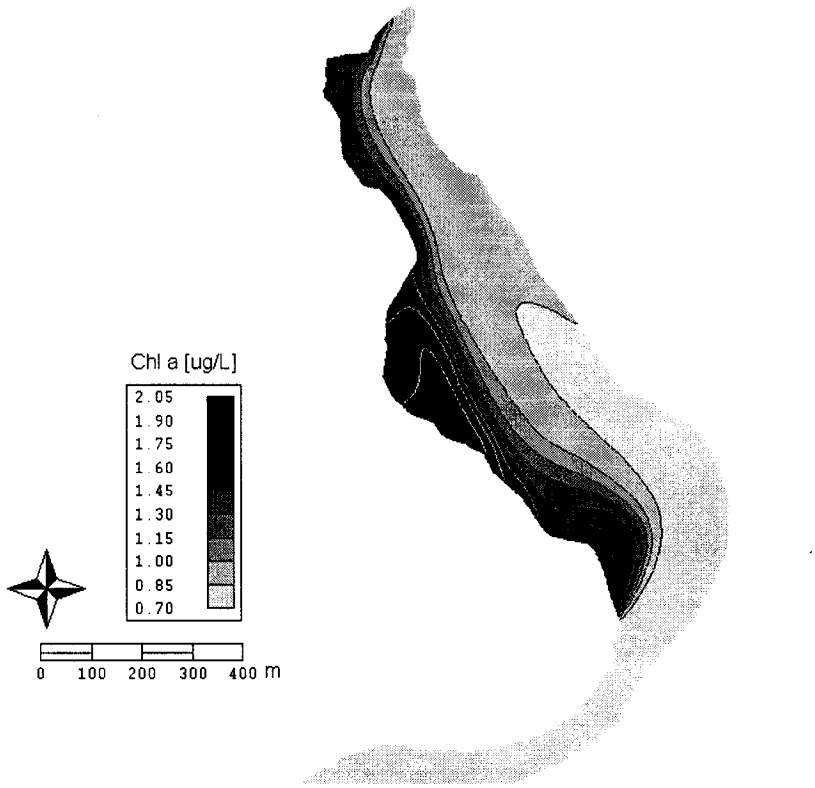

Figure 5.3 Simulated Chl *a* Concentrations in Mooney's Bay for July 03, 2000

Mass exchange between dead zones and the main flow is a complex phenomenon. At the interface of dead zones and main flow, eddies exist. The path of these eddies is not always the same. Sometimes they get trapped in the dead zone and sometimes they travel further downstream without any additional influence of the particular dead zone depending upon the flow conditions [Weitbrecht et al., 2001]. A mixing layer also exists at the interface, which has a three-dimensional circulation pattern. The exchange depends on the difference in concentrations between the main flow and the dead zones [Fischer et al., 1979]. These mechanisms govern the mass exchange between the main flow and dead zones.

Table 5.8 shows the comparison between measured and simulated Chl *a* concentrations. July 03, 2000 simulation gives the best comparison as only 2% error whereas there is –59% error for August 08, 2000.

Period	Station	Measured Chl *a* [ug L^{-1}]	Simulated Chl *a* [ug L^{-1}]	Error
June 05, 2000	RRBP 167A	1.29	1.06	-18 %
July 03, 2000	RRBP 167A	0.86	0.88	2 %
July 20, 2000	RRBP 167B	1.21	1.54	27 %
August 08, 2000	RRBP 167A	3.86	1.60	-59 %

Table 5.8 Comparison of Simulated and Measured Chl *a* Concentrations

In the months of June and August, the predicted values were on the lower side of measurements. The errors in simulated and measured Chl *a* concentrations were associated with the following sources, a) internal loading of phosphorus is not currently modelled; b) error in values adopted for PAR; c) error due to ignoring point load sources; d) error due to modelling of phytoplankton as a single group; e) errors in sampling and laboratory analysis. Considering that the errors associated with sampling and laboratory analysis were minor, the other sources of errors are discussed in Section 5.10.

5.8 Sensitivity Analysis

As discussed earlier, temperature, light and nutrients control the growth of phytoplankton. The main losses modelled in this study are losses due to respiration and settling. Most of the processes are modelled through first order and saturated type growth equations. In the following section the model is tested for its sensitivity to various constants and coefficients.

5.8.1 Response of Growth to Light

The model was tested to photoperiod (*f*). The range of photoperiod from June to August was 0.6 to 0.65 based on actual data. Figure 5.4 shows the change in light limitation due to variations in photoperiod. The increase in light attenuation factor from June to August was about 8%.

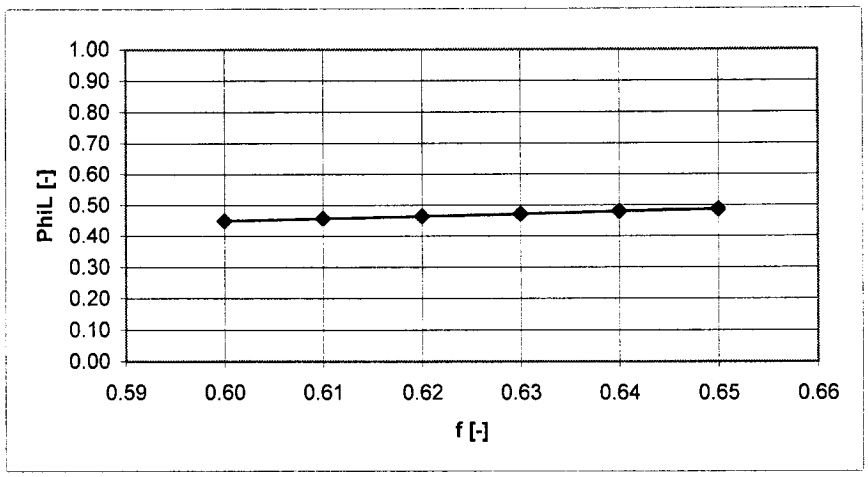

Figure 5.4 Response of Light Limitation (PhiL) to Photoperiod (f)-Data for July 03, 2000: I_a=516 ly d^{-1}, I_s=300 ly d^{-1}, D=5 m, K_e=0.5

The model was also tested for its response to changes in the light extinction coefficient (k_e). Figure 5.5 shows the response of light limitation to extinction coefficient and it can be observed that the light limitation was sensitive to k_e. According to WASP 6.0, the range of k_e is 0.1 to 5 and k_e for Lake Ontario was on the order of 0.5 m^{-1} [Thomann et al., 1987].

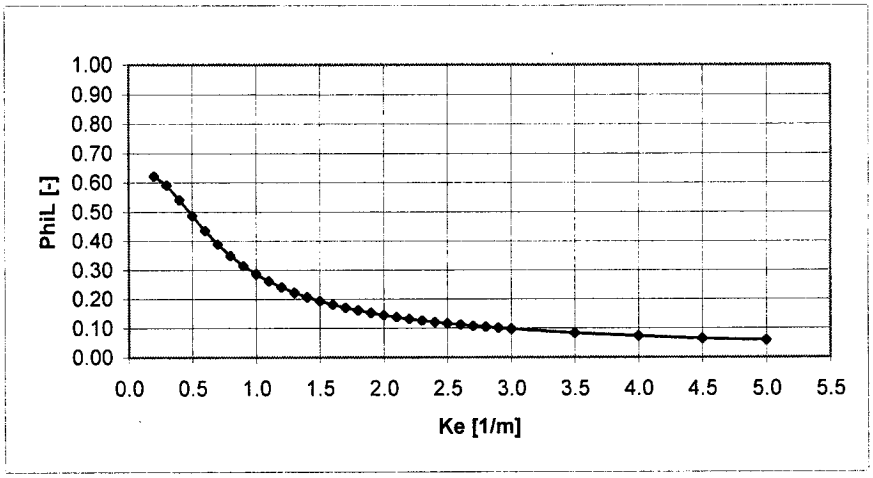

Figure 5.5 Response of Light Limitation (PhiL) with Light Extinction Coefficient (K_e)- Data for July 03, 2000: I_a=516 ly d^{-1}, I_s=300 ly d^{-1}, D=5 m, f=0.65

According to a study on Rideau River [Preece, 2001], the value of k_e was computed as 0.96 to 2.97 m^{-1} in the month of July, 2000. All the sampling sites were located between Merrickville and upstream of Jock River in that study (Fig. 5.6). It can be observed from Fig. 5.6 that the Chl *a* concentrations decreased in the downstream reach of the Rideau River, which is the modelled area in the present study. In the present study k_e is modelled as a global property but if data at sampling stations were available, it would be better to model k_e as a nodal property.

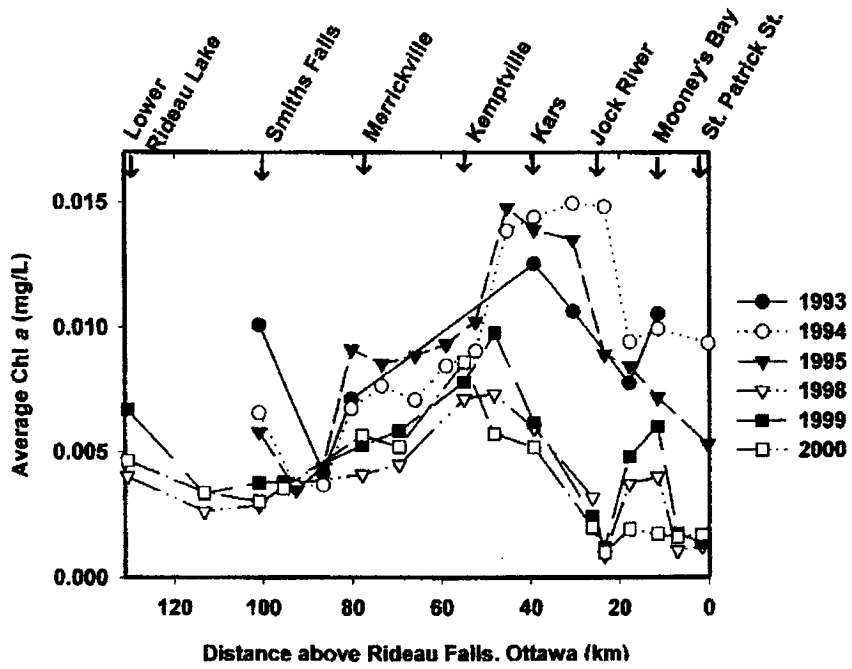

Figure 5.6 Average Annual Chl *a* Concentration, 1993-2000 [Rideau River Round Table, 2001]

In Steele's model, I_s is the optimal light level at which the algal growth rate is equal to the maximum growth rate. I_s values for a mixed population of phytoplankton are about 100 to 400 ly d^{-1} with 300 ly d^{-1} as an approximate average [Thomann et. al., 1987]. The model was tested for a range of I_s between 200 and 500 ly d^{-1}. Figures 5.7 and 5.8 show the results of this analysis.

Two analyses were done with depths of 5 and 10 m, other parameters used in the analysis were as follows, $k_e = 0.5$ and $f = 0.65$, which were the values adopted from the July 03, 2000 simulation. The light attenuation effect, at 5 m depth, is less than for 10 m depth for a range of values of I_s.

Effect of photoinhibition is more pronounced in 5 m depth analysis. From Figs. 5.7 and 5.8, it can be seen that light attenuation is a function of many parameters and analyzing them independently may not represent the true picture.

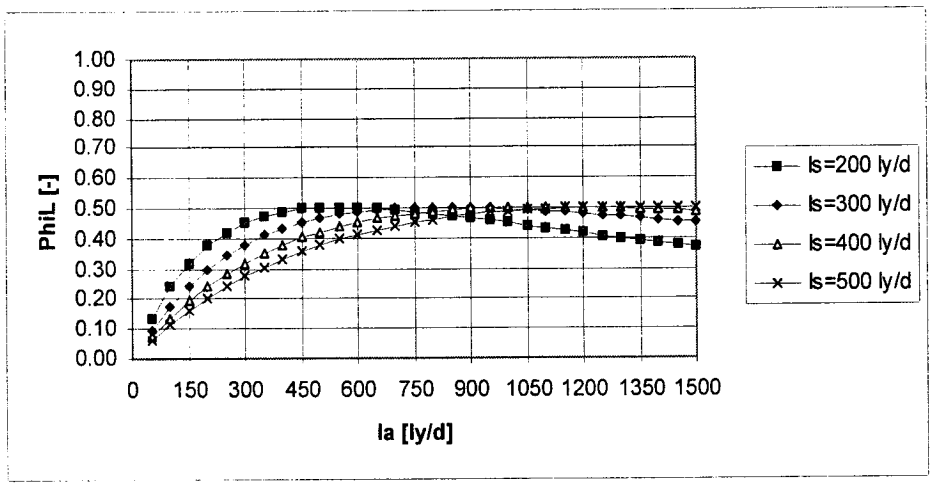

Figure 5.7 Response of Light Limitation (PhiL) to Optimum Light Intensity (I_s) for Depth of 5 m

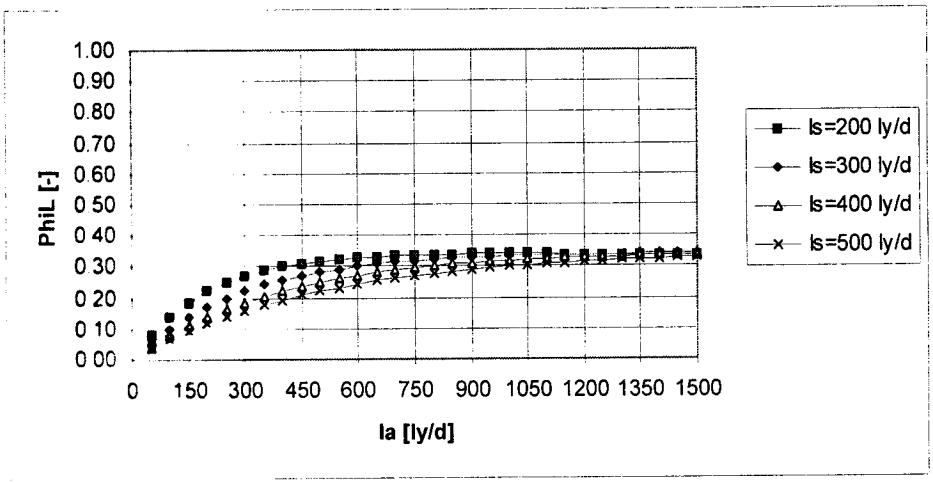

Figure 5.8 Response of Light Limitation (PhiL) to Optimum Light Intensity (I_s) for Depth of 10 m

Simulations were carried out to see the effect of PAR on concentrations of Chl *a* at station RRBP 167B for different periods. The results of this analysis are shown in Fig. 5.9.

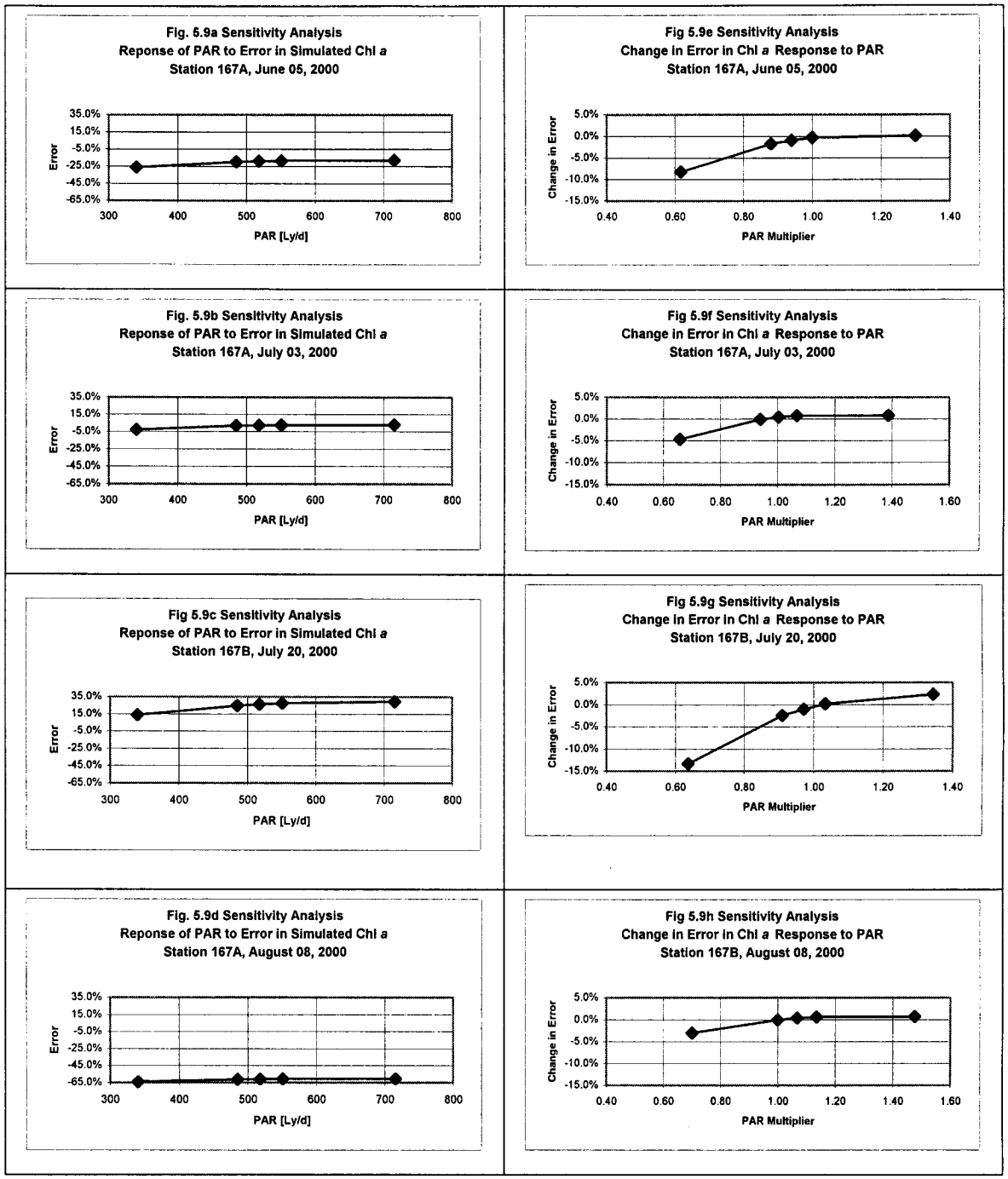

Figure 5.9 Response of Chl *a* Concentrations to PAR

Figures 5.9a to 5.9d give the variation in simulated Chl *a* concentration for a particular period with response to a range of PAR between 350 and 750 ly d^{-1}. Figures 5.9e to 5.9h show the variation in simulated Chl *a* concentration as a function of PAR multiplier, where 1 is the value

corresponding to the PAR used in that specific simulation. PAR measurements were not available for Ottawa for the year 2000 during the time frame of this study. Since the PAR measurements were not available, the range for above analysis was adopted from Lide et al., (1995), which gives the total solar radiation in a cloudless sky for various latitudes. PAR was assumed to be 45% [Chapra, 1997] of the energy in the complete standard spectrum [Chapra, 1997]. Effect of cloud was also not simulated in the present study and it can be observed from Figs. 5.9e to 5.9h that cloud cover may have an impact on growth of phytoplankton.

5.8.2 Response of Growth to Temperature

The range of measured temperatures at all sampling stations for the sampling period, May 02, 2000 to Sep. 25, 2000 was 12.56 to 24.24^{0}C with the maximum values observed on August 08, 2000. Figure 5.10 shows the model sensitivity to temperature for two theta values. It is important to remember that growth rate is a first order function and change in growth limitation factor can affect the results for phytoplankton growth exponentially.

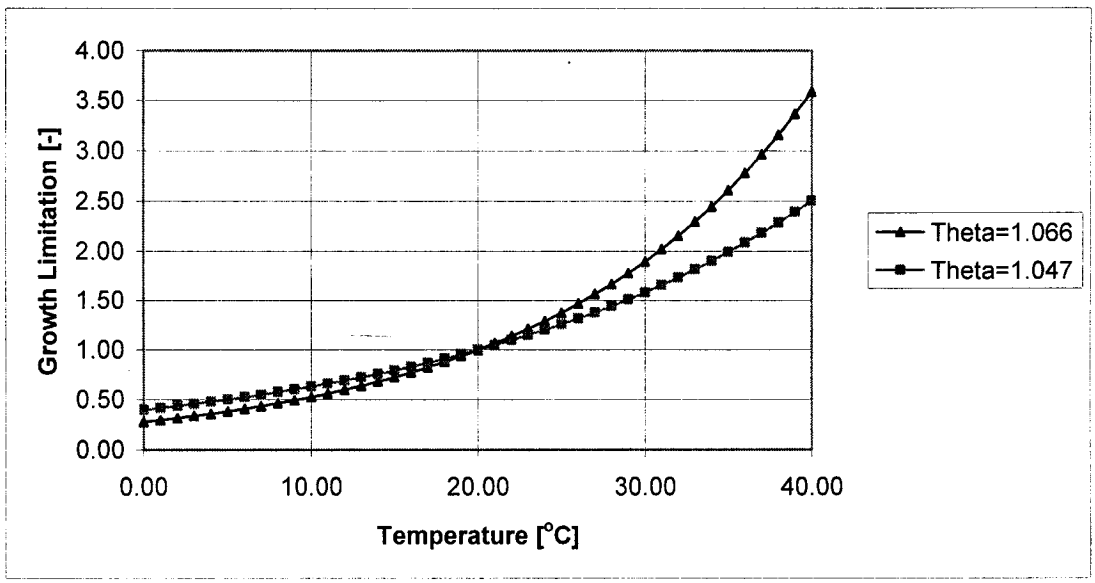

Figure 5.10 Response of Phytoplankton Growth to Temperature

5.8.3 Response of Growth to Flow

Simulations were carried out to understand the impact of flow on phytoplankton growth. Figure 5.11 shows the results of such simulations. The flow was normalized to the measured flow on July 20, 2000. The rate constants, coefficients and parameters were kept the same as in the July 20, 2000 simulation.

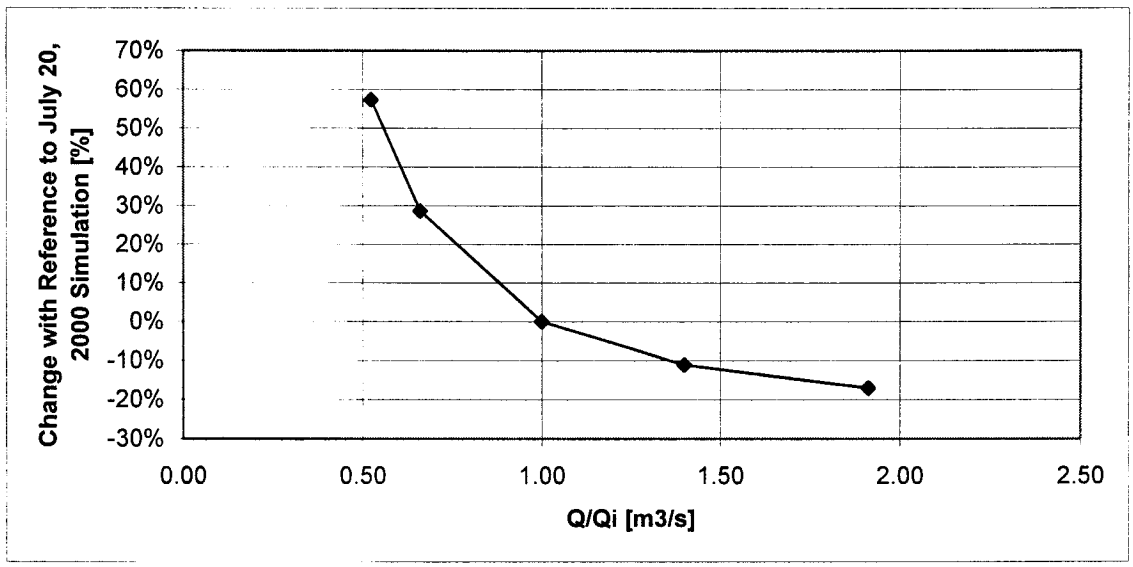

Figure 5.11 Response of Phytoplankton Growth to Flow Simulation for July 20, 2000 ($Q=28.6\ m^3 s^{-1}$), Station RRBP 167B

It can be observed from Fig. 5.11 that growth is a non-linear function of (normalized) flow. The slope for low flows is more pronounced than the higher flows. This can be associated to the fact that as the flow decreases the age of water or retention time increases. The growth is an exponential function of age of water or time and this effect causes the non-linearity observed in Fig. 5.11.

5.8.4 Response of Growth to Limiting Nutrient

Phosphorus is the limiting nutrient in the study reach. Figure 5.12 shows the response of growth to RP. The limits of RP in the study reach from June to August 2000 were 0.016 to 0.04 mg-P L^{-1}. The selected value of k_{SP} in the simulations was 0.01 mg-P L^{-1}. Section 3.5.1 provides more detail on selection of k_{SP}. It can be observed from Fig. 5.12 that k_{SP} equal to 0.01 mg-P L^{-1} represents the Michaelis-Menten saturated type model although lower values may also be used for better calibration. It is suggested in later sections that k_{SP} should be computed from experiments in order to get better calibration of the model.

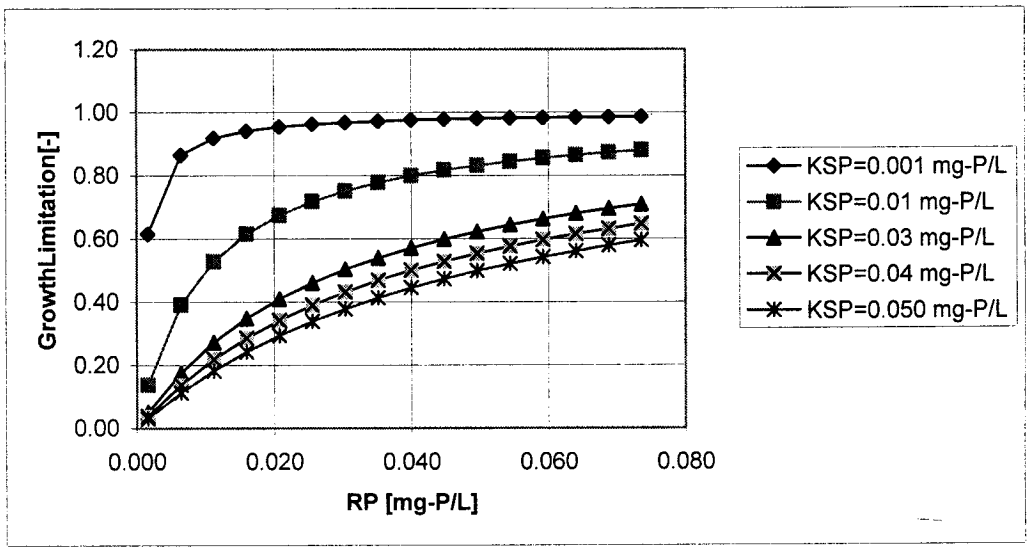

Figure 5.12 Response of Growth to Reactive Phosphorus for Various K_{SP} Values

5.9 Water Age Modelling

More discussion is given on modelling of age of water in Section 2.8. As discussed before, one of the primary interests in water quality modelling is not only to estimate the average residence time at a location but also to compute the age of a particle at different locations in a river such as dead zones. By doing so, one is able to evaluate whether a steady-state simulation is appropriate or not. As a rule-of-thumb, one needs to have relatively steady boundary conditions for a time

period of the same magnitude as the maximum age of water in the domain to make the steady-state simulation relevant.

The following equation was incorporated in DISPERSIM to compute the age of water in the domain [Li Xianting et al., 1999].

$$U_x H\frac{\partial A_w}{\partial x}+U_y H\frac{\partial A_w}{\partial y}-\frac{\partial}{\partial x}\left(H\left(D_{xx}\frac{\partial A_w}{\partial x}+D_{xy}\frac{\partial A_w}{\partial y}\right)\right)-\frac{\partial}{\partial y}\left(H\left(D_{xy}\frac{\partial A_w}{\partial x}+D_{yy}\frac{\partial A_w}{\partial y}\right)\right)=H(1) \tag{5.7}$$

Where A_w is the water age and D is the diffusion coefficient. The source term 1 represent the aging process of 1 s s^{-1}. This analogy was applied to the transport equation for water flow and water particle age at any arbitrary location in the river was computed, assuming that the age of the water entering the domain under analysis to be 0.

Three steady-state simulations were carried out with different flows. The summary of results of the three simulations is presented in Table 5.9.

Simulation Period	Flow [$m^3 s^{-1}$]	Age of Water at Station 167A [hrs]	Maximum Age of Water in Dead Zone [Days]	Age (Exit-Entrance) of Mooney's Bay [hrs]
July 03, 2000	54.7	14.70	3.7	6.92
July 20, 2000	28.6	30.14	5.8	20.69
June 05, 2000	18.9	43.72	5.8	27.79

Table 5.9 Water Age for Various Flows

The results are plotted in Figure 5.13, which show that there is a negative non-linear relationship between flow and water age. Figures 5.14 to 5.19 show the distribution of water age in the River for various flows. It was found out that the oldest particles of water were present in the dead zone, west of Mooney's Bay.

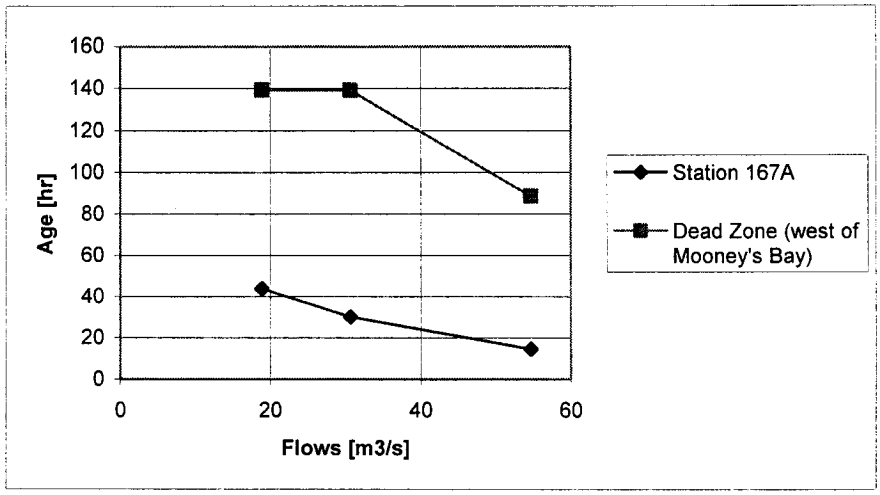

Figure 5.13 Plot of Water Age for Various Flows

The water age in dead zones becomes constant at 5.8 days. This phenomenon may not be true in nature and it appears that in the dead zone, during low flows, the effect of advection is so small that numerical diffusion is controlling the transport of material. In other zones, the effect of numerical diffusion is less and the water age varies with flow.

It is reported [Duffe et al., 1995] that the average annual residence time in Mooney's Bay is on the order of 2.4 days. The average residence time depicts the average of the residence time in main flow zones and dead zones whereas water age modelling gives the distribution of water age over the domain. The water age was computed in the Mooney's Bay by subtracting the water age just upstream of the Bay from the exit and the results are given in Table 5.9. This gives the residence time along the main flow on the eastern bank of the Mooney's Bay and does not include the effect of dead zones along the western bank. No measurements or tracer test results were available to compare the numerical model study results but a trend of higher Chl *a* concentrations in the dead zones was observed in Mooney's Bay [Duffe et al., 1995], which suggests that the areas with oldest age support the habitat for phytoplankton growth.

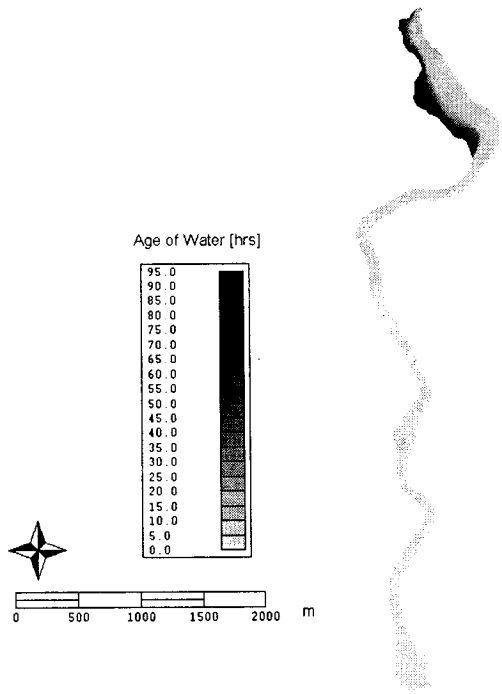

Figure 5.14 Age of Water for Flow of 54.7 $m^3 s^{-1}$ in Black Rapids-Hog's Back Reach

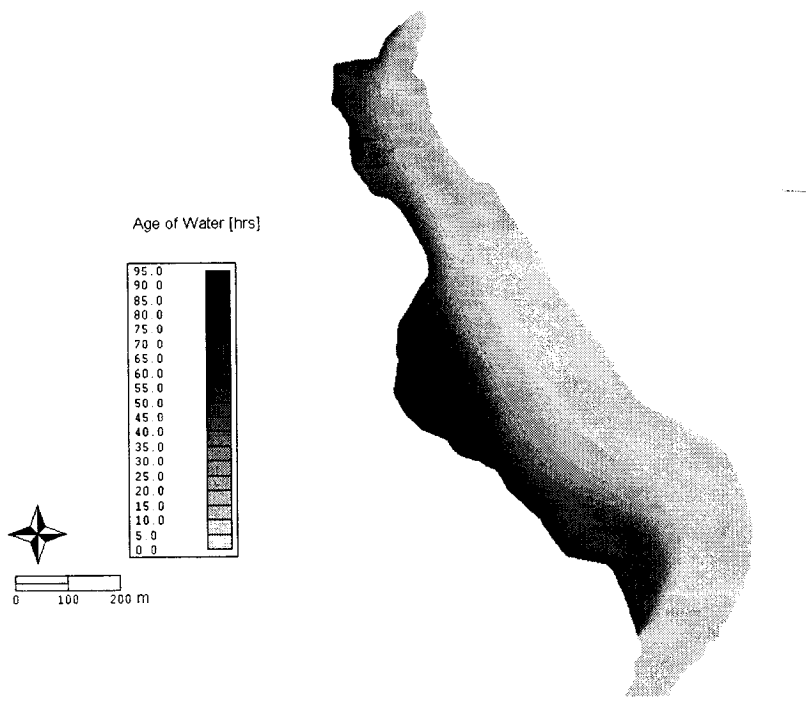

Figure 5.15 Age of Water for Flow of 54.7 $m^3 s^{-1}$ in Mooney's Bay

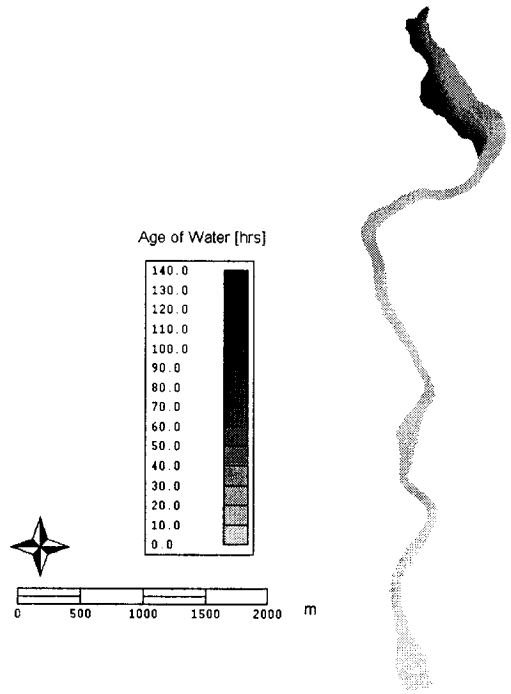

Figure 5.16 Age of Water for Flow of 30.7 $m^3 s^{-1}$ in Black Rapids-Hog's Back Reach

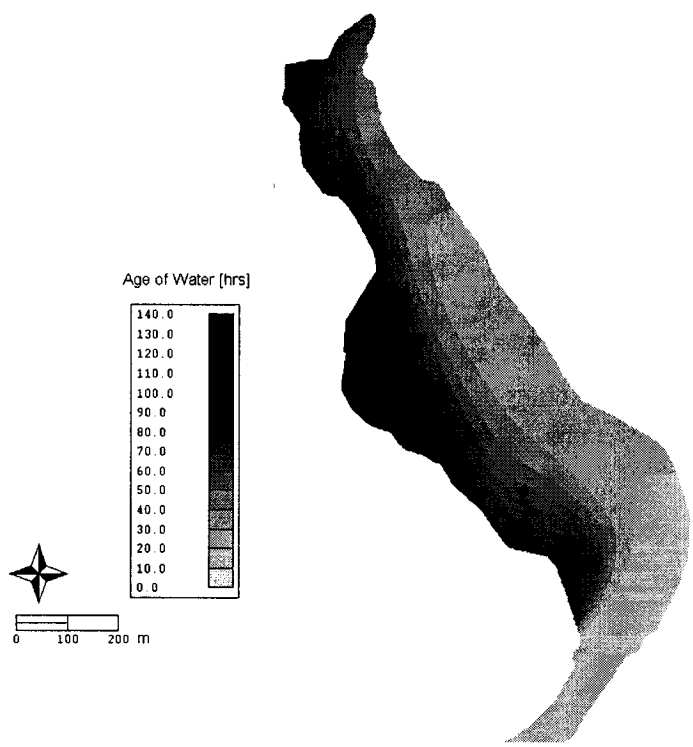

Figure 5.17 Age of Water for Flow of 30.7 $m^3 s^{-1}$ in Mooney's Bay

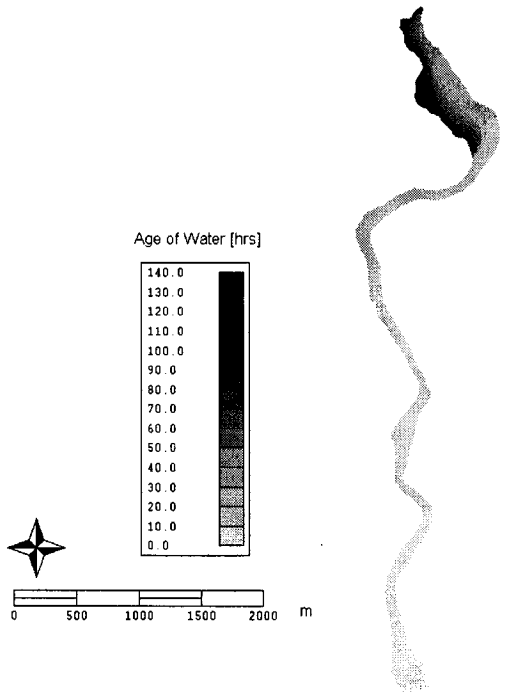

Figure 5.18 Age of Water for Flow of 18.9 $m^3 s^{-1}$ in Black Rapids-Hog's Back Reach

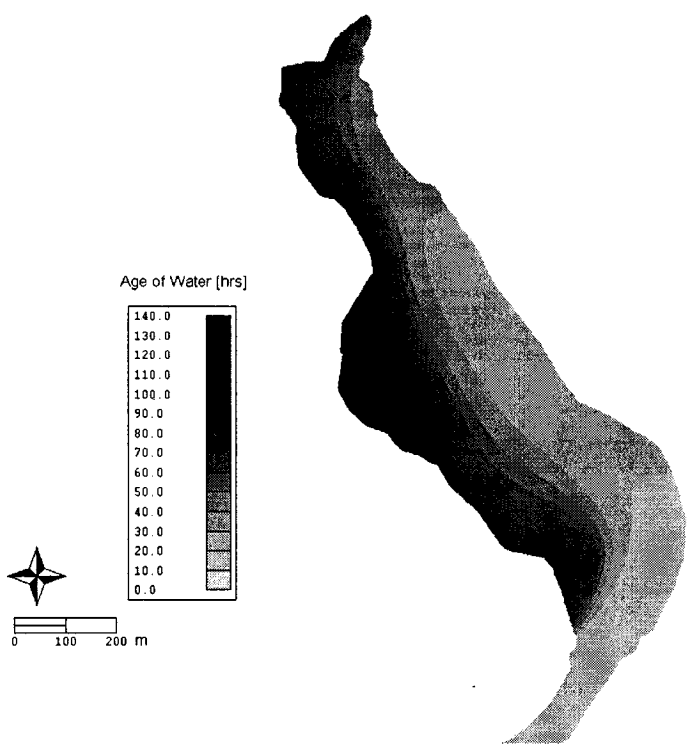

Figure 5.19 Age of Water for Flow of 18.9 $m^3 s^{-1}$ in Mooney's Bay

5.10 Discussion

Steady state simulations were done for June 05, 2000, July 03, 2000, July 20, 2000 and August 08, 2000. The results of the phytoplankton growth and transport model matched well with the measurements in the Mooney's Bay for July 03, 2000 simulation. Keeping in mind the sampling and analytical errors, the simulated values for June 05, 2000 and July 20, 2000 were also reasonably close to the measured values. The model under-estimated the measured values for August 08, 2000 simulation by 59%. The growth and water age elements developed in the present study were validated with analytical/numerical solutions of the developed equations.

The developed model has some limitations and one is that variables such as k_e and T are modelled as global properties, whereas it might be more appropriate to model them as a nodal property (variable in space). No data on k_e for the sampling stations were available to try to model it as a nodal property. It is expected that modelling k_e and T as nodal property will improve the results but still a difference of 59% on August 08, 2000 is not expected to be reduced much by doing so.

Anoxic conditions at station 167B developed close to bottom of Mooney's Bay on August 08, 2000 as shown in Fig. 3.8. Since the numerical model underestimated the measured Chl *a* by 59% on August 08, 2000 simulation, internal loading of phosphates could be a source of error. One limitation of the model is that currently, the internal cycle of phosphorus is not modelled and measured values of *RP* were used in computing the growth limitation factor for phosphorus. Analyses of data show that phosphorus values did not vary much in space but somewhat varied in time. This would mean that during most of the summer the upstream boundary condition and point sources for phosphorus primarily affects the phosphorus concentrations downstream but during August when anoxic conditions developed in the Mooney's Bay, the internal phosphorus loading could be a source of food for phytoplankton. In order to model the phosphorus cycle more data on particulate organic phosphorus and reactive phosphorus are required.

Grazing losses are also not currently modelled as more data are required on the spatial distribution of zooplankton and/or zebra mussels. If the spatial distribution were not uniform in the present study reach, then this would have an impact on the predicted values.

Flow data and water quality data of point sources were not available and thus these point sources were ignored. Figure 3.3 shows the location of major point load sources in the study reach. More data including flow measurements and water quality are required to assess the impact of these point load sources on phytoplankton dynamics in the Rideau River. The point sources and upstream boundary conditions have an influence on phytoplankton dynamics. Considering the importance of other variables and limitations in the model, it is expected that the effect of lateral inflows will have a major impact on phytoplankton growth.

One interesting observation regarding Chl *a* measurements was that the concentrations were higher at station DH 318 than station DH 317 for May 02 and July 17, 2000 (Fig. 3.10). Station DH 317 is downstream at about 1.4 km of station DH 318. No Chl *a* data were available for upstream stations at RRBP 118A and RRBP 118B on the dates for which Chl *a* data are available for DH 317 and DH 318. One possible reason for this behaviour could be that two point sources discharge at station DH 318 namely, Bentley and Riverwalk Park. Bentley is a wet pond and Riverwalk Park is a wetland type treatment facility. It could be possible that wetland/wet pond type of facility have higher concentrations of Chl *a* in their effluent but more measurements are required to determine this.

In the present study phytoplankton are modelled as single group. It is known that the growth rates of various species are different [Chapra, 1997]. Apart from other variables, the net growth of specific species is a function of settling rate, light and temperature. The settling rates also differ for various species. Diatoms can spontaneously increase their sinking rate under unfavorable conditions [Reynolds, 1984]. On the other hand planktonic cyanobacteria are buoyant organisms that can float [Reynolds, 1984].

In Steele's equation for light limitation (refer to Section 3.5.1.2), I_s is the optimal light level at which growth rate is equal to maximum growth rate. I_s ranges from about 100 to 400 ly d^{-1} and lower values are used for species, which adapt to low light and the higher values are for high

light adapted species. [Chapra, 1997]. A test simulation was carried out by lowering the value of I_s to 200 ly d^{-1} for August 08, 2000 and an increase of only 3% was observed in Chl *a* concentration at station RRBP 167A. This shows that I_s would not have a strong impact on the growth.

In the present study, the Theta model for temperature correction was used. The Theta model is typically used when phytoplankton are simulated as single state variable or group [Chapra, 1997]. It implies that there will always be species that grow at any particular temperature. Studies have shown that the major algal groups have different sensitivities to temperature (Fig. 3.12). Groups such as diatoms grow at lower temperatures and blue-green algae grow faster at higher temperatures [Chapra, 1997].

Based on the above discussion it seems that modelling phytoplankton as different species would be a better approach but for that data regarding taxonomy would be required to assess the type of species in a particular period and location.

Predicting the distribution of the age of the water is a better approach than estimating the average residence time. The model successfully computed the water age in zones of main flow for a range of flows but under low flows the results were not satisfactory in the dead zones. Under low flows the effect of advection in the dead zones is so small that numerical diffusion is controlling the transport of material. Water age modelling also helped to evaluate whether a steady-state simulation was appropriate or not. The results in the dead zone suggest that one should be careful in depicting the phytoplankton model results in the dead zone unless data are available to verify the results.

CHAPTER 6

6 CONCLUSIONS & RECOMMENDATIONS

A two-dimensional phytoplankton growth modelling was successfully carried out. The developed model showed a good agreement with the measurements for the three out of four simulation periods considering the sampling and analytical errors. The model can be useful in the assessment of the relative responses of the river to various management options. The following paragraphs give a summary of the conclusions drawn from the present study and recommendations for future studies and improvements of the model are also presented.

6.1 Conclusions

The simulated values of the flow model agree with the measurements and MIKE3D model

HYDROSIM was successfully used to model the flows in the Rideau River (Black Rapids-Hog's Back Reach). The simulated results of velocity vectors showed an agreement with the AFFRA measurements although the simulated values were always on the lower side. The modelling results of MIKE3D and the study carried out in 1997 [Baird & Associates, 1997] support the results of the flow modelling in the present study.

Simulated values of phytoplankton in transport model agreed well with the measurements except for the August 08, 2000 simulation

The phytoplankton element was successfully added in the DISPERSIM model. The results of the phytoplankton growth and transport model matched well with the measurements in the Mooney's Bay for July 03, 2000 simulation. The simulated values for June 05, 2000 and July 20, 2000 were

also reasonably close to the measured values. The model under-estimated the measured values for August 08, 2000 simulation by 59%.

Modelling of phosphorus may have an impact on the results during anoxic conditions development

At station 167B, anoxic conditions developed on August 08, 2000 as shown in Fig. 3.8. Since the numerical model underestimated the measured Chl *a* by 59% on the August 08, 2000 simulation, internal loading of phosphates might be a source of error. One limitation of the model is that currently, the internal cycle of phosphorus is not simulated and measured values of *RP* were used in computing the growth limitation factor for phosphorus. In order to model the phosphorus cycle more data on particulate organic phosphorus and reactive phosphorus are required.

Point sources could have an impact on phytoplankton dynamics

Station DH 318 is upstream of station DH 317 but the available measurements of Chl *a* showed higher concentration at DH 318 than DH 317. Since no point sources were modelled in the present study, this phenomenon could not be simulated. Two point sources, namely: Bentley (wet pond) and Riverwalk Park (wetland), discharge near upstream station DH 318 and it appears that the higher concentrations of phytoplankton are the result of these point sources. It is anticipated that if more refinement of the model is desired then point sources have to be simulated in the model.

Water age modelling is a useful tool for estimating the reaction time of the domain

Water age was modelled and the distribution of water age was computed in the river for various flows. Water age modelling helped to evaluate whether a steady-state simulation was appropriate or not. The results in the dead zone suggest that one should be careful in depicting the phytoplankton model results in the dead zone unless data are available to verify the results.

Refinement of the model and revised water quality sampling could improve the predictions

Simulating the phytoplankton dynamics in transient state could have an impact on the predictions. Modelling the variables such as k_e and T as nodal properties will improve the results but still a difference of 59% on August 08, 2000 is not expected to be reduced much by doing so. Modelling phytoplankton as several different groups of species would be a better approach but for that data regarding taxonomy would be required to assess the type of species in a particular period and location. Currently, the grazing losses are not simulated and if the distribution of predators is not uniform in the study reach, this could have an impact on the results.

6.2 Recommendations

6.2.1 Continuation of the Study

It is recommended to continue the present research in order to fine-tune the present model and simulate the phytoplankton dynamics in other reaches of the Rideau River. A work plan is proposed below to continue the present work and fields of further studies have also been identified where improvements in the model and the measurements are still required.

6.2.1.1 Proposed Work Plan

It is proposed that the first step in the continuation of present study would be the refinement of the existing model in the Black Rapids-Hog's Back Reach of the Rideau River. In order to do so following recommendations are listed in the order of priority.

1. Since the system is phosphorus limited and the internal loading could be a important source of nutrients during anoxic conditions, data to confirm the development of such conditions and also data on particulate organic phosphorus and soluble reactive phosphorus are required to model the phosphorus cycle. Analysis for computing half saturation growth constant for phosphorus would also help in fine-tuning the model. Based on these data the phosphorus cycle could be then modelled.
2. Measurements for inflows from Bentley (wet pond) and Riverwalk Park (wetland) point sources should be carried out or daily flow data from these point sources should be collected, if available. Water quality parameters should be measured close to the outfall of these point sources.
3. Two sampling stations are proposed along with the existing stations for future water quality sampling in the Black Rapids-Hog's Back Reach. One water quality sampling station is proposed at downstream of the Black Rapids Lock. The station should be

in the middle of the River and at about 50 m downstream of the fall to represent the average conditions downstream of the Black Rapids. A second station is proposed in the dead/recirculation zone along the north-west side of the Mooney's Bay as identified in Fig. 4.10.

4. It is recommended that water quality sampling be done at all stations with a shortest interval of time possible. May, June, July and August is a good period for sampling and the measurements as the phytoplankton densities are maximum in this period. Attempt should be made to do the sampling and measurements at the sampling stations in one day. This may be repeated over four to five times in each month. This will give true temporal and spatial variations along the river.
5. The following water quality parameters are recommended for sampling and analyses in the laboratory: Chl *a*, *PAR*, *T*, particulate organic phosphorus, *SRP*, *DO*, *Eh*, k_e.

   The depth profiles of temperature, dissolved oxygen, *Eh* are to be measured in Mooney's Bay only to check if the Bay stratifies and also to see if internal loading of phosphorus occurs. Other measurements should be depth-averaged. Measurements for *PAR* should also be carried out to properly incorporate the impact of light on growth. Measurements on zooplankton and zebra mussels will also help to incorporate the grazing losses in the growth equation, if there is a strong spatial variation in their density.

6. Accurate depth-averaged current velocities should be measured to properly calibrate the flow model at the sampling stations. Water levels at downstream of water control structures such as Black Rapids should also be measured for better calibration of the model.
7. Growth rate and settling rate of various species of phytoplankton are different. In the present study the phytoplankton were modelled as a single group. It would be interesting to analyze the taxonomy of the phytoplankton so that the assessment of the species could be done in time and space. This would fine tune the model as various species respond in a different way to the state variables.
8. After fine tuning the model, it is recommended that in the next step the model be extended to upstream reaches of the Rideau River.

7 BIBLIOGRAPHY

1. Baird and Associates, June, 1994. *Mooney's Bay Hydraulic Study, Draft Report.*
2. Baird and Associates, September, 1997. *Development of a Numerical Model of Mooney's Bay, Final Report.*
3. Baird and Associates, 1998. *Numerical Modelling of the Rideau River: Phase II. Final Report.*
4. Baird and Associates, 2000. *Assessment of Discharge Criteria for Stormwater Facilities on the Rideau River. Draft Report.*
5. Baird and Associates, 2001. *Numerical Modelling of Bacterial Dispersion in Mooney's Bay.*
6. Basu B. K. and Pick F. R. 1996. "Factors Regulating Phytoplankton and Zooplankton Development in Temperate Rivers". *Limnol. Oceanogr.*, 41: 1572-1577.
7. Basu B. K. and Pick F. R. 1997. "Phytoplankton and Zooplankton Development in a Lowland Temperate River". *Journal of Plankton Research*, 19 (2): 237-253
8. Bowie, G.L., W.B. Mills, D.B. Porcella, C.L. Campbell, J.R. Pagenkopf, G.L. Rupp, K.M. Johnson, P.W.H. Chan, S.A. Gherini and C.E. Chamberlin, 1985. "Rates, Constants, and Kinetics Formulations in Surface Water Quality Modeling". Second Edition. U.S. Environmental Protection Agency Athens, GA. *EPA-600/3-85-040.*
9. Canadian Museum of Nature: http://www.nature.ca/rideau
10. Chapra, S. C., 1997. *Surface Water Quality Modeling.* ISBN: 0-07-011364-5, McGraw Hill, USA.
11. Chaudhry M. H, 1994. *Open Channel Flow.* ISBN: 81-203-0863-8
12. Chow, Ven Te, 1973. *Open Channel Hydraulics*, McGraw Hill, Inc.
13. City of Ottawa. Information Technology Branch. 1:15 000 Photomosaic Mapping. [computer file]. Ottawa : City of Ottawa, 2000.
14. Darley W. Marshall, 1982. *Algal Biology: A Physical Approach.* Blackwell Scientific Publications.
15. Deas M. L. and Orlob G.T., 1999. "Klamath River Modeling". *Report No. 99-04. University of California, Davis.*

16. Descy J. P. and Gosselain V. 1994. "Development and Ecological Importance of Phytoplankton in a Large Low-Land River (River Meuse, Belgium)". *Hydrobiologia*, 289: 139-155.
17. Duffe J & RMOC, 1995. *An Assessment of the Plankton in the Lower Reaches of the Rideau River and Mooney's Bay in 1995.*
18. E. Everbecq, V. Gosselain, L. Viroux and J. P Descy. 2001. "POTAMON: A Dynamic Model for Predicting Phytoplankton Composition and Biomass in Lowland Rivers". *Water Resources*, Vol. 35, No. 4, Elsevier Science Ltd.
19. Environment Canada, 1998. *HYDAT CD-ROM:*, Ver. 96-1.04, July 24, 1998.
20. Environment Canada, 2001. Canadian Daily Climate Data on CD-ROM-Eastern Canada.
21. Fischer H. B. et. al., (1979): Mixing in Inland and Coastal Waters. Academic Press.
22. Gouri Dhatt, 1992. "Finite Element Modelling of Fluids, Lecture Notes". Université de Technologie de Compiegne, France.
23. Heniche, M., Secretan, Y & Leclerc, M. 2000. *HYDROSIM User's Guide 1.0a06.* Québec, INRS-Eau
24. INRS-EAU. 2000. DISPERSIM: Research Report on DISPERSIM. No. R-558.
25. Kadlec R. H. Knight R. L, 1996. *Treatment Wetlands*. CRC/Lewis Publishers.
26. Kalff, J., (2002). *Limnology-Inland Water Ecosystems*. Prentice Hall, ISBN: 0-13-033775-7.
27. King, I. P., 2002. RMA models- Technical Aspects.
28. Leopold, L. B., M. G. Wolman and J. P. Miller, 1964. *Fluvial Processes in Geomorphology*. W. H. Freeman, San Francisco, California, USA.
29. Waterloo Maple Inc., 2001. Maple 7.00.
30. Martin J. L. and McCutcheon S. C., 1999. *Hydrodynamics and Transport for Water Quality Modeling*. Lewis Publishers
31. Moss, B.., Booker I., Balls, H., and Manson K. 1989. "Phytoplankton Distribution in a Temperate Flood Plain Lake and River System I". *Hydrology, Nutrient Sources and Phytoplankton Biomass. J. Plankton Res.*, 11: 813-838.
32. Palmer M. D., 2001. *Water Quality Modeling-A Guide to Effective Practice*. The World Bank, Washington, D.C.
33. Preece J., 2001. *The Role of Hydraulic "Dead Zones" in the Development of Phytoplankton in the Rideau River, Ontario*. M.Sc. Thesis, University of Ottawa .

34. QUAL2E, 1987. *The Enhanced Stream Water Quality Models QUAL2E and QUAL2E-UNCAS.* Documentation and Users' Manual, Environmental Research Laboratory, USEPA.
35. Reynolds, C. S., 1984. *Freshwater Phytoplankton Ecology.* Cambridge University Press, New York.
36. Reynolds, C. S., 1995. "River Plankton: The Paradigm Regained. The Ecological Basis for River Management". John Wiley and Sons, 161-174
37. Reynolds C.S., 2000. "Hydroecology of River Plankton: The Variability in Channel Flow". *Hydrological Processes*, 14: 3119-3132.
38. The Rideau River Roundtable, 2001. *The Rideau River-State of the River Report.*
39. RMA2 User's Guide, 2001. US Army, Engineer Research and Development Center Waterways Experiment Station Coastal and Hydraulics Laboratory.
40. RMOC, 1992. *Rideau River Stormwater Management Study*, 1990-91. Final Draft Report.
41. Rodi Wolfgang, 1984. "Turbulence Models and Their Application in Hydraulics. State-of-the-Art Paper". *IAHR.*
42. Secretan, Y., Roy, Y. & al., 2000. *MODELEUR: User's Guide 1.0a07.* Québec, INRS-Eau
43. Soballe, D.M and Kimmel, B. L. 1987. "A Large Scale Comparison of Factors Influencing Phytoplankton Abundance in Rivers, Lakes and Impoundments". *Ecology*, 68: 1943-1954.
44. SOBEK Technical Reference Manual , 2001. WL | Delft Hydraulics.
45. Stephen J. T. and Rubitschum C., 1981. "Comparisons of Soluble Reactive Phosphorus and Orthophosphorus Concentrations at an Offshore Station in Southern Lake Michigan". *J. Great Lakes. Res.* 7(3): 290-298.
46. Thomann R. V and Mueller J. A., 1987. *Principles of Surface Water Quality Modeling and Control.* Harper Collins Publishers Inc.
47. Walks D and Cyr Helene, 2001. "Does it Makes Sense to Use Leopold's Water Residence Time Equation for River Plankton?" Poster Presentation. Department of Zoology, University of Toronto, Canada
48. WASP Ver 6.0. *Draft User's Manual.* USEPA.

49. Weitbrecht V. & Jirka G. H., 2001. "Flow Patterns and Exchange Processes in Dead Zones of Rivers". Proceedings of the *IAHR Congress, 2001, Beijing.*

50. Wetzel, R.G. 1983. *Limnology*, 2nd Ed. Harcourt Brace College Publishers, New York, NY.

51. Lide D. R, Frederikse H.P.R, 1995. *CRC Handbook of Chemistry and Physics*. CRC Press, 76th Edition.

52. Li Xianting, Wang Xin, Li Xiaofeng and Li Yang, 1999. "Investigation on the Relationship Between Flow Pattern and Air Age". Proceedings of *Building Simulation '99*, Vol I, 423-429I.BPSA.

53. Yang, J. –R., B. K. Basu, P. B. Hamilton, F. R. Pick, 1997. "The Development of a True Riverine Phytoplankton Assemblage along a Lake-Fed Lowland River". *Arch. Hydrobiol.* 140 (2): 243-260.

APPENDIX-A

- **Bathymetry/Digital Elevation Model Maps**
- **Water Depth Maps**
- **Velocity Maps**

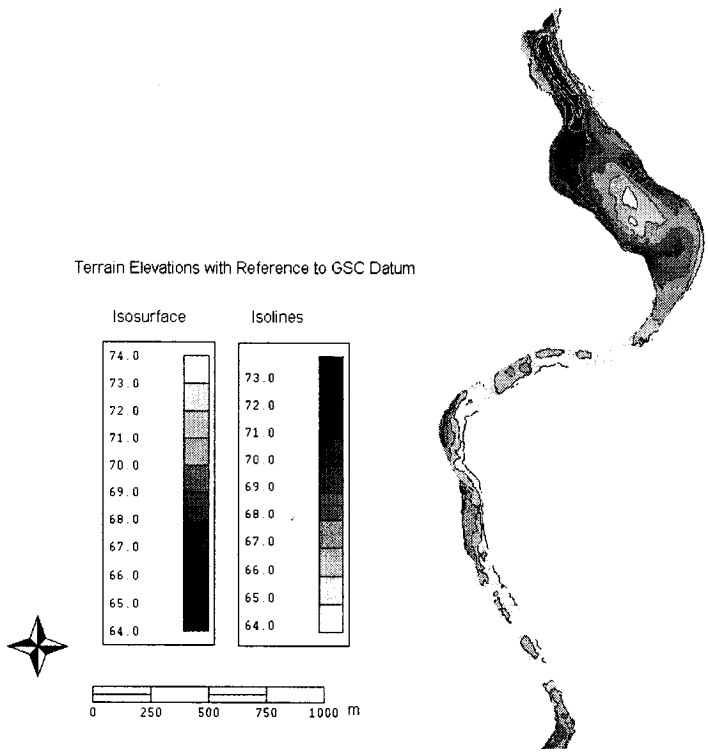

Figure A.1 Digital Terrain Model of Rideau River (Upstream of Hog's Back)

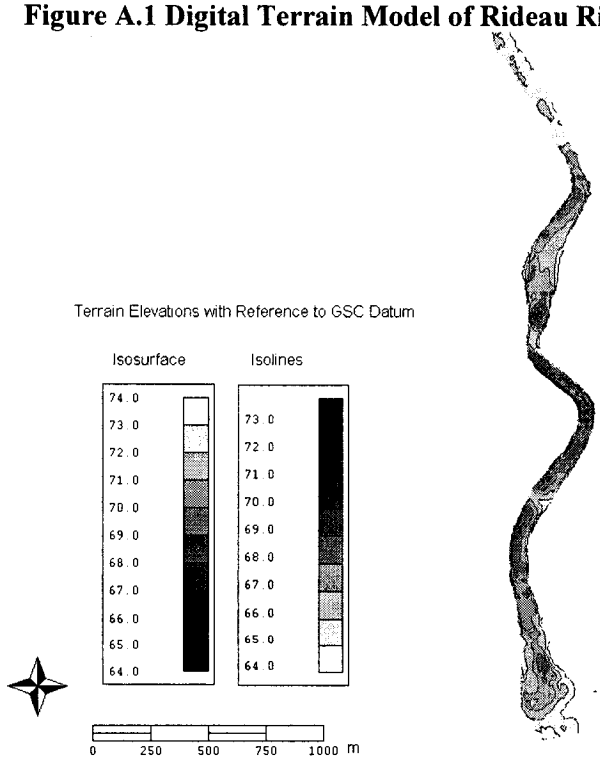

Figure A.2 Digital Terrain Model of Rideau River (Downstream of Black Rapids)

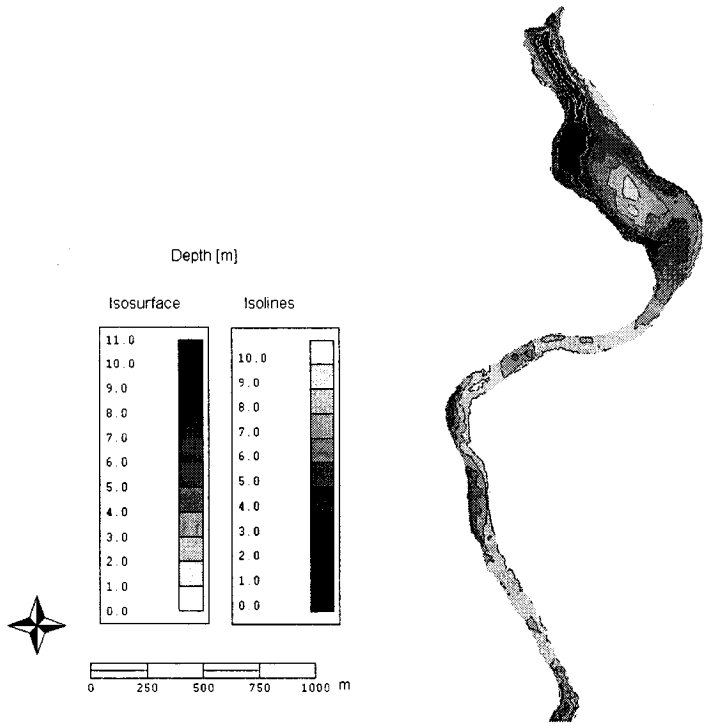

Figure A.3 Water Depth Upstream of Hog's Back for Flow of 28.6 $m^3 s^{-1}$ (July 20, 2000)

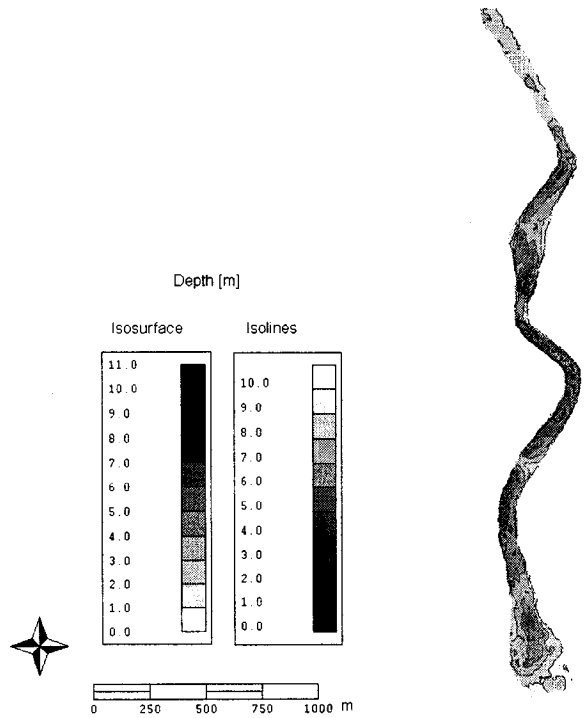

Figure A.4 Water Depth Downstream of Black Rapids for Flow of 28.6 $m^3 s^{-1}$

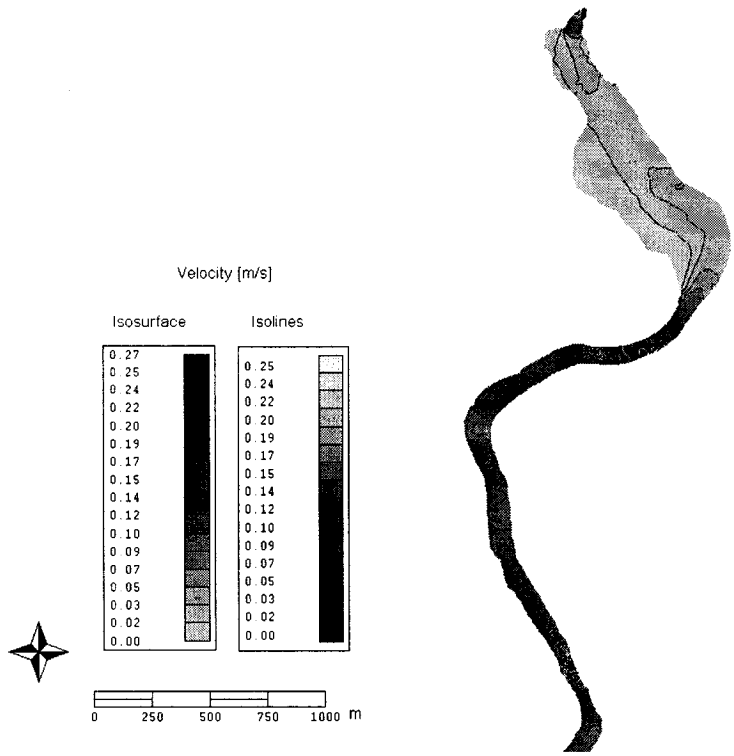

Figure A.5 Velocity Map Upstream of Hog's Back for Flow of 28.6 $m^3 s^{-1}$ (July 20, 2000)

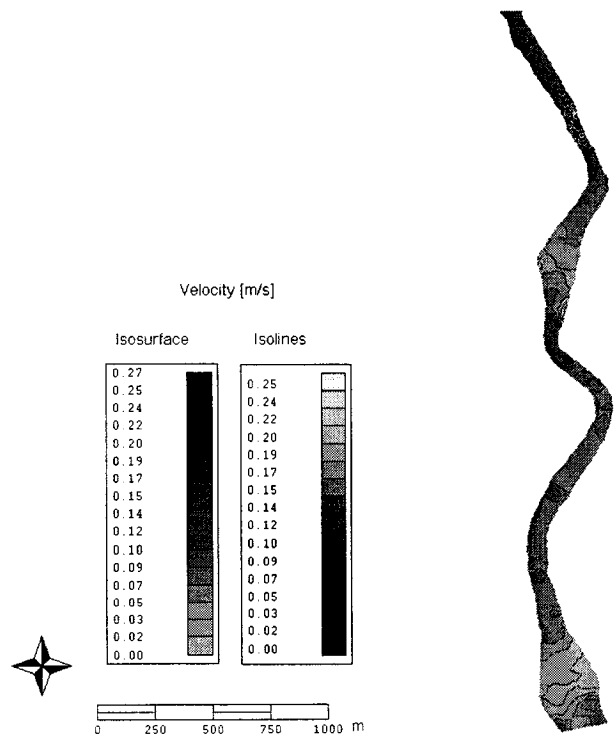

Figure A.6 Velocity Map Upstream of Hog's Back for Flow of 28.6 $m^3 s^{-1}$ (July 20, 2000)

APPENDIX-B

- **Chl *a* Maps for June 05, 00 Simulation**
- **Chl *a* Maps for July 03, 00 Simulation**
- **Chl *a* Maps for July 20, 00 Simulation**
- **Chl *a* Maps for August 08, 00 Simulation**

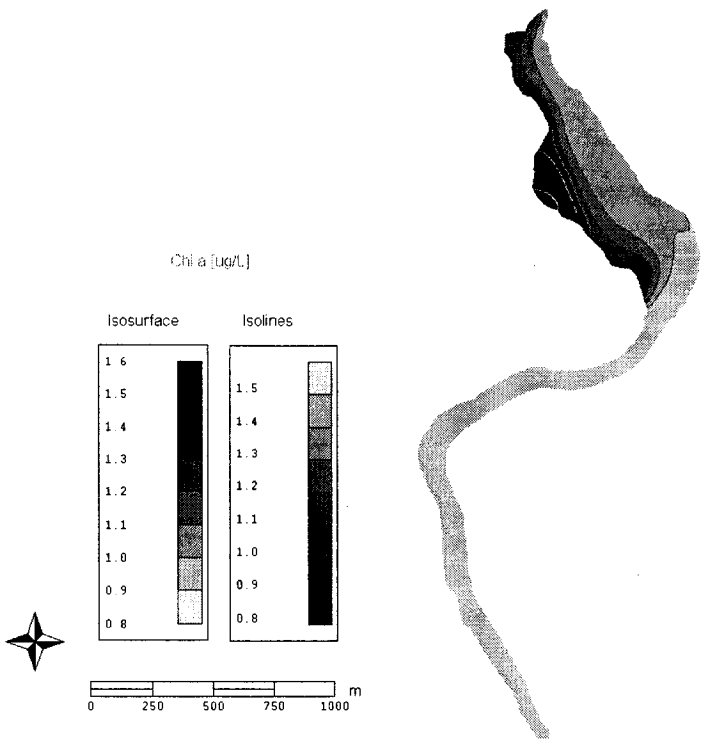

Figure B.1 Simulated Chl *a* Concentrations in Upstream of Hog's Back for June 05, 00

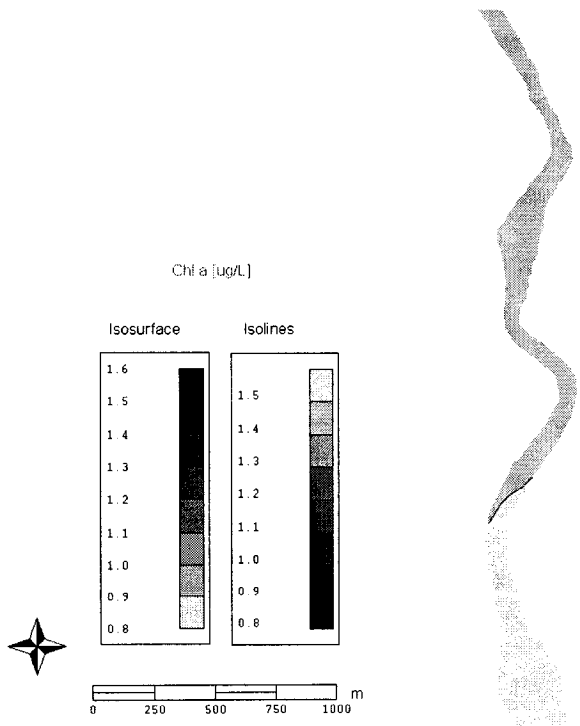

Figure B.2 Simulated Chl *a* Concentrations in Downstream of Black Rapids for June 05, 00

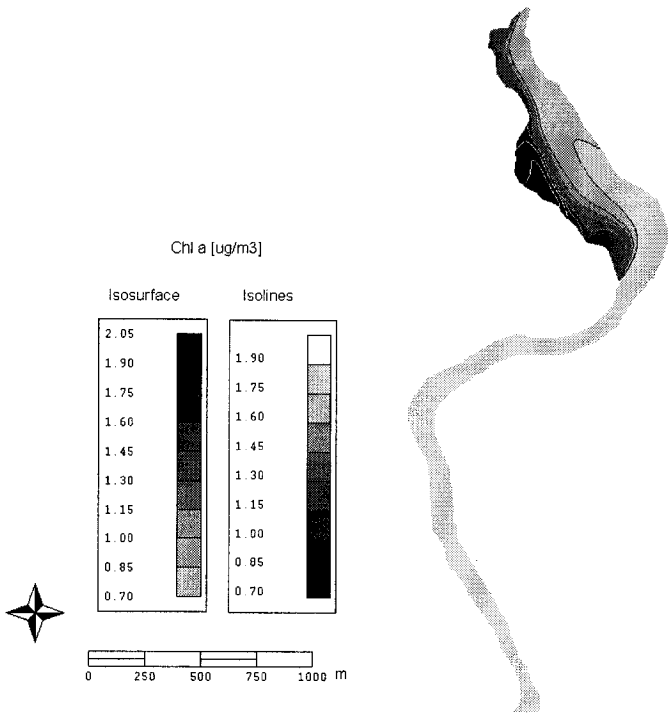

Figure B.3 Simulated Chl *a* Concentrations in Upstream of Hog's Back for July 03, 00

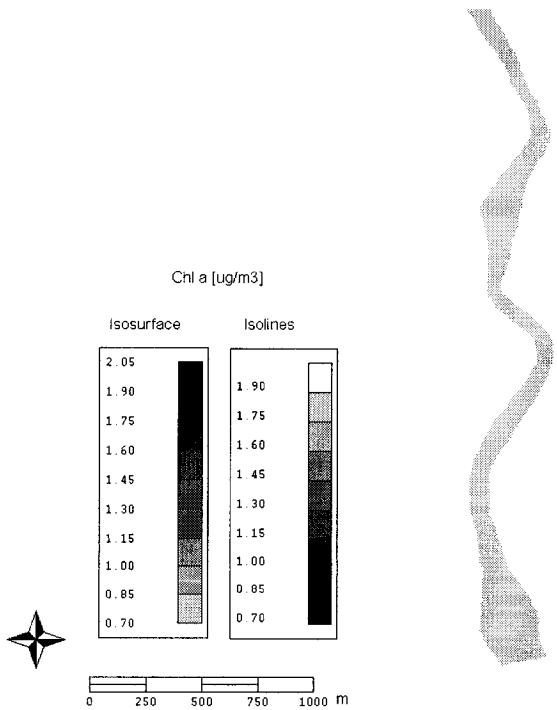

Figure B.4 Simulated Chl *a* Concentrations in Downstream of Black Rapids for July 03, 00

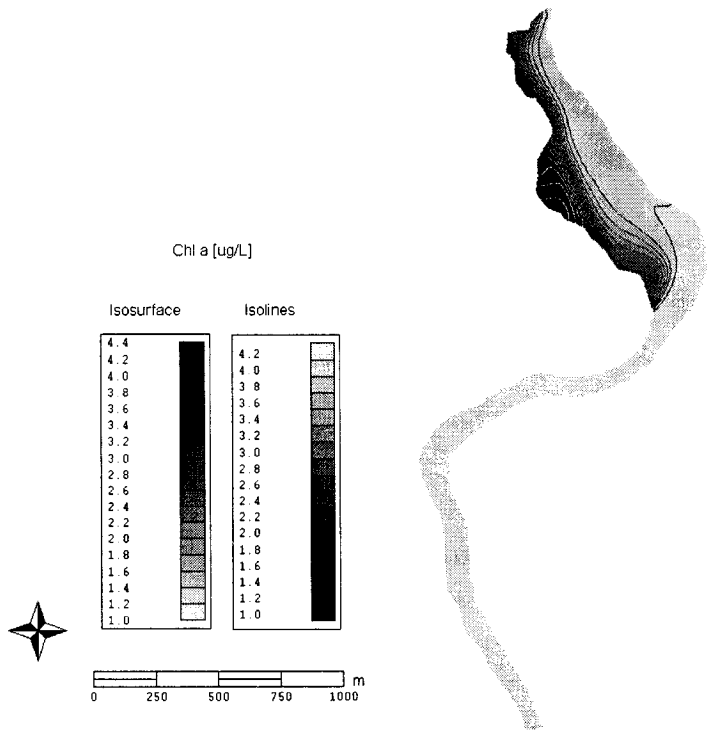

Figure B.5 Simulated Chl *a* Concentrations in Upstream of Hog's Back for July 20, 00

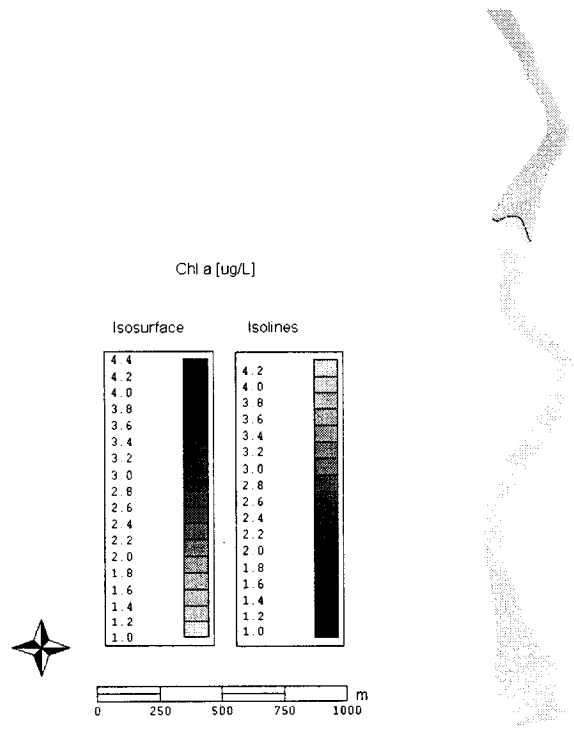

Figure B.6 Simulated Chl *a* Concentrations in Downstream of Black Rapids for July 20, 00

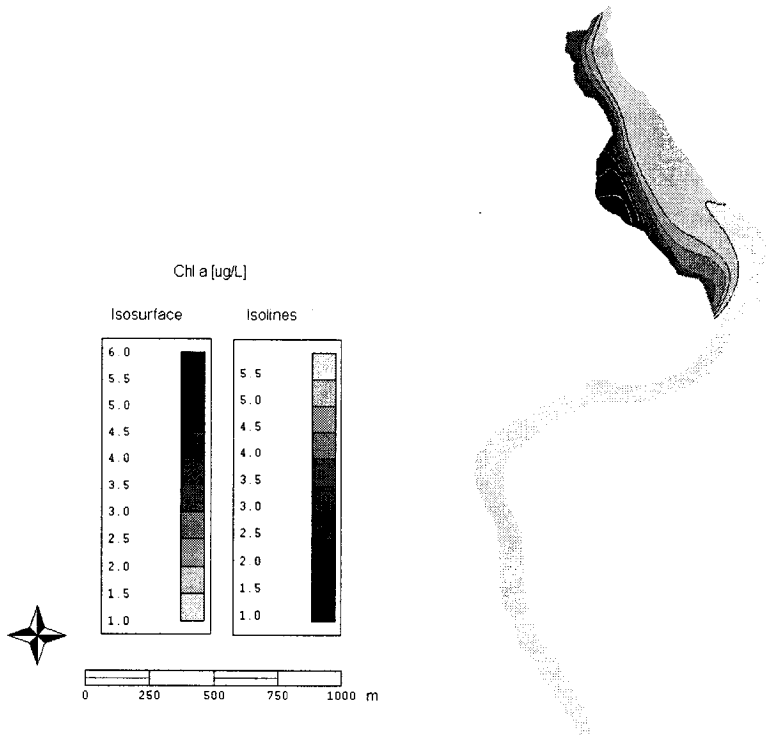

Figure B.7 Simulated Chl *a* Concentrations in Upstream of Hog's Back for August 08, 00

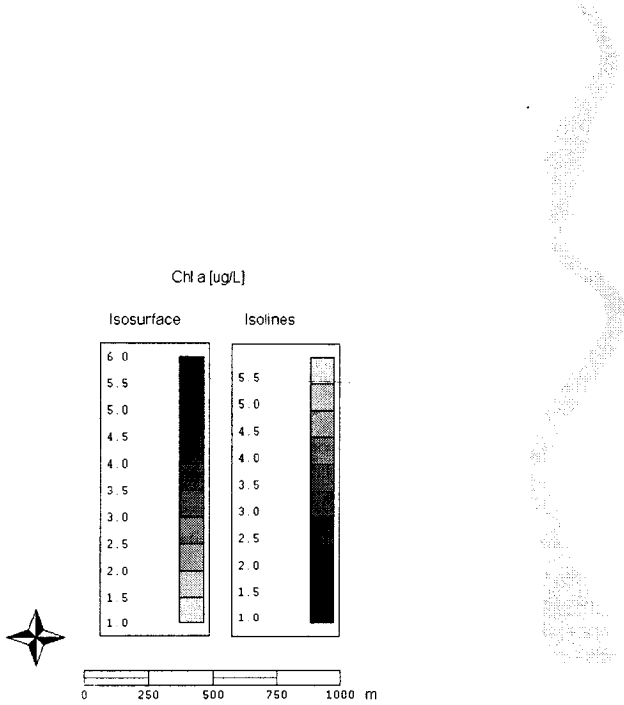

Figure B.8 Simulated Chl *a* Concentrations in Downstream of Black Rapids for Aug. 08, 00

APPENDIX-C

- **Growth Model Analytical/Numerical Solution in Maple 7.0**

```
> restart;
> H:=x->Hent+Sb*x;
```

$$H := x \rightarrow Hent + Sb\,x$$

```
> alpha1:=x->Ia/Is*exp(-ke*H(x));
alpha0:=Ia/Is;
```

$$\alpha 1 := x \rightarrow \frac{Ia\ \mathbf{e}^{(-ke\ \mathrm{H}(x))}}{Is}$$

$$\alpha 0 := \frac{Ia}{Is}$$

```
>      kgp:=x->kg20*theta^(T-20)*(2.718*f/ke*(exp(-alpha1(x))-exp(-
alpha0)))*p/(ksp+p);
```

$$kgp := x \rightarrow 2.718\ \frac{kg20\ \theta^{(T-20)}\ f\ (\mathbf{e}^{(-\alpha 1(x))} - \mathbf{e}^{(-\alpha 0)})\ p}{ke\ (ksp + p)}$$

```
> C:=x->Cent*exp(1/q*(int(kgp(xp)-vs-kR*H(xp),xp=0..x)));
```

$$C := x \rightarrow Cent\ \mathbf{e}^{\left(\frac{\int_0^x \mathrm{kgp}(xp) - vs - kR\ \mathrm{H}(xp)\ dxp}{q}\right)}$$

```
> C(x);
```

$$Cent\ \mathbf{e}^{\left(-.002000000000\left(-1359.\ kg20\ \theta^{(T-20.)}\ fp\ \theta^{20}\ \mathrm{Ei}\left(1,\ \frac{Ia\ \mathbf{e}^{(-1.\ ke\ (Hent + Sb\,x))}}{Is}\right)\right.\right.$$

$$+ 1359.\ kg20\ \theta^{(T-20.)}\ fp\ \theta^{20}\ \mathbf{e}^{\left(-1.\ \frac{Ia}{Is}\right)}\ x\ ke\ Sb + 500.\ vs\ x\ \theta^{20}\ ke^2\ Sb\ ksp + 500.\ vs\ x\ \theta^{20}\ ke^2\ Sb\ p$$

$$+ 500.\ kR\ x\ \theta^{20}\ ke^2\ Sb\ Hent\ ksp + 500.\ kR\ x\ \theta^{20}\ ke^2\ Sb\ Hent\ p + 250.\ kR\ x^2\ \theta^{20}\ ke^2\ Sb^2\ ksp + 250.\ kR\ x^2\ \theta^{20}\ ke^2\ Sb^2\ p$$

$$\left.\left. + 1359.\ kg20\ \theta^{T}\ fp\ \mathrm{Ei}\left(1,\ \frac{\mathbf{e}^{(-1.\ Hent\ ke)}\ Ia}{Is}\right)\right) \Big/ (q\ \theta^{20}\ ke^2\ (ksp + p)\ Sb)\right)$$

```
> kg20:=1.968e-5;
theta:=1.047;
T:=23.78;
f:=0.6;
ke:=0.5;
Ia:=485;
Is:=300;
ksp:=0.01;
p:=.034;
vs:=8.681e-6;
kR:=2.315e-6;
Cent:=1e-6;
Sb:=0.1;
Hent:=1;
q:=1;
```

$$kg20 := .00001968$$

$$\theta := 1.047$$

$$T := 23.78$$

$$f := .6$$

$$ke := .5$$

$$Ia := 485$$

$$Is := 300$$

$$ksp := .01$$

$$p := .034$$

$$vs := .8681\ 10^{-5}$$

$$kR := .2315\ 10^{-5}$$

$$Cent := .1\ 10^{-5}$$

$$Sb := .1$$

$$Hent := 1$$

$$q := 1$$

```
> alpha1(25);
evalf(alpha0);
```

$$.2809345420$$

$$1.616666667$$

```
> H(37.5);
```

$$4.75$$

```
> C(37.5);
```

$$.1000443789\ 10^{-5}$$

```
> plot(C(x),x=0..50);
```

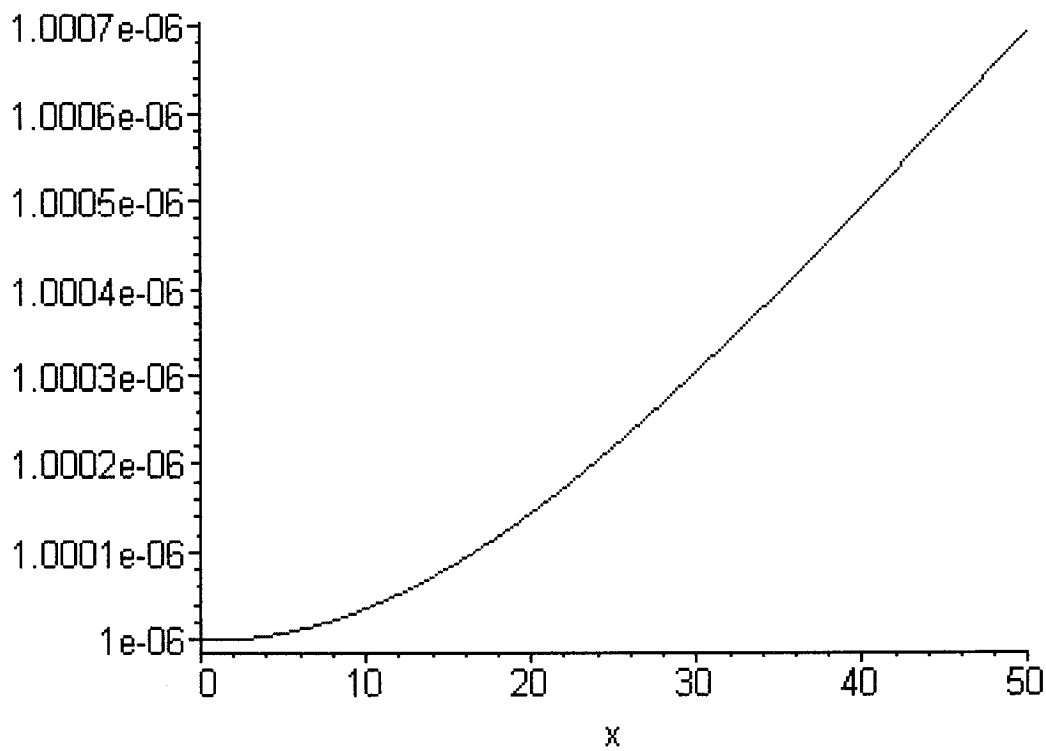
1.0007e-06
1.0006e-06
1.0005e-06
1.0004e-06
1.0003e-06
1.0002e-06
1.0001e-06
1e-06
0
10
20
30
40
50
x